AN ABSTRACT OF THE DISSERTATION OF

Dmitry N. Kosterev for the degree of Doctor of Philosophy in Electrical Engineering presented on February 28, 1996.

Title: PLANNING FOR CONTROLLABLE NETWORK DEVICES IN POWER TRANSMISSION SYSTEMS

Abstract approved: Redacted for Privacy

Wojtek J.Kolodziej

The full capacity of the existing transmission lines is often underutilized due to the system stability requirements. Controllable network devices represent the effective means of improving the system stability, and their deployment allows better use of the existing transmission facilities and can help to avoid construction of new lines. This dissertation addresses system analysis and modeling of controllable network devices.

Transient angle stability is one of the major requirements limiting transfer capability of the power transmission systems. The theoretical concepts of transient angle controllability using controllable network devices are considered in this dissertation. The main results are derived for a general transmission network structure and applied to series and shunt compensators as well as braking resistors. The proposed approach allows to quantify controllability and to relate it to the control device size, type and location in the transmission network.

Transient stability controllers are needed to maximize the device effect on the transient angle stability enhancement. The transient stability controller functional structure is discussed and the design requirements for each component are specified. The examples of controller designs are presented.

Emerging technologies such as Thyristor-Controlled Series Compensators and Synchronous Voltage Sources offer superior control capabilities and performance characteristics as compared to conventional compensators. Unlike conventional compensators, the new controllable network devices are very complex dynamical systems and require more comprehensive modeling for time-domain studies and controller designs. Detailed models of a Thyristor-Controlled Series Compensator and a Synchronous Voltage Source for powerflow, transient stability, and electro-magnetic transient studies are presented.

Finally, a detailed planning study for increasing transfer capability of the Montana transmission system using controlled series compensation is presented. A variety of design and performance requirements is considered in this study, which makes it a useful reference for similar planning projects.

# PLANNING FOR CONTROLLABLE NETWORK DEVICES IN POWER TRANSMISSION SYSTEMS

by

Dmitry N. Kosterev

A dissertation

submitted to

Oregon State University

in partial fulfillment of
the requirements for the
degree of

Doctor of Philosophy

Completed February 28, 1996
Commencement June 1996

Doctor of Philosophy thesis of Dmitry N. Kosterev presented on February 28, 1996

APPROVED:

Redacted for Privacy

03-25-96

Major Professor, representing Electrical Engineering

Redacted for Privacy

Chair of the Department of Electrical and Computer Engineering

Redacted for Privacy

Dean of the Graduate School

I understand that my thesis will become part of the permanent collection of Oregon State University libraries. My signature below authorizes release of my thesis to any reader upon request.

Redacted for Privacy

Dmitry N. Kosterev, Author

## ACKNOWLEDGMENT

I am very grateful to people who helped me to develop professionally as an engineer and as a researcher.

I am very thankful to Dr.Wojtek Kolodziej, my major professor, for giving me solid theoretical foundation in the area of systems,signals and controls. His guidance and advice, technical and personal, are greatly appreciated.

I am very grateful to Mr.William Mittelstadt, Principal Engineer at the Bonneville Power Administration, for his guidance, directions, vision, and leadership. I am very thankful for his vital impact on my professional and personal development, and for giving me opportunity to work with him on the leading edge power system projects.

I thank Dr.Ronald Mohler, Professor at Oregon State University, for his valuable contributions to this dissertation.

I am thankful to Dr.Alan Wallace, Professor at Oregon State University, and Mr.Carson Taylor, Principal Engineer at the Bonneville Power Administration, for their contributions to my professional development, and their valuable advices in the area of power system analysis and controls.

I am thankful to my friend Richard Lewison for giving me support and encouragement in the time of adversity.

Finally, I would like to thank my parents for their love, faith, self-sacrifice and encouragement.

## TABLE OF CONTENTS

## TABLE OF CONTENTS (Continued)

## TABLE OF CONTENTS (Continued)

## TABLE OF CONTENTS (Continued)

## LIST OF FIGURES

## LIST OF FIGURES (Continued)

## LIST OF TABLES

# PLANNING FOR CONTROLLABLE NETWORK DEVICES IN POWER TRANSMISSION SYSTEMS

## 1. INTRODUCTION

Acquiring new transmission rights of way is becoming more difficult due to environmental and economic considerations. New transmission lines are expensive and environmentally undesirable, and it takes considerable time to permit and to build them. The power transfer capability of a transmission system is constrained by line design limitations (such as its thermal capacity) and system stability requirements (such as transient stability, voltage stability, sub-synchronous resonance). Typically, transmission lines are loaded below their thermal capacities due to the system stability requirements. It is economically attractive and environmentally beneficial to achieve full utilization of existing transmission lines by reducing constraints resulting from the system stability requirements.

Controllable network devices provide a means of improving the system stability, and in many cases are more cost-effective and environmentally benign transmission system reinforcements than new lines. Controllable network devices include:

- Series Compensation:
  - Mechanically and thyristor switched series capacitors [2, 3]
  - Thyristor-Controlled Series Compensator (TCSC) [4, 5]
  - Static Synchronous Series Compensator (SSSC) [6, 8]
- Shunt Compensation:

  - Mechanically and thyristor switched shunt capacitors and reactors
  - Thyristor-controlled shunt reactors
  - Static Condenser (Statcon) [7–9]
  - Battery Energy Storage device [10]
- Dynamic Braking Resistors [11]
- Unified Power Flow Controller [8, 12]

Employing controllable network devices will result in a better utilization of existing transmission resources and reduce construction of new transmission lines.

Transient stability is one of the major stability requirements limiting power transfer capability of a transmission system. The IEEE Standard Dictionary of Electrical and Electronics Terms [1] defines transient stability as "a condition that exists in a power system if, after an aperiodic disturbance, the system regains steady-state stability." Depending on the instability mechanism and dynamic elements involved, various types of transient instability (stability) are considered. This dissertation focuses on the transient angle stability. Transient angle stability relates to the capability of synchronous AC machines to retain synchronism among them following an aperiodic disturbance. Angle stability is a wide-area phenomenon, involving relative behavior of generators in the entire system. Disturbances, when occurring in power systems, create imbalance between generator electrical power output and mechanical power input from a prime mover. If mechanical power exceeds electrical output the generator rotor will accelerate, conversely a mechanical power deficiency will cause the rotor to decelerate. After an aperiodic disturbance is removed, the system experiences a post-disturbance transient. If there is not enough synchronizing power between the generators in the system, generator groups can lose synchronism

and go out-of-step. Out-of-step conditions result in system islanding and, very likely, in interrupted power delivery to the customers.

It is important to show that controllable network devices can control transient angle dynamics in power systems. Controllability is one of the key concepts in the systems theory. Thus, theoretical concepts of the transient angle controllability using controllable network devices are considered first in this dissertation. The presented results are derived for a general transmission system structure, and apply to series and shunt compensators as well as braking resistors. The derived concepts allow to quantify controllability and to relate it to the control device size, type and location in transmission network. After the transient angle controllability is demonstrated for a classical power system model, the dissertation addresses functional structure of a transient stability controller. Such controllers are needed to maximize the device effectiveness for transient stabilization. The dissertation outlines the fundamental principles of the transient stability controller for controllable network devices.

Conventional compensators (such as mechanically and thyristor- switched devices, thyristor-controlled shunt reactors) have been effectively used to reinforce power transmission systems. Emerging technologies such as TCSC, SSSC, Statcon, Unified Power Flow Controller offer superior control capabilities and performance characteristics to those of conventional compensators. Recent TCSC installations at 230kV and 500kV systems [4, 5] demonstrated numerous benefits provided by the device for poweflow control, sub-synchronous resonance mitigation, and transient stability enhancement. New devices such as SSSC and Statcon represent a Synchronous Voltage Source (SVS) connected in series or in shunt with a transmission line and are based entirely on power electronics converter technology. To include these devices in consideration for existing and future transmission system

planning projects, their appropriate models have to be derived for the time-domain studies. Unlike conventional compensators, the new controllable network devices are very complex dynamical systems, and modeling of these systems is not a trivial task. This dissertation develops time-domain models for Thyristor-Controlled Series Compensators and Synchronous Voltage Sources. These models are used next in power system performance studies and controller designs.

Finally, the dissertation presents a detailed planning study for the Montana transmission system uprate using controlled series compensation. The example goes step-by-step through the key points of the developed planning procedure and serves as a useful reference for similar planning projects.

# 2. TRANSIENT ANGLE CONTROLLABILITY USING CONTROLLABLE NETWORK DEVICES

This chapter presents concepts of the transient angle controllability and principles of the transient stability controls for controllable network devices.

## 2.1. Evolution of the Controllability Concept

The ability of controllable network devices to benefit transient angle stability has been known and used by power utilities. Reference [2] proposed to use switched series capacitors to enhance transient stability in power systems. An equal-area criteria was used to demonstrate effect of the capacitor switching on the first swing stability margin. The next significant step was made in [11], where phase-plane techniques were used to develop control strategy for switching the dynamic braking resistor. It was demonstrated that by a proper application of a braking resistor, the system trajectory can be driven to a neighborhood of the post-disturbance equilibrium. In reference [14], a phase-plane approach was used to design switching lines for bang-bang control of series capacitors. Robustness issues of switching lines were discussed, and target-set instead of target-point control was proposed. Despite significant developments in the area of controllable network devices and their applications for transient angle stability enhancement, there was no formal proof of the fact of transient angle controllability.

The modeling approach which was used in the above papers to develop controllability concepts has considered only radial type transmission systems (two machines interconnected by a single link, or a single-machine infinite bus system). If

series compensator was used, it controlled only power transfer capability of the link, and if the dynamic brake was used, it controlled only power loading of the link. Such description of a transmission system is limited to a radial system only and is not representative of realistic multi-bus transmission networks. Because of inadequate representation of the transmission system, the existing approach

- is limited to radial transmission networks
- does not allow to quantify controllability
- does not allow to determine effect of device location in transmission network and device size on controllability
- does not allow to compare various types of compensators.

Since controllable network devices affect the transient angle dynamics by altering parameters of the transmission network, a more comprehensive representation of transmission network is needed to determine the compensation device effect on network parameters. This novel approach is taken in this dissertation.

## 2.2. Power System Model

A power system model with controllable network devices is constructed in this section, and the relationship between device compensation and model parameters is established.

### 2.2.1. Transmission System Equations

A power transmission system is represented by linear algebraic equations with composite electrical loads given by constant admittance shunts. The nodal equation representing the transmission system is

$$\begin{bmatrix} \bar{\mathbf{I}}_G \\ \bar{\mathbf{I}}_D \\ 0 \end{bmatrix} = \begin{bmatrix} \bar{\mathbf{Y}}_{GG} & 0 & \bar{\mathbf{Y}}_{GN} \\ 0 & \bar{\mathbf{Y}}_{DD} & \bar{\mathbf{Y}}_{DN} \\ \bar{\mathbf{Y}}_{NG} & \bar{\mathbf{Y}}_{ND} & \bar{\mathbf{Y}}_{NN} \end{bmatrix} \begin{bmatrix} \bar{\mathbf{E}}_G \\ \bar{\mathbf{E}}_D \\ \bar{\mathbf{E}}_N \end{bmatrix}, \tag{2.1}$$

where:

$\bar{\mathbf{Y}}_{(\bullet\bullet)}$ - bus admittance matrices

$\bar{\mathbf{E}}_{(\bullet)}$ - bus voltage vector

$\bar{\mathbf{I}}_{(\bullet)}$ - vector of injected bus currents

subscripts: G - generator, D - controllable network devices, N - uncontrolled transmission network.

Submatrix $\bar{\mathbf{Y}}_{DD}$ includes inputs from controllable network devices, and submatrices $\bar{\mathbf{Y}}_{ND}$ and $\bar{\mathbf{Y}}_{DN}$ determine locations of these devices in the transmission network. Representation of various controllable network devices in submatrix $\bar{\mathbf{Y}}_{DD}$ is discussed below.

**Shunt compensators** ( mechanically and thyristor-switched shunt capacitors and reactors, thyristor-controlled reactors) at the *p-th* bus are modeled as a controlled admittance $Y_C$. This admittance is added to the uncontrollable self-admittance $\bar{Y}_{DD}^{pp}$ of the *p-th* bus. This results in a single entry in submatrix $\bar{\mathbf{Y}}_{DD}$:

$$\bar{Y}_{DD} = [\bar{Y}_{DD}^{pp} + jY_C].$$

$Y_C$ is positive for capacitive compensation and negative for inductive compensation.

**Series compensators** ( mechanically and thyristor-switched series capacitors, thyristor-controlled series compensators ) enter the transmission system model

as a controlled reactance $X_C$ in the $p$-$q$ branch. The devices require addition of 2×2 diagonal block in submatrix $\bar{\mathbf{Y}}_{DD}$:

$$\bar{\mathbf{Y}}_{DD} = \begin{bmatrix} \bar{Y}_{DD}^{pp} - j/X_C & j/X_C \\ j/X_C & \bar{Y}_{DD}^{qq} - j/X_C \end{bmatrix} \begin{matrix} p-\text{bus} \\ q-\text{bus} \end{matrix}$$

**Dynamic braking resistors** ( switched and thyristor-controlled ) are modeled by a controlled admittance $Y_R$ added to the uncontrolled self-admittance $\bar{Y}_{DD}^{pp}$ of the *p-th* bus. The corresponding entry in submatrix $\bar{\mathbf{Y}}_{DD}$ is

$$\bar{Y}_{DD} = [\bar{Y}_{DD}^{pp} + Y_R].$$

Admittances $Y_C, Y_R$ and reactance $X_C$ are controlled variables and will be denoted by $\mathbf{u}$. Controls $\mathbf{u}$ appear linearly in submatrix $\bar{\mathbf{Y}}_{DD}$.

### 2.2.2. Transmission Network Reduction

**Step 1.** System 2.1 dimension can be reduced first by eliminating the uncontrolled transmission network buses and retaining only generation and controlled buses. This can be done by solving the third line of equation (2.1) for $\bar{\mathbf{E}}_N$:

$$\bar{\mathbf{E}}_N = -\bar{\mathbf{Y}}_{NN}^{-1}(\bar{\mathbf{Y}}_{NG}\bar{\mathbf{E}}_G + \bar{\mathbf{Y}}_{ND}\bar{\mathbf{E}}_D).$$

The solution is substituted in the first two lines of equation (2.1), resulting in the following reduced-order transmission network equation:

$$\begin{bmatrix} \bar{\mathbf{I}}_G \\ \bar{\mathbf{I}}_D \end{bmatrix} = \begin{bmatrix} \bar{\mathbf{Y}}_{gg} & \bar{\mathbf{Y}}_{gd} \\ \bar{\mathbf{Y}}_{dg} & \bar{\mathbf{Y}}_{dd}(\mathbf{u}) \end{bmatrix} \begin{bmatrix} \bar{\mathbf{E}}_G \\ \bar{\mathbf{E}}_D \end{bmatrix}, \tag{2.2}$$

where

$$\bar{\mathbf{Y}}_{ij} = \bar{\mathbf{Y}}_{IJ} - \bar{\mathbf{Y}}_{IN}\bar{\mathbf{Y}}_{NN}^{-1}\bar{\mathbf{Y}}_{JG}, \qquad i,j = \{g,d\}, \qquad I,J = \{G,D\}$$

The submatrix $\bar{\mathbf{Y}}_{dd}(\mathbf{u})$ represents controlled compensation in the transmission network, and control inputs appear linearly in equation (2.2). Admittances $\bar{\mathbf{Y}}_{gd}$ and $\bar{\mathbf{Y}}_{dg}$ determine locations of network control devices with respect to the generation buses in the system. These submatrices depend on the device location and type. Admittances in equation (2.2) represent equivalent distances between the retained buses, and model (2.2) does not preserve the original transmission system structure.

**Step 2.** Since the considered controllable network devices enter the transmission system model only in submatrix $\bar{\mathbf{Y}}_{dd}(\mathbf{u})$, vector $\bar{\mathbf{I}}_D = \mathbf{0}$. Then, by solving the second line of equation (2.2) for $\bar{\mathbf{E}}_D$ and substituting this solution in the first line of equation (2.2), the following transmission system equation is obtained:

$$\bar{\mathbf{I}}_G \;=\; [\,\bar{\mathbf{Y}}_{gg} - \bar{\mathbf{Y}}_{gd}\bar{\mathbf{Y}}_{dd}^{-1}(\mathbf{u})\bar{\mathbf{Y}}_{dg}\,]\;\bar{\mathbf{E}}_G \;=\; \bar{\mathbf{Y}}(\mathbf{u})\;\bar{\mathbf{E}}_G. \tag{2.3}$$

The matrix $\bar{\mathbf{Y}}(\mathbf{u})$ represents equivalent admittances between generation nodes, and is affected nonlinearly by controls $\mathbf{u}$.

### 2.2.3. Generator Model

The generators are represented by classical models: constant transient voltage $E_G$ = const behind the transient reactance. The electrical output of the *i-th* generator to the transmission network is

$$P_G^i = \sum_{j=1}^{g} E_G^i E_G^j Y^{ij} \sin(\delta_i - \delta_j + \alpha_{ij}),$$

where:

$E_G^i$ - a magnitude of $\bar{E}_G^i$,

$\delta_i$ - an argument of $\bar{E}_G^i$,

$Y^{ij}$ - a magnitude of $\bar{Y}^{ij}$,

$\alpha_{ij}$ - conductance angle, equal 90 degrees minus argument of $\bar{Y}^{ij}$.

$P_G^i$ depends on the compensation provided by a controllable network device through the admittances $\bar{Y}^{ij}(\mathbf{u}), \quad j = 1 \ldots g$.

The *i-th* generator swing equation is

$$\dot{\delta}_i = \omega_i, \qquad M_i\dot{\omega}_i = P_M^i - P_G^i,$$

where

$\omega_i$ - *i-th* generator rotor speed deviation

$M_i$ - the *i-th* generator inertia

$P_M^i$ - the *i-th* generator mechanical input power.

### 2.2.4. Dependence of the Swing Equation Parameters on the Compensation

Let us establish a relationship between the compensation provided by a controllable network device and swing equation parameters. We start with a transmission system model 2.2 where the control inputs from network devices appear linearly, and go through a model reduction step to obtain equation 2.3. We investigate impact of control signal on parameters of the admittance matrix $\bar{\mathbf{Y}}$, and consequently parameters of the swing equation.

**Shunt Compensation.** Consider *i-th* and *j-th* generation buses and the shunt compensator at the *p-th* bus. This sub-network is represented by the following block

$$\begin{array}{l} i-\text{bus} \\ j-\text{bus} \\ p-\text{bus} \end{array} \begin{bmatrix} \bar{Y}_{gg}^{ii} & \bar{Y}_{gg}^{ij} & \bar{Y}_{gd}^{ip} \\ \bar{Y}_{gg}^{ji} & \bar{Y}_{gg}^{jj} & \bar{Y}_{gd}^{jp} \\ \bar{Y}_{dg}^{pi} & \bar{Y}_{dg}^{pj} & \bar{Y}_{dd}^{pp} + jY_C \end{bmatrix}$$

in the admittance matrix of equation 2.2. Admittance $\bar{Y}_{gg}^{ij}$ represents a mutual uncontrolled admittance between the generators, admittances $\bar{\mathbf{Y}}_{gd}$ and $\bar{\mathbf{Y}}_{dg}$ determine

electrical location of the *p-th* shunt compensator bus with respect to the *i-th* and *j-th* buses respectively. Then, the equivalent controlled admittance between *i-th* and *j-th* generation buses in the reduced-order system (2.3) is

$$\bar{Y}^{ij}(Y_C) = \bar{Y}^{ij}_{gg} - \frac{\bar{Y}^{ip}_{gd}\bar{Y}^{pj}_{dg}}{\bar{Y}^{pp}_{dd} + jY_C}.$$

The second term in the above expression represents a shunt compensator effect on the mutual admittance $\bar{Y}^{ij}$. The admittance magnitude $Y^{ij}$ is finite for $\bar{Y}^{pp}_{dd} \neq -jY_C$. In the typical case when $\bar{Y}^{pp}_{dd}$ has a real part representing line resistances, the admittance magnitude $Y^{ij}$ is bounded for all values of $Y_C$..

**Series Compensation.** Consider *i-th* and *j-th* generation buses and the series compensator between the *p-th* and *q-th* buses. The corresponding sub-network is represented by the following block

$$\begin{array}{c} i-\text{bus} \\ j-\text{bus} \\ p-\text{bus} \\ q-\text{bus} \end{array} \begin{bmatrix} \bar{Y}^{ii}_{gg} & \bar{Y}^{ij}_{gg} & \bar{Y}^{ip}_{gd} & \bar{Y}^{iq}_{gd} \\ \bar{Y}^{ji}_{gg} & \bar{Y}^{jj}_{gg} & \bar{Y}^{jp}_{gd} & \bar{Y}^{jq}_{gd} \\ \bar{Y}^{pi}_{dg} & \bar{Y}^{pj}_{dg} & \bar{Y}^{pp}_{dd} - j/X_C & \bar{Y}^{pq}_{dd} + j/X_C \\ \bar{Y}^{qi}_{dg} & \bar{Y}^{qj}_{dg} & \bar{Y}^{qp}_{dd} + j/X_C & \bar{Y}^{qq}_{dd} - j/X_C \end{bmatrix}$$

in the admittance matrix of equation 2.2. Then, the equivalent controlled admittance between *i-th* and *j-th* generation buses in the reduced-order system (2.3) is

$$\bar{Y}^{ij}(X_C) = \bar{Y}^{ij}_{gg} - [\bar{Y}^{ip}_{gd} \quad \bar{Y}^{iq}_{gd}] \begin{bmatrix} \bar{Y}^{pp}_{dd} - j/X_C & \bar{Y}^{pq}_{dd} + j/X_C \\ \bar{Y}^{qp}_{dd} + j/X_C & \bar{Y}^{qq}_{dd} - j/X_C \end{bmatrix}^{-1} \begin{bmatrix} \bar{Y}^{pj}_{dg} \\ \bar{Y}^{qj}_{dg} \end{bmatrix}.$$

The admittance magnitude $Y^{ij}$ is finite for nonzero determinant of the matrix

$$\begin{bmatrix} \bar{Y}^{pp}_{dd} - j/X_C & \bar{Y}^{pq}_{dd} + j/X_C \\ \bar{Y}^{qp}_{dd} + j/X_C & \bar{Y}^{qq}_{dd} - j/X_C \end{bmatrix}.$$

**Dynamic Braking Resistor** This case is similar to that with the shunt compensation. For a given compensation value $Y_R$, the equivalent controlled admittance between *i-th* and *j-th* generation buses in the reduced-order system (2.3)

is

$$\bar{Y}^{ij}(Y_R) = \bar{Y}^{ij}_{gg} - \frac{\bar{Y}^{ip}_{gd}\bar{Y}^{pj}_{dg}}{\bar{Y}^{pp}_{dd} + Y_R}.$$

The admittance magnitude $Y^{ij}$ is finite for $\bar{Y}^{pp}_{dd} \neq -Y_R$. In the typical case when $\bar{Y}^{pp}_{dd}$ has an imaginary part representing line reactances, the admittance magnitude $Y^{ij}$ is bounded for all compensation values of $Y_R$.

Conclusions:

- The controls from controllable network devices affect parameters of the swing equation non-linearly. The effect of the control signal on the swing equation parameters depends on the controllable network device type and location.

- Compensation generally will affect all electrical parameters in the swing equation, and these parameters will be finite numbers in all practical cases.

- The relationship between control signals and parameters of the swing equation is not one-to-one. Increase in control can in some cases decrease mutual admittance (and hence the transfer capability) between generators in the system. E.g. a shunt compensator with infinite admittance is a fault. Large control signal may enhance stability of one group of generators and at the same disturb stability of another group of generators. For example, 1400MW dynamic brake application at the Chief Joseph in the Bonneville Power Administration can be a very positive effect on stability between Pacific Northwest and Southwest, and at the same time lead to instability of the Chief Joseph generators with respect to the rest of the system.

## 2.3. Transient Angle Controllability of a Two-Machine Multi-Bus System

Concepts of the transient angle controllability are demonstrated for a two-machine multi-bus system.

### 2.3.1. Model of a Two-Machine Multi-Bus System

Consider a two-generator system, interconnected by a multi-bus transmission network ($g = 2$). Introduce notations

$$P_e = E_G^{(1)} E_G^{(2)} Y^{(12)},$$

$$P_{mi} = P_M^{(i)} - (E_G^{(i)})^2 Y^{(ii)} \sin \alpha_{ii}, \qquad i = 1, 2.$$

Then the two-machine system is represented by the following set of the swing equations

$$\dot{\delta}_1 = \omega_1,$$
$$M_1 \dot{\omega}_1 = P_{m1} - P_e \sin(\delta_1 - \delta_2 - \alpha),$$

$$\dot{\delta}_2 = \omega_2,$$
$$M_2 \dot{\omega}_2 = P_{m2} - P_e \sin(\delta_2 - \delta_1 - \alpha).$$

Since transient angle stability involves relative generator behavior, new states are introduced

$$\delta = \delta_1 - \delta_2, \quad \text{and} \quad \omega = \omega_1 - \omega_2$$

representing swing angle and speed differences between the generators. Parameters $P_e \geq 0, P_{mi}, \alpha$ are controlled by the network control devices, parameters $M_i > 0$ are fixed. All the parameters have finite values.

Then, the above equation can be written as

$$\begin{aligned} \dot{\delta} &= \omega, \\ M\dot{\omega} &= P_M - P_E \sin(\delta - \varphi), \end{aligned} \tag{2.4}$$

where:

$M = M_1 M_2/(M_1 + M_2)$ - total system inertia;

$P_M = (M_2 P_{m1} - M_1 P_{m2})/(M_1 + M_2)$ - power to be transmitted;

$P_E = P_e \sqrt{(M_1 + M_2)^2 \cos^2\alpha + (M_1 - M_2)^2 \sin^2\alpha}\ /(M_1 + M_2)$ - transfer capability;

$\varphi = \text{atan2}[(M_1 - M_2)\sin\alpha/(M_1 + M_2)\cos\alpha]$ - conductance angle.

In equation (2.4), $M > 0$, $P_E \geq 0$, and $P_M$ can be positive or negative depending on the powerflow direction in the system. Assume that $P_M > 0$, i.e. the power is transferred in one direction. Since the admittance matrix elements are finite, $P_E$ and $P_M$ are also finite.

### 2.3.2. Properties of the Swing Equation

First, the properties of system 2.4 are investigated for a constant control **u**.

**Proposition 1.** Differential equation (2.4) has unique solution for all $t$.

Proof: The function in equation (2.4) is Lipshitz continuous. Then, the unique solution of (2.4) exists for all $t$ [13]. ∎

The phase-plane trajectory can be derived by eliminating time from equation (2.4).

$$\frac{d\omega}{d\delta} = \frac{P_M - P_E \sin(\delta - \varphi)}{M\,\omega}. \tag{2.5}$$

Integrating by parts, the trajectory equation is obtained

$$\frac{1}{2}M(\omega^2 - \omega_0^2) = P_M(\delta - \delta_0) + P_E[\cos(\delta - \varphi) - \cos(\delta_0 - \varphi)]. \tag{2.6}$$

**Proposition 2.** System (2.4) has a periodic phase portrait with a period $2\pi$ on the $\delta$-axis.

Proof: It follows from equation (2.6). If the quadruple $(\omega, \omega_0, \delta, \delta_0)$ satisfies condition (2.6), so does $(\omega, \omega_0, \delta \pm 2k\pi, \delta_0 \pm 2k\pi)$, where $k$ is an integer. ∎

Thus, system (2.4) trajectories are considered only on the interval $\delta \in (-\pi + \varphi, \pi + \varphi]$.

**Proposition 3.** If $|P_M| > P_E$, system (2.4) has no equilibria.

If $|P_M| = P_E$, system (2.4) has one equilibrium on $(-\pi + \varphi, \pi + \varphi]$.

If $|P_M| < P_E$, system (2.4) has two equilibria on $(-\pi + \varphi, \pi + \varphi]$:

$$(\delta_e,\ \omega_e) = (\varphi + \arcsin(P_M/P_E),\ 0)$$

One equilibrium is a center, and the other one is a saddle point. The center-type equilibrium is denoted by $(\delta_{ec},\ 0)$, and the saddle-type equilibrium is denoted by $(\delta_{es},\ 0)$.

Define a set

$$\mathcal{R}\ (\delta, \omega) = \{\ \delta,\ \omega\ | \frac{1}{2} M\omega^2 < P_M(\delta - \delta_{es}) + P_E[\cos(\delta - \varphi) - \cos(\delta_{es} - \varphi)]\ \}$$

**Proposition 4.** If

- $(\delta, \omega) \in \mathcal{R}$ then a trajectory passing through $(\delta, \omega)$ is closed and periodic. A closed trajectory encloses the center-type equilibrium $(\delta_{ec}, 0)$.

- $(\delta, \omega) \in \partial(\mathcal{R})$ (boundary of the set $\mathcal{R}$), a trajectory passing through $(\delta, \omega)$ approaches the saddle-type equilibrium $(\delta_{es}, 0)$ as $t \to \infty$.

- $(\delta, \omega) \notin cl(\mathcal{R})$ (closure of the set $\mathcal{R}$) then:
  (i) if $\mathcal{R} = \emptyset$, a trajectory through $(\delta, \omega)$ is monotonically increasing in $\omega$;
  (ii) if $\mathcal{R} \neq \emptyset$, $\delta < \delta_{ec}$, a trajectory through $(\delta, \omega)$ intersects a line $\delta = \theta, \theta > \delta_{es}$ at $\omega \neq 0$.

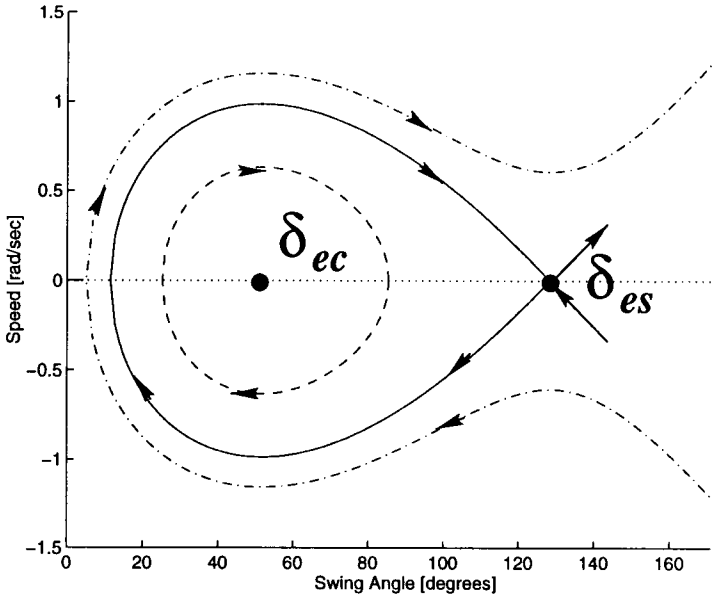


FIGURE 2.1. Phase-plane trajectories of a swing equation

Phase-plane trajectories for the above conditions are depicted in Figure 2.1. The solid line represents boundary of the set $\mathcal{R}$, the broken line represent a closed trajectory originating and staying within the set $\mathcal{R}$, and the dash-dotted line represents an unbounded trajectory originating outside the set $\mathcal{R}$.

Define functions

$$K(\omega) = 1/2\ M\ \omega^2$$

$$P(\delta) = -P_M \delta - P_E \cos(\delta - \varphi)$$

$$T(\delta, \omega) = K(\omega) + P(\delta)$$

These functions have energy interpretation, where $K(\omega)$ is kinetic energy, $P(\delta)$ is potential energy, and $T(\delta, \omega)$ is total system energy. Equation $T(\delta, \omega) = \text{const}$ defines a transient trajectory (2.6), i.e. the total energy is constant along a transient trajectory.

Since every trajectory originating in $\mathcal{R}$ encloses the center-type equilibrium $(\delta_{ec}, 0)$ (Proposition 4), it intersects the $\delta$-axis on both sides of $\delta_{ec}$. Due to the uniqueness of system (2.4) solution, all trajectories originating in $\mathcal{R}$ can not intersect the $\delta$-axis beyond the saddle-type equilibrium $(\delta_{es}, 0)$. Thus, all the trajectories originating in $\mathcal{R}$ intersect $\delta$-axis on the interval $[\ \delta_{ec},\ \delta_{es}\ )$.

Since every trajectory in $\mathcal{R}$ intersects the interval $[\ \delta_{ec},\ \delta_{es}\ )$ and the function $T(\delta, \omega)$ is constant along a trajectory, to evaluate the functions $T(\delta, \omega)$ at $(\delta, \omega) \in \mathcal{R}$, it is sufficient to evaluate the functions $T(\delta, 0) = P(\delta)$ for $\delta \in [\ \delta_{ec},\ \delta_{es}\ )$. Elementary calculus shows that the function $P(\delta)$ is continuous and has one isolated minimum at $\delta_{ec}$ on the interval $[\ \delta_{ec},\ \delta_{es}\ )$, and that the function $P(\delta)$ is monotonically increasing along the interval $[\delta_{ec}, \delta_{es})$. Denote $T_{ec} = T(\delta_{ec}, 0) = P(\delta_{ec})$ and $T_{es} = T(\delta_{es}, 0) = P(\delta_{es})$.

**Proposition 5.**

- Trajectories originating in $\mathcal{R}$ are described by equations $T(\delta, \omega) = T_i$, where $T_i \in [\ T_{ec},\ T_{es}\ )$.
- $T_i \in [\ T_{ec},\ T_{es}\ )$ uniquely defines a transient trajectory in $\mathcal{R}$.
- Assume that $(\delta_0, \omega_0) \in cl(\mathcal{R})$ and $(\delta_f, \omega_f) \in cl(\mathcal{R})$, and that $T(\delta_0, \omega_0) = T_0 < T_f = T(\delta_f, \omega_f)$. Then a line connecting $(\delta_0, \omega_0)$ and $(\delta_f, \omega_f)$ intersects all trajectories $T(\delta, \omega) = T_i$ where $T_i \in [T_0,\ T_f]$.

### 2.3.3. Transient Angle Controllability

**Definition.** The system $\dot{\mathbf{x}} = f(\mathbf{x}, \mathbf{u})$ is *controllable on a set* $\mathcal{R}$ if given any $\mathbf{x}_0 \in \mathcal{R}$ and $\mathbf{x}_f \in \mathcal{R}$ there exists control $\mathbf{u}(t)$ and finite $t_f$ such that $\mathbf{x}(0) = \mathbf{x}_0$ and $\mathbf{x}(t_f) = \mathbf{x}_f$.

Consider two controls: maximum compensation $\mathbf{u}_{max}$, and minimum compensation $\mathbf{u}_{min}$. These controls affect all swing equation parameters $P_E, P_M, \varphi$ simultaneously. Assume that the center-type equilibrium $(\delta_{ec}^{max}, 0)$ for the system under $\mathbf{u}_{max}$ exists. The set $\mathcal{R}(\mathbf{u}_{max})$ is denoted by $\mathcal{R}_{max}$, and the set $\mathcal{R}(\mathbf{u}_{min})$ is denoted by $\mathcal{R}_{min}$. Let

$$\mathcal{R}_{min} \subset \mathcal{R}_{max}.$$

**Controllability Problem Statement.** Given $(\delta_0, \omega_0) \in \mathcal{R}_{max}$ and $(\delta_f, \omega_f) \in \mathcal{R}_{max}$, show that there exists a switching policy of $\mathbf{u}$ between $\mathbf{u}_{min}$ and $\mathbf{u}_{max}$ such that

$$\delta(0) = \delta_0, \omega(0) = \omega_0, \delta(t_f) = \delta_f, \omega(t_f) = \omega_f.$$

A point $(\delta_i, \omega_i) \in \mathcal{R}_{max}$ can be reached from any point on a trajectory $T(\delta, \omega, \mathbf{u}_{max}) = T(\delta_i, \omega_i, \mathbf{u}_{max})$. Thus, the controllability problem is to have a path from a trajectory $T(\delta, \omega, \mathbf{u}_{max}) = T(\delta_0, \omega_0, \mathbf{u}_{max}) = T_0(\mathbf{u}_{max})$ to a trajectory $T(\delta, \omega, \mathbf{u}_{max}) = T(\delta_f, \omega_f, \mathbf{u}_{max}) = T_f(\mathbf{u}_{max})$.

**Theorem 1.** Let $(\delta_{ec}^{max}, 0) \notin cl(\mathcal{R}_{min})$. Then at most two switches are needed to drive the system from $(\delta_0, \omega_0)$ to $(\delta_f, \omega_f)$.

Proof:

1. Let a trajectory $T(\delta, \omega, \mathbf{u}_{min}) = T(\delta_{ec}^{max}, 0, \mathbf{u}_{min})$ be a switching line $S(\delta, \omega)$. Divide the switching line into two curves, Figure 2.2:

$$S_+(\delta, \omega) = \{(\delta, \omega) \in S(\delta, \omega) \mid (\delta, \omega) \in cl(\mathcal{R}_{max}),\ \omega \geq 0\}$$

and

$$S_-(\delta, \omega) = \{(\delta, \omega) \in S(\delta, \omega) \mid (\delta, \omega) \in cl(\mathcal{R}_{max}),\ \omega < 0\}.$$

2. Since $\mathcal{R}_{min} \subset \mathcal{R}_{max}$, the $\delta$-angles of the saddle-type equilibria are $\delta_{es}^{max} > \delta_{es}^{min}$. Since the center-type equilibrium $(\delta_{ec}^{max}, 0) \notin cl(\mathcal{R}_{min})$, a trajectory

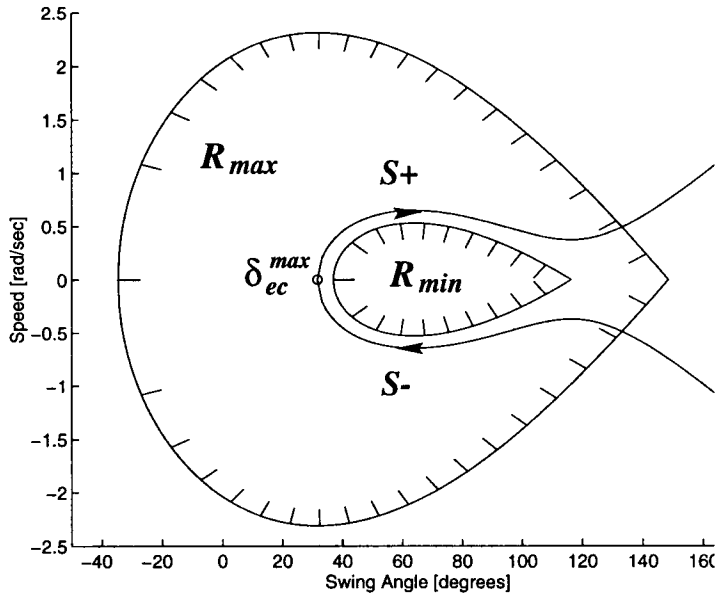


FIGURE 2.2. Switching curves for Theorem 1

$T(\delta, \omega, \mathbf{u}_{min}) = T(\delta_{ec}^{max}, 0, \mathbf{u}_{min})$ intersects the line $\delta = \delta_{es}^{max}$ at $\omega \neq 0$ (Proposition 4). The point $(\delta_{es}^{max}, \omega \neq 0) \notin cl(\mathcal{R}_{max})$.

3. Thus, the curve $S_+$ starts at the equilibrium $(\delta_{ec}^{max}, 0)$ and ends on the boundary of the set $\mathcal{R}_{max}$. The curve $S_-$ starts on the boundary of the set $\mathcal{R}_{max}$ and ends at the equilibrium $(\delta_{ec}^{max}, 0)$. Consequently, each curve intersects all trajectories $T(\delta, \omega, \mathbf{u}_{max}) = T_i$, where $(\delta, \omega) \in \mathcal{R}_{max}$ and $T_i \in [T_{ec}(\mathbf{u}_{max}), T_{es}(\mathbf{u}_{max}))$ (Proposition 5). As a representative point moves along the curve $S_+$, the function $T(\delta, \omega, \mathbf{u}_{max})$ increases from $T_{ec}(\mathbf{u}_{max})$ at $(\delta_{ec}^{max}, 0)$ to $T_{es}(\mathbf{u}_{max})$ on the boundary of the set $\mathcal{R}_{max}$, passing through all the values in between. As a representative point moves along the curve $S_-$, the function $T(\delta, \omega, \mathbf{u}_{max})$ decreases from $T_{es}(\mathbf{u}_{max})$ on the boundary of the set $\mathcal{R}_{max}$ to $T_{ec}(\mathbf{u}_{max})$ at $(\delta_{ec}^{max}, 0)$, assuming all the values in between.

This results in the following switching policy.

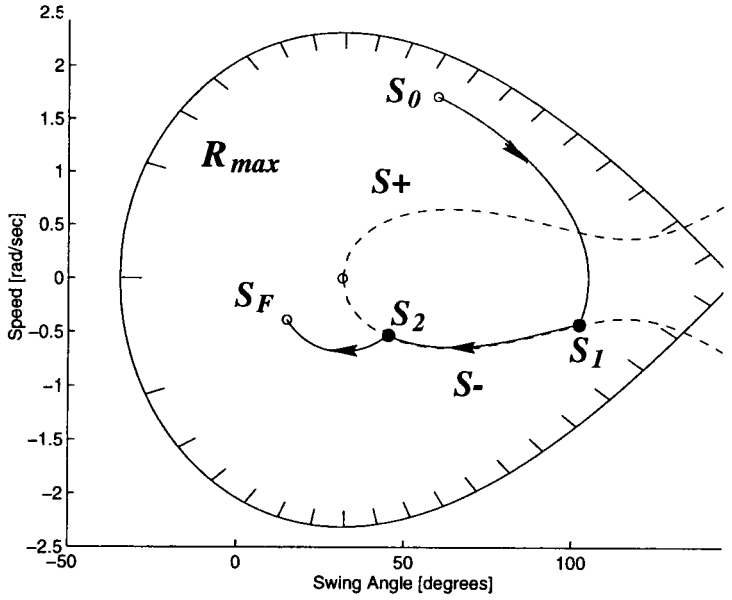


FIGURE 2.3. Switching policy for Theorem 1

*Case 1.* $T_f(\mathbf{u}_{max}) < T_0(\mathbf{u}_{max})$ (Figure 2.3). Here the control $\mathbf{u}_{max}$ is applied first. When a representative point reaches the curve $S_-$ (point $S_1$), the control is switched to $\mathbf{u}_{min}$, and a representative point moves along the curve $S_-$. When $T(\delta, \omega, \mathbf{u}_{max}) = T_f(\mathbf{u}_{max})$ at the point $S_2$, the control is switched to $\mathbf{u}_{max}$. With the control $\mathbf{u}_{max}$, the representative point reaches the target point $S_f = (\delta_f, \omega_f)$.

*Case 2.* $T_f(\mathbf{u}_{max}) > T_0(\mathbf{u}_{max})$ (Figure 2.4). Here the control $\mathbf{u}_{max}$ is applied first. When a representative point reaches the curve $S_+$ (point $S_1$), the control is switched to $\mathbf{u}_{min}$, and a representative point moves along the curve $S_+$. When $T(\delta, \omega, \mathbf{u}_{max}) = T_f(\mathbf{u}_{max})$ at the point $S_2$, the control is switched to $\mathbf{u}_{max}$. With the control $\mathbf{u}_{max}$, the representative point reaches the target point $S_f = (\delta_f, \omega_f)$. ∎

**Theorem 2.** Let $\delta_{ce}^{max} < \delta_{ce}^{min}$. Then the system is controllable on $\mathcal{R}_{max}$.

Proof: We need to show that there is a path from the equilibrium $(\delta_{ec}^{max}, 0)$ to the boundary of the set $\mathcal{R}_{max}$. The function $T(\delta, \omega, \mathbf{u}_{max})$ evaluated along such a

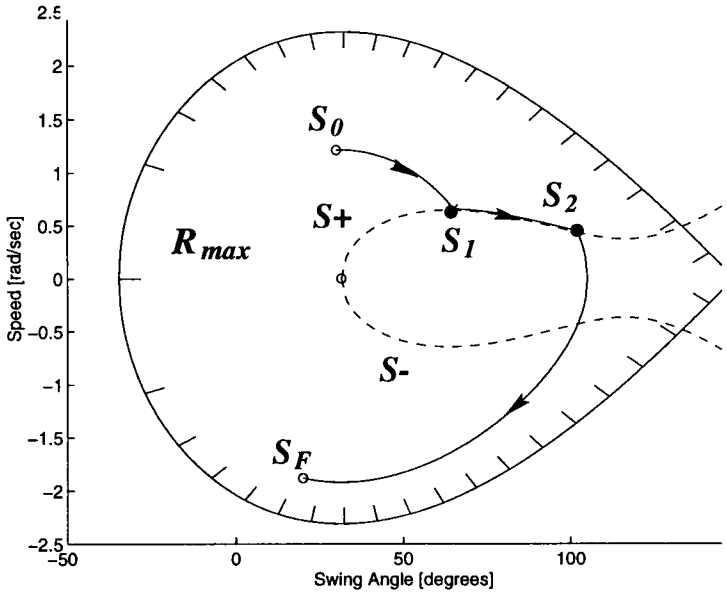


FIGURE 2.4. Switching policy for Theorem 1

path assumes all the values from $T_{ec}(\mathbf{u}_{max})$ at the equilibrium $(\delta_{ec}^{max}, 0)$ to $T_{es}(\mathbf{u}_{max})$ on the boundary of the set $\mathcal{R}_{max}$.

A case when $(\delta_{ec}^{max}, 0) \notin cl(\mathcal{R}_{min})$ is considered in Theorem 1. Here, it is assumed that $(\delta_{ec}^{max}, 0) \in \mathcal{R}_{min}$. Construction of the path is shown in Figure 2.5. The solid lines represent transient trajectories under $\mathbf{u}_{max}$, and the broken lines represent trajectories under $\mathbf{u}_{min}$. The dotted line encloses the set $\mathcal{R}_{min}$, and the solid line with dashes represents the set $\mathcal{R}_{max}$.

1. The starting point is $S_0 = (\delta_0, \omega_0) = (\delta_{ec}^{max}, 0)$. Plot a trajectory $T(\delta, \omega, \mathbf{u}_{min}) = T(\delta_{ec}^{max}, 0, \mathbf{u}_{min})$. Since $(\delta_{ec}^{max}, 0) \in \mathcal{R}_{min}$, this trajectory encloses the center equilibrium $(\delta_{ec}^{min}, 0)$ (point $O$) and intersects the $\delta$-axis at the point $S_1 = (\delta_1, 0)$ such that $T(\delta_1, 0, \mathbf{u}_{min}) = T(\delta_{ec}^{max}, 0, \mathbf{u}_{min})$. Notice that $\delta_1 > \delta_{ec}^{min} > \delta_{ec}^{max}$. The function $T(\delta, \omega, \mathbf{u}_{max})$ is evaluated at $S_1$: $T(\delta_1, 0, \mathbf{u}_{max}) = T_1(\mathbf{u}_{max})$. The function $T(\delta, \omega, \mathbf{u}_{max})$ takes all values from the interval $T_{ec}(\mathbf{u}_{max})$ to $T_1(\mathbf{u}_{max})$, as

a representative point moves along the trajectory $T(\delta, \omega, \mathbf{u}_{min}) = T(\delta_{ec}^{max}, 0, \mathbf{u}_{min})$ (Proposition 5).

2. Since $S_1 \in \mathcal{R}_{min}$ and $\mathcal{R}_{min} \subset \mathcal{R}_{max}$, $S_1 \in \mathcal{R}_{max}$. Also, $\delta_1 > \delta_{ec}^{max}$. Plot a trajectory $T(\delta, \omega, \mathbf{u}_{max}) = T_1(\mathbf{u}_{max})$. The trajectory intersects the $\delta$-axis at point $S_2$ : $(\delta_2, 0)$. Since $S_1 \in \mathcal{R}_{max}$, the point $S_2 \in \mathcal{R}_{max}$. Also, $\delta_2 < \delta_{ec}^{max}$ and $T(\delta_2, 0, \mathbf{u}_{max}) = T_1(\mathbf{u}_{max})$.

3. If $S_2 \notin \mathcal{R}_{min}$, the trajectory $T(\delta, \omega, \mathbf{u}_{min}) = T(\delta_2, 0, \mathbf{u}_{min})$ intersects all the trajectories in the set $\mathcal{R}_{max}$ with the function $T(\delta, \omega, \mathbf{u}_{max})$ in the range from $T_1(\mathbf{u}_{max})$ to $T_{es}(\mathbf{u}_{max})$. If $S_2 \in \mathcal{R}_{min}$ , a trajectory $T(\delta, \omega, \mathbf{u}_{min}) = T(\delta_2, 0, \mathbf{u}_{min})$ intersects the $\delta$-axis at the point $S_3$ : $(\delta_3, 0)$, $T(\delta_3, 0, \mathbf{u}_{min}) = T(\delta_2, 0, \mathbf{u}_{min})$. Due to the uniqueness of solution, $\delta_3 > \delta_1 > \delta_{ec}^{max}$. Consequently, the function $T(\delta_3, 0, \mathbf{u}_{max}) = T_3(\mathbf{u}_{max}) > T_1(\mathbf{u}_{max}) > T_{ec}(\mathbf{u}_{max})$. The function $T(\delta, \omega, \mathbf{u}_{max})$ takes all values from the interval $T_1(\mathbf{u}_{max})$ to $T_3(\mathbf{u}_{max})$, as a representative point moves along the trajectory $T(\delta, \omega, \mathbf{u}_{min}) = T(\delta_2, 0, \mathbf{u}_{min}) = T_1(\mathbf{u}_{max})$. The trajectory $T(\delta, \omega, \mathbf{u}_{max}) = T_3(\mathbf{u}_{max})$ intersects the $\delta$-axis at point $S_4 : (\delta_4, 0) \in \mathcal{R}_{max}$. Due to the uniqueness of solution, $\delta_4 < \delta_2 < \delta_{ec}^{max}$. This process continues as that for the point $S_2$.

4. Since $\mathcal{R}_{min} \subset \mathcal{R}_{max}$, there is a point $S_K(\delta_K, 0)$ ($K = 4$ in Figure 2.5) such that $S_K \in \mathcal{R}_{max}$, and $S_K \notin \mathcal{R}_{min}$. A trajectory $T(\delta, \omega, \mathbf{u}_{min}) = T(\delta_K, 0, \mathbf{u}_{min})$ intersects the trajectories in $\mathcal{R}_{max}$ with the function $T(\delta, \omega, \mathbf{u}_{max})$ in the range from $T_K(\mathbf{u}_{max})$ to $T_{es}(\mathbf{u}_{max})$.

A representative point moving along thus constructed switching line will assume all the values in the interval [ $T_{ec}(\mathbf{u}_{max})$, $T_{es}(\mathbf{u}_{max})$ ), and thus will intersect all trajectories under $\mathbf{u}_{max}$ originating in $\mathcal{R}$. ∎

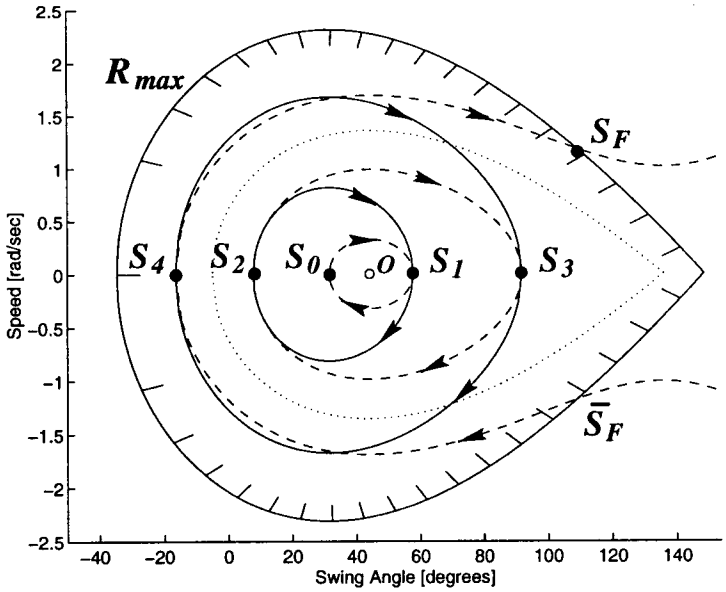


FIGURE 2.5. Switching policy for Theorem 2

## 2.4. Conclusions and Directions for Future Research in Transient Angle Controllability

The previous section shows transient angle controllability for a two-machine multi-bus system with controllable network devices. The presented controllability results apply to series and shunt series compensators as well as braking resistors. By considering a multi-bus system, the controllability can be quantified by a size of the set $\mathcal{R}_{max}$ and related to the controllable device type, size and location in the power transmission network.

The developed concepts of transient angle controllability can be extended to a multi-machine power system. This dissertation makes the first step in this direction by showing how parameters in a multi-machine swing equation depend on device compensation. From a practical standpoint, it will be more useful to consider output

instead of state controllability [16]. Generators states (rotor angle and speed) can be projected on lower dimensional sub-space, representing for example an inter-area swings [14, 16].

## 2.5. Transient Stability Control

A Transient Stability Controller (TSC) is employed to maximize impact of controllable network devices on transient angle stabilization. The TSC objective is to utilize optimally controllable network devices and their available control capabilities to maintain the power system stability in the first swing. The TSC is an emergency controller, and is normally kept off-line. It should be activated only for severe disturbances and conditions threatening the system stability. The TSC should identify such conditions and activate control law timely. After the TSC executes its control law and the control objective is achieved, the TSC should be taken off-line safely to prevent adverse effects on stability in a weakened post-disturbance system.

The following functional structure of a transient stability controller is proposed [14, 15] :

(i) operating characteristic;

(ii) control law;

(iii) restraint characteristic.

### 2.5.1. Operating Characteristic

The transient stability control of network devices is an emergency control which responds to major power system disturbances, and is a part of Remedial Action Schemes (RAS). Transient stability control usually is a very powerful action

affecting power system performance and stability. During the TSC operation, the controllable network devices can be operated in their transient overload ratings. For example, a thyristor-controlled series compensator can increase its compensation for a short time by using full transient overvoltage capabilities of series capacitors [22]. Use of transient overload capabilities is limited per lifetime of series capacitors, and frequent operation of capacitors under transient overvoltages is undesirable. Frequent TSC operation for small disturbances may lead to undesirable effects on equipment and power system performance. For example, a dynamic brake operation close to a steam-turbine generator may create a large stress on the generator shaft. Frequent brake application will fatigue the shaft and may result in early loss of life of generation equipment, which is highly undesirable. Thus, the transient stability controller should be activated mainly for disturbance events which can result in instability of the uncontrolled system.

Most of the present TSC activation schemes (e.g. transient stability control at Slatt TCSC, tripping bus-connected reactors at Garrison, BPA) are open-loop and driven by line opening events. Typically, when a loss-of-line logic detects that circuit breakers on a major Extra High-Voltage (EHV) line change their status from "closed" to "open," a pre-determined RAS sequence is executed if armed. The RAS arming usually depends on pre-disturbance power flows and is controlled from a control center. Such open-loop control can be used as a part of the TSC activation scheme for expected severe disturbances. However, the open-loop scheme is proven to be ineffective when dealing with disturbance events under unplanned operating conditions and multi-contingency events. The performance of the TSC activation schemes can be improved by augmenting them with response-based control systems.

The response-based operating characteristic employs real-time measurements (possibly wide-area measurements transmitted using communication networks) to

perform on-line stability assessment. There are two requirements for the response-based operating characteristic: (i) sensitivity and (ii) selectivity. The sensitivity requires that disturbances and system conditions leading to instability (and to violation of the reliability criteria) be recognized promptly to initiate appropriate actions minimizing transient severity. The selectivity requirement prevents the TSC activation for small disturbances which do not threaten the system stability and result in the acceptable system performance. Using the controller for small disturbances is undesirable because of the equipment stress and possible adverse effects on the system dynamic performance.

Successful designs of operating characteristics which combine both, the pre-programmed responses to large disturbances [5] and response-based criteria are presented in [14, 15]. The operating characteristic is designed in the phase-plane of the inter-area swing angle $\delta$ and its rate of change $\omega$. When a transient trajectory attempts to leave the operating region, the TSC is activated. Since the system is more prone to instability when it operates under stressed conditions with line outages, the operating characteristic is made adaptive, i.e. it depends on the scheduled power transfer and status of the circuit breakers on EHV lines.

Operating characteristics can be coordinated for several network devices. Unselective operation by some devices, if infrequent, can be tolerated. Such devices should be activated first, which is provided by reducing selectivity of their operating characteristics.

Properly designed response-based operating characteristic, together with the pre-programmed actions, can achieve high sensitivity and selectivity of the TSC activation schemes. Measurement choice in the response-based controls is very important to provide required observability of transients of interest.

### 2.5.2. Control Law

The control law determines a compensation policy meeting the TSC objective. The control law can be either continuous or discontinuous. For transient angle stability control, a discontinuous control law in the form of switching curves has several advantages. Discontinuous controls can be implemented for both, mechanically-switched and thyristor-controlled devices, while continuous controls are realizable only with thyristor-controlled devices. Mechanically-switched devices are more widely used and more economical than thyristor-controlled units.

Successful design of the bang-bang control policy for the series-capacitor transient stability control is presented in [14]. Under consideration are two sub-systems (receiving and sending areas) interconnected by an intertie with series-compensated lines. Stability of interconnected power system is particularly vulnerable to power system disturbances. The controller objective is to insert series capacitors to achieve maximum first swing stabilization, and to dampen power swing. The switching policy is designed using $(\delta, \omega)$ phase-plane of the inter-area swing angle and its rate of change. Phase angle measurements at major generator terminals in both, sending and receiving areas are used to synthesize the inter-area swing angle $\delta$ and its rate of change $\omega$. The control law objective is to drive a representative point in $(\delta, \omega)$ plane to the target set representing the stability region for the post-disturbance power system. The control consists of pre-computed switching lines. Of concern is sensitivity of the switching policy with respect to the system parameters which in turn depend on transmission line outages, line power loadings, scheduled generation, etc. To account for all these contingencies with only one switching line is non-feasible and accordingly some adaptation is needed. One option is to use a contingency classifier for these purposes. Several switching lines can be pre-computed for vari-

ous system conditions. The on-line contingency classifier can use information from control centers on line status of major transmission lines and scheduled transfer, as well as local measurements to arm an appropriate switching line. In addition, each switching line is robustified and extended to a switching strip.

An example of the continuous robust control law for TCSCs is presented in [15]. A robust static controller is designed in the following form

$$u = h(\delta - \delta_{ref}) + g(\omega) + u_0, \tag{2.7}$$

where

$u$ is the series compensation request,

$h(\cdot)$ and $g(\cdot)$ are monotonic functions,

$\delta_{ref}$ is the reference angle,

$u_0$ is the steady-state compensation set-point.

The control law should satisfy the following requirements:

1. The compensation policy determined by (2.7) should use the full transient overvoltage capabilities of the TCSC capacitors during the first swing conditions.

2. The function $g(\cdot)$ should provide positive damping.

3. The function $h(\cdot)$ and reference $\delta_{ref}$ are selected using results of powerflow studies such that for the post-disturbance steady-state ($\omega = 0$), the compensation request determined $u$ stays within the temporary overload capabilities of TCSC capacitors. It also minimizes transients related to the compensation adjustment at the end of the control interval.

The TSC is an emergency controller, and to act promptly, it should use a simple control law with a well-defined response. To this end, a simple static control

law is used. The control law is derived using an intuitive geometrical phase-plane approach, and its output is uniquely defined by its inputs. A dynamic control law with "memory" may not be suitable for the TSC, since its response is a function not only of the controller inputs, but also of controller states (dynamic "memory"). Dynamic control law is more appropriate for power swing damping controllers [19], which follow the transient stability control to provide complete damping of transient angle oscillations.

### 2.5.3. Restraint Characteristic

The device application can be restricted in time. For example, the TCSC can increase its compensation by using the transient overvoltage capabilities of capacitors only for up to 10 seconds, and then the compensation has to be reduced to stay within the temporary overload capabilities of the device [5]. The braking resistor is designed to be applied multiple times with total time not more than 3 seconds [11]. There may be system performance limitations, for example series capacitor bank insertion combined with a parallel line outage can create overvoltage on the bus side of capacitors [17], thus overexciting bus transformers.

The TSC disconnection (braking resistor opening, TCSC compensation adjustment) creates a disturbance for already weakened post-disturbance system. Thus, the TSC should be disconnected safely to prevent adverse effects on the system stability and performance. Restraint characteristic performs this function. If the system measurements are confined to the target set for a specified time interval, the TSC is re-set. The designed restraint characteristic should be based on the system performance and account for the device time-overload capabilities.

# 3. MODELING THYRISTOR-CONTROLLED SERIES COMPENSATORS IN PLANNING STUDIES

Thyristor-Controlled Series Compensators (TCSC) have significant impact on the transmission system performance [5, 22]. This chapter presents time-domain TCSC models for EMTP(Electro-Magnetic Transient Program), powerflow and transient stability studies.

A variable reactance model represents a TCSC in powerflow studies sufficiently well. However, a TCSC representation in transient stability studies may require more detailed modeling, and is the primary focus of this chapter.

A variable-reactance model proposed in [20] approximates a TCSC transient response by a first-order lag system, where the input is the reactance set-point and the output is the effective net reactance of the TCSC. The model assumes that the device natural response can be compensated by internal controls. The model also incorporates the TCSC time-overload capability characteristics as a function of the line current. The need for a more detailed TCSC modeling for stability studies is argued in [21], where it is pointed out that internal controls can compensate but can not eliminate the TCSC natural response completely. A more detailed TCSC model for stability studies is proposed in [21]. The TCSC power circuits are modeled by differential equations, control, protection and synchronization schemes are fully represented, so that the actual response of the TCSC circuit is obtained. The model inputs are the thyristor firing angle and the line current, and the model output is the thyristor current.

Although the TCSC model proposed in [21] represents the device response accurately, the model can be enhanced and simplified significantly. This dissertation

extends approach proposed in [21] and derives a simpler and more practical version of the TCSC model for transient stability studies.

In many cases, the performance of a controllable network device model is limited by the performance of a transmission system model. Existing transient stability simulators use one-line representation of the transmission network by algebraic equations. Such representation neglects line transients, unbalances and electro-magnetic interactions between the TCSC and transmission lines. In some cases, this oversimplification can result in inaccurate conclusion of the TCSC effect on power system performance. The problem and a solution will be discussed in this chapter.

## 3.1. Device Circuit, Operating Principles and Waveforms in Steady-State

A TCSC module shown in Figure 3.1 consists of a series capacitor bank and a parallel branch with a surge reactor and thyristor valves [5, 20, 22]. A metal-oxide varistor is used in parallel with a module for overvoltage protection. When the thyristors are blocked, the device acts as a conventional series compensator. When the thyristors are conducting continuously (capacitor bypass mode), the device represents inductive and capacitive branches in parallel. These two modes are identical to those of a thyristor-switched series compensator. There is also a vernier mode of operation (point-of-wave switching) when the thyristors are partially conducting.

The inductance $L$ of the surge reactor is such that for a given capacitance $C$ of the capacitor bank, the TCSC natural frequency $\omega_n = 1/\sqrt{LC}$ is higher than the fundamental frequency $\omega_0 = 120$ rad/sec, (60Hz). Natural frequencies used in the present installations are 164Hz (Slatt) and 145Hz (Kayenta). Given ohmic values (at the fundamental frequency) of the TCSC capacitor bank reactance $X_C$ and the

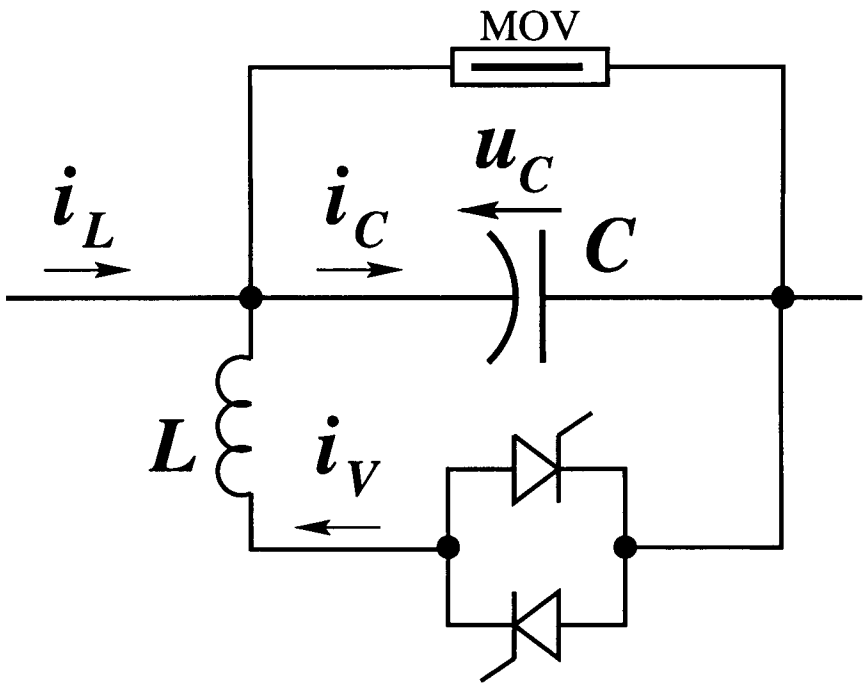


FIGURE 3.1. Thyristor-controlled series compensator

surge inductor reactance $X_L$, the natural frequency can be expressed in terms of the fundamental frequency as $\omega_n = \omega_0 \sqrt{X_C/X_L}$.

For steady-state operation, it is assumed that the line current $i_L$ is sinusoidal of amplitude $I_L$ at the fundamental frequency $\omega_0$, $i_L = I_L \cos \omega_0 t$, and that the thyristors are firing at a constant angle synchronized perfectly with the line current (so-called equidistant firing). The following control angles are considered:

$\alpha$ : firing delay angle (after the beginning of the forward valve voltage)

$\sigma$ : thyristor conduction angle

The angles are constant in the steady state, and the thyristor gating times are displaced by $\pi$ radians.

The TCSC steady-state operation is described by a hybrid model consisting of differential equations representing the TCSC power circuits and events related to the thyristor firing. Let $\theta = \omega_0 t$

- for $\nu_i \leq \theta < \eta_{i+1}$,

$$C\dot{u}_C = I_L \cos\theta;$$

- for $\eta_i \leq \theta < \nu_i$,

$$C\dot{u}_C = -i_V + I_L \cos\theta,$$

$$L\dot{i}_V = u_C$$

where

$\eta_i = \alpha + \pi(i-1)$ - beginning of thyristor conduction

$\nu_i = \eta_i + \sigma$ - end of thyristor conduction

$i$ - number of the switching event

$i_V(\eta_i) = 0, i_V(\nu_i) = 0$ - initial and terminal conditions for thyristor current

Initial conditions for the capacitor voltage are determined from the waveform periodicity and symmetry conditions.

Figure 3.2 shows TCSC operating waveforms for the capacitive vernier mode. Time is given in degrees, where $360^O$ corresponds to one electrical cycle. The line current amplitude is 1,000 Amperes, the ohmic size of the capacitor bank is $1\Omega$ at the fundamental frequency, and the surge inductor reactance is $0.1329\Omega$. The capacitor current $i_C$ is given in Figure 3.2(a), and the capacitor voltage $u_C$ is shown in Figure 3.2(b). The solid lines represent waveforms when thyristors are blocked and the device acts as a fixed capacitor. In this case, the capacitor current $i_C$ is equal to the line current $i_L$. The broken lines represent waveforms in the capacitive vernier mode. During thyristor conduction intervals, the thyristor current $i_V$ adds to the line current $i_L$, resulting in higher capacitor current $i_C$, and thus larger voltage

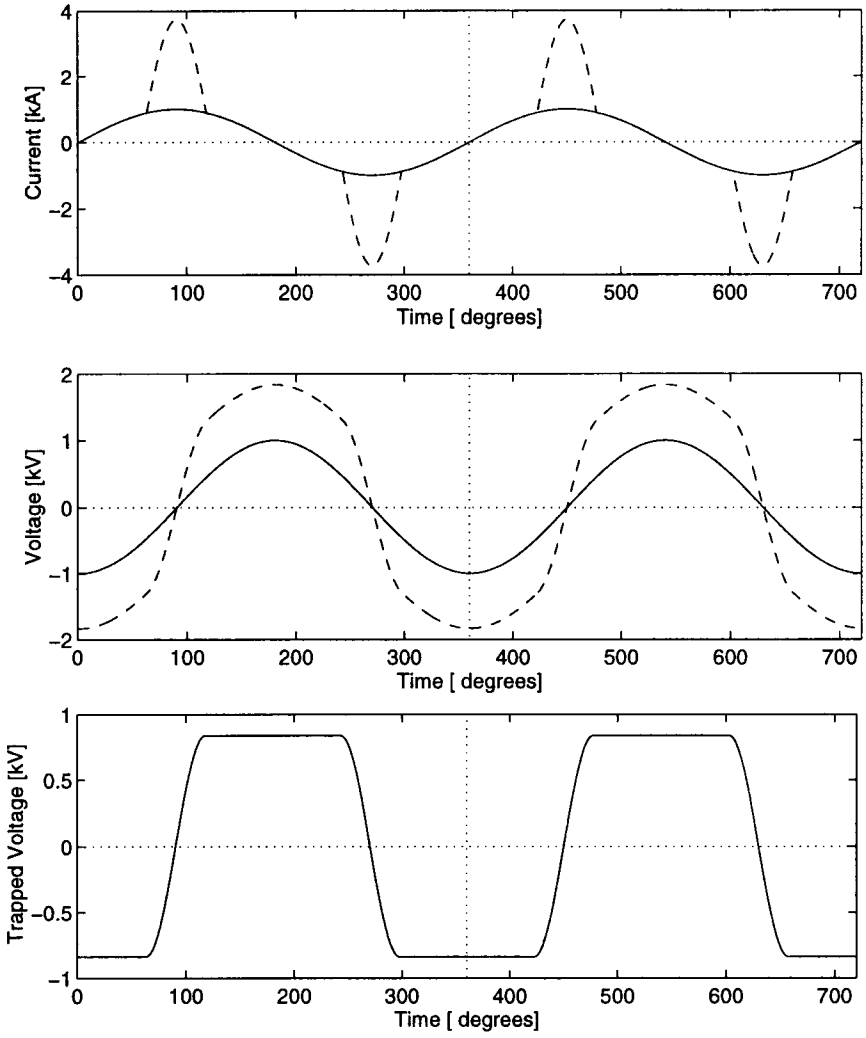


FIGURE 3.2. TCSC operating waveforms: capacitive vernier mode

$u_C$ across the capacitor bank. The TCSC operation in the capacitive vernier mode can be described using a synchronous voltage reversal concept [23]. Figure 3.2(c) shows the capacitor trapped voltage, which is equal to the voltage across the TCSC capacitor bank minus voltage across the same fixed capacitor bank under the same line current. During the thyristor conduction interval, the trapped voltage reverses its polarity.

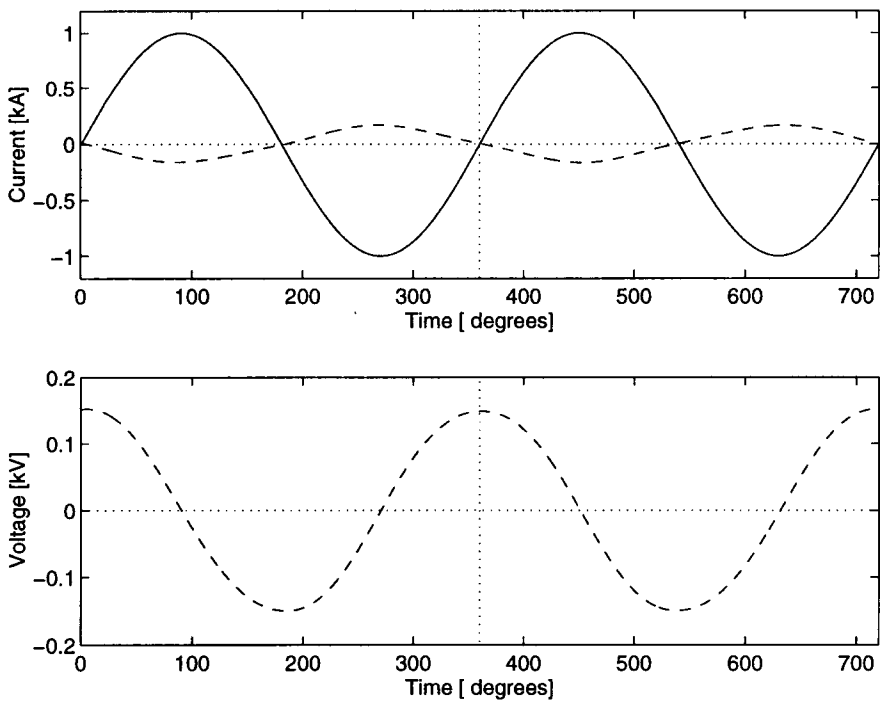


FIGURE 3.3. TCSC operating waveforms: bypass mode

Figure 3.3 shows TCSC operation in the bypass mode (continuous thyristor conduction). The capacitor current (broken line) is in opposite phase with the line current (solid line), and the capacitor voltage is leading the line current. Thus, the device appears as a small inductance at the fundamental frequency, as seen from the transmission line.

Figure 3.4 shows capacitor (a) current and (b) voltage waveforms for the inductive vernier mode. The line current $i_L$ is shown in Figure 3.4(a) by the solid line, and the thyristor current is shown by the broken line. During thyristor conduction periods, the thyristor current $i_V$ subtracts from the line current, and results in the fundamental component of the capacitor current in opposite phase with the line current. Consequently, the fundamental component of the capacitor voltage is leading the line current, and the device reactance at the fundamental frequency is

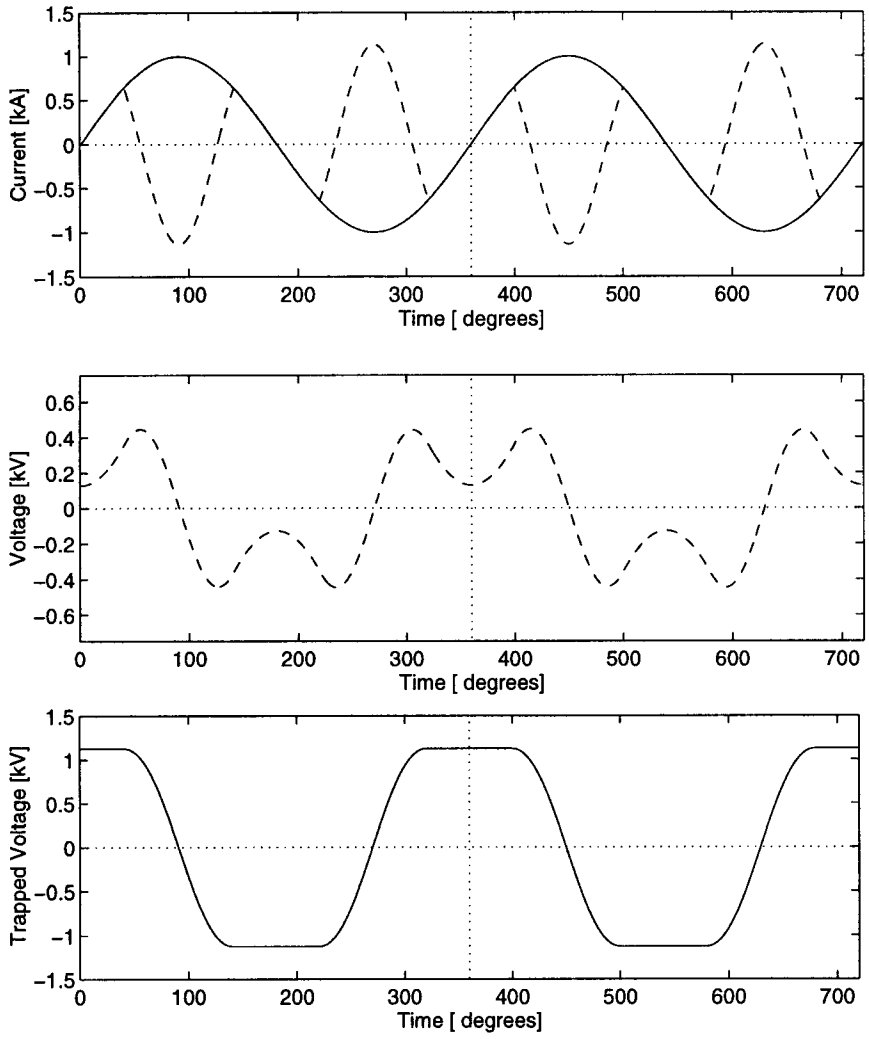


FIGURE 3.4. TCSC operating waveforms: inductive vernier mode

inductive. Figure 3.4(c) shows capacitor trapped voltage in the inductive vernier mode.

## 3.2. EMTP Model

A thyristor-controlled series compensator is modeled in detail using EMTP (BPA-ATP version). The power circuits are represented according to Figure 3.1.

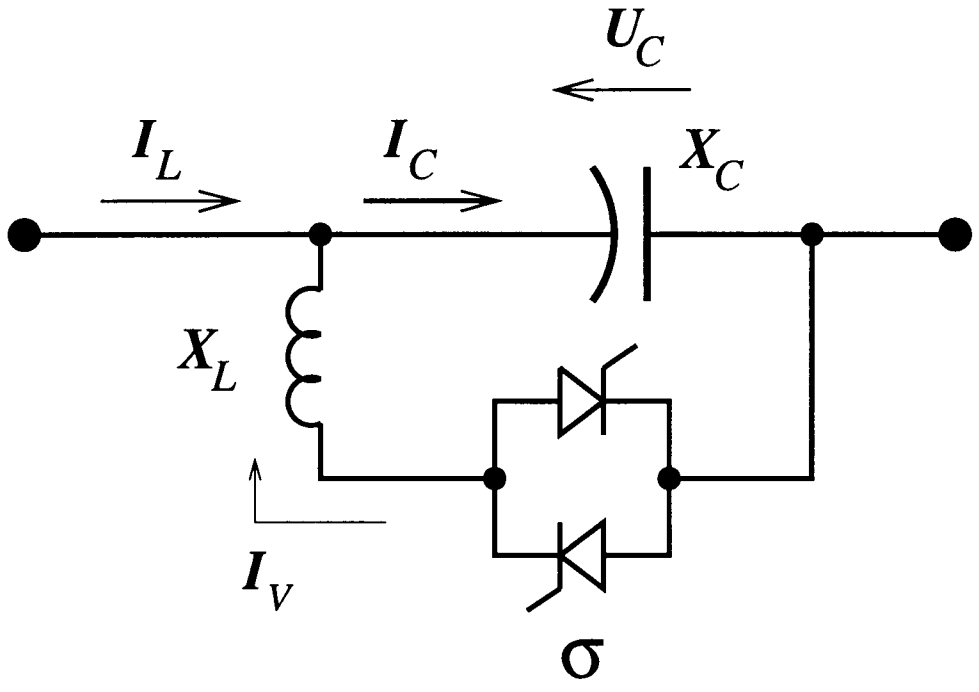


FIGURE 3.5. TCSC representation at the fundamental frequency

Thyristor valves are modeled as type 11 TACS-controlled switches. Snubber circuits are represented in parallel with the switches. TCSC circuit responses are shown in Figures 3.2-3.4. The firing angle control and synchronization circuits are represented using ATP control language Models [24]. Thyristor firing is synchronized with the line current. An interface for various user-defined controls is also provided in Models.

### 3.3. TCSC Representation at the Fundamental Frequency

For powerflow and transient stability studies, of interest are the fundamental voltage and current components, as well as reactances at the fundamental frequency. Tthe fundamental frequency quantities are represented by phasors. The TCSC model at the fundamental frequency is shown in Figure 3.5.

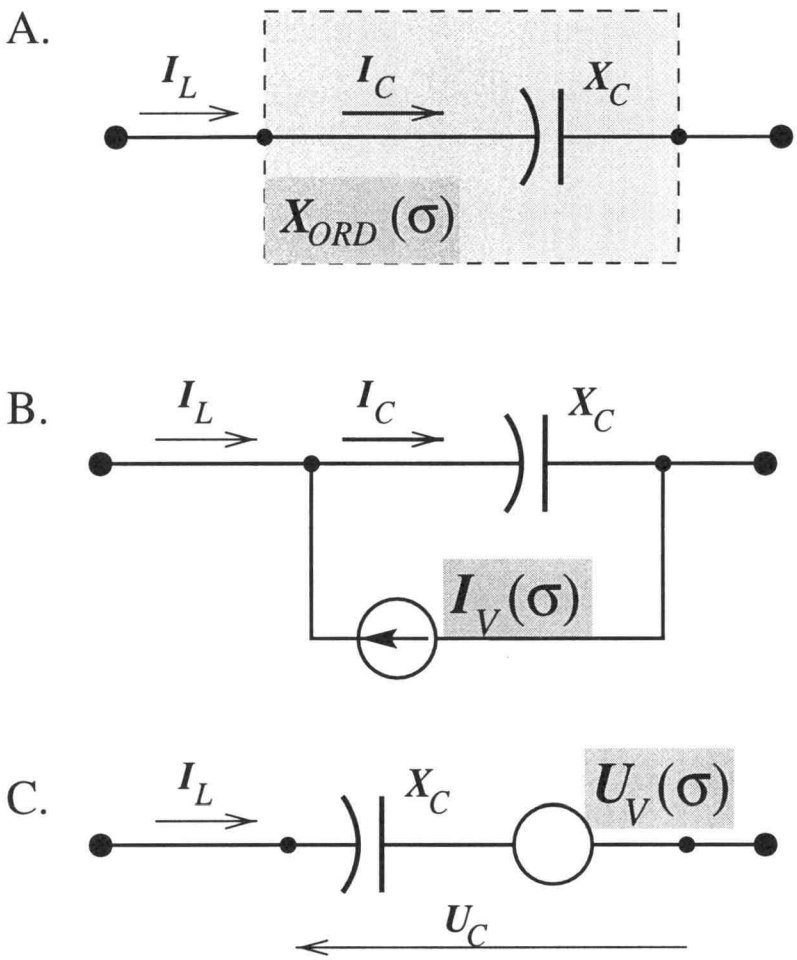


FIGURE 3.6. TCSC models at the fundamental frequency

Figure 3.6 shows various TCSC representations: (a) X-order (as a function of conduction angle) model; (b) thyristor current model, (c) capacitor trapped voltage model. The models are equivalent under the same line current $I_L$.

**A. X-order model**

Using the TCSC steady-state operating waveforms, the fundamental component of the capacitor voltage and the TCSC net reactance $X_{net}$ at the fundamental frequency can be expressed as functions of the conduction angle $\sigma$ [4]. The TCSC X-order is defined as $X_{ord}(\sigma) = X_{net}(\sigma)/X_C$, and is

$$X_{ord}(\sigma) = 1 - \frac{X_C}{X_C - X_L}\frac{\sigma + \sin\sigma}{\pi} + 4\cos^2(\sigma/2)\,\frac{X_C X_L}{(X_C - X_L)^2}\left[\frac{k\tan(k\sigma/2) - \tan(\sigma/2)}{\pi}\right], \tag{3.1}$$

where $k = \sqrt{X_C/X_L}$.

The X-order $X_{ord}(\sigma)$ is the controlled variable in this model.

**B. Thyristor current model.**

In this model, the thyristor current $I_V$ is the controlled variable. In the capacitive vernier mode, the thyristor current adds to the line current $I_L$ and results in a higher capacitor current $I_C$. The higher capacitor current increases the voltage drop across the capacitor bank, thereby increasing the device net reactance as seen from the line. The TCSC X-order defines a relationship between the capacitor and line currents, $I_C = X_{ord}\ I_L$. The thyristor current $I_V$ can be also represented in terms of the line current using the X-order as $I_V = (1 - X_{ord})I_L$. In the inductive vernier mode, the thyristor current subtracts from the line current, resulting in the capacitor current of opposite phase with the line current. Thus, the TCSC X-order is negative and the TCSC net reactance is inductive.

**C. Capacitor trapped voltage model**

In this model, the fundamental component of the capacitor trapped voltage $U_V$ is the control variable. In the capacitive vernier mode, the voltage $U_V$ adds to the voltage $I_L X_C$, resulting in a higher voltage drop across the TCSC capacitor. The voltage $U_V$ is related to the thyristor current by $U_V = I_V X_C$, and $U_V = (1 - X_{ord})X_C I_L$. In the inductive vernier mode, the trapped voltage $U_V$ subtracts from $I_L X_C$, resulting in the negative net voltage across the capacitor bank.

The thyristor conduction angle is plotted versus the TCSC X-order for a single module in Figure 3.7 for $X_C/X_L = 7.52$, using equation (3.1). There is a gap between capacitive and inductive vernier modes, i.e. some X-order values are

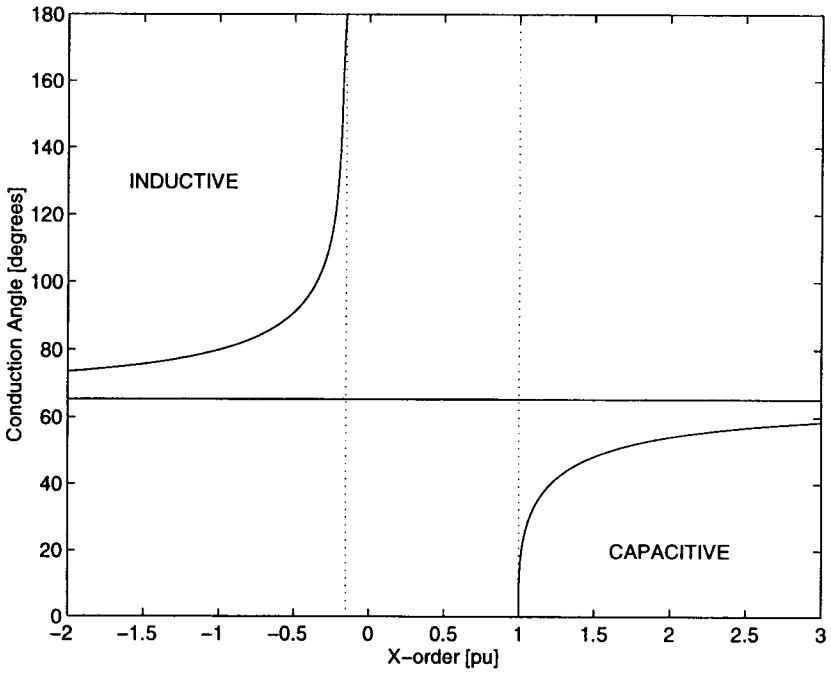


FIGURE 3.7. Thyristor conduction angle versus the TCSC X-order

unavailable. Also, there is an asymptote corresponding to a conduction angle at which resonance conditions occur. To avoid risk of resonance in the device $LC$ circuit, a margin for conduction angle is provided, restricting the X-order range to $X_{ord} \leq X_{ord}^{max}$ for the capacitive vernier (maximum firing advance), and $X_{ord} \geq X_{ord}^{min}$ for the inductive vernier (maximum firing delay).

## 3.4. TCSC Ratings and Capability Characteristics

To represent TCSC control range accurately in powerflow and transient stability studies, the device capability characteristics should be considered as a function of the line current. These capability characteristics are established based on the device ratings and capacitor ohmic size, and are discussed below.

### 3.4.1. TCSC Ratings

#### Capacitor Ratings

Typically, the following rated currents of a capacitor bank are considered and used in planning studies [5, 22, 20]

$I^c_{rat}$ : rated (continuous) current

$I^c_{temp}$ : temporary (30-minute) overload current

$I^c_{tran}$ : transient (10-second) overload current

IEEE Standards give relationships between the capacitor current ratings: $I^c_{temp} = 1.35 I^c_{rat}$, $I^c_{tran} = 2.0 I^c_{rat}$.

For a given ohmic size of a TCSC capacitor bank, $X_C$, the TCSC voltage ratings are defined as

$U^c_{rat} = I^c_{rat} X_C$ : rated (continuous) voltage

$U^c_{temp} = I^c_{temp} X_C$ : temporary (30-minute) overload voltage

$U^c_{tran} = I^c_{tran} X_C$ : transient (10-second) overload voltage.

#### Thyristor ratings

Thyristor ratings include voltage and current ratings of thyristor valves. Typically, a thyristor valve consists of several thyristors in series with at least one thyristor added for redundancy. Break-Over-Diodes are used for the overvoltage protection of individual thyristors in the valve. The thyristor current ratings relate to the thyristor thermal capabilities. Thyristors have limited time-overcurrent characteristics depending on the design of their heat sinks and cooling systems.

#### MOV arrester ratings

MOV arresters are used to protect a series capacitor bank from overvoltages [25]. MOV is made from zinc oxide disks connected directly across the capacitor. MOV shunts excess current around the capacitor to hold the capacitor voltage below the

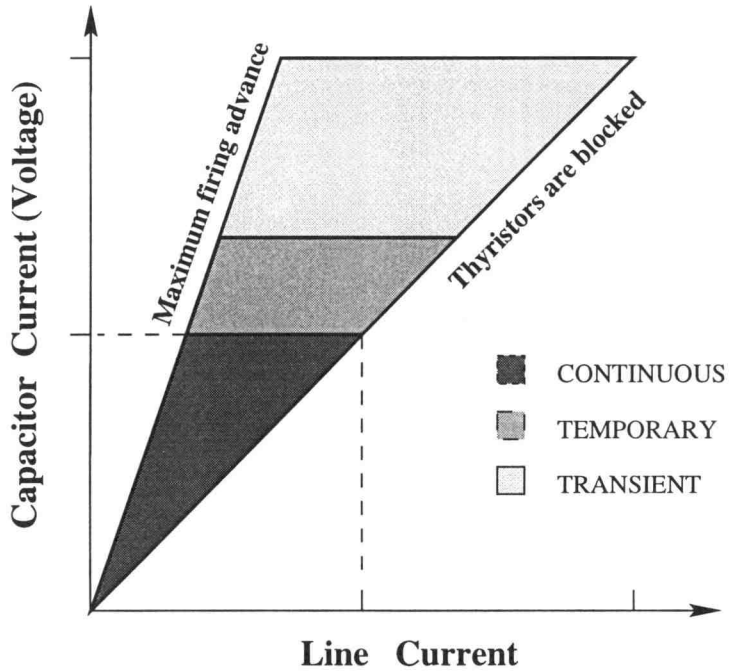


FIGURE 3.8. TCSC capability characteristics: capacitor current (voltage) vs. line current

protected level. MOV ratings include voltage, energy ratings, and protected voltage level. MOV models are developed and used in existing transient stability programs.

### 3.4.2. Capability characteristics

TCSC current (voltage) versus line current $U_C$ $(I_C) - I_L$ characteristics are presented in Figure 3.8 for a single module. TCSC X-order versus line current $X_{ord} - I_L$ characteristics are presented in Figure 3.9 for a single module. The capability characteristics are derived only for the capacitive vernier mode and bypass modes. The inductive mode is not utilized at the present installations, and is not likely to be used in future applications.

The TCSC capability characteristics for the capacitive vernier mode are established based on the capacitor current (voltage) ratings:

- $I^c_{rat} \geq I_C = X_{ord} I_L$, $(U^c_{rat} \geq U_C = X_{ord} X_C I_L)$ for continuous loading,
- $I^c_{temp} = 1.35\ I^c_{rat} \geq I_C = X_{ord} I_L$, $(1.35\ U^c_{rat} \geq U_C)$ for temporary 30-minute overload,
- $I^c_{tran} = 2\ I^c_{rat} \geq I_C = X_{ord} I_L$, $(2\ U^c_{rat} \geq U_C$ for transient 10-second overload.

Since TCSC X-order is constrained to $[1,\ X^{max}_{ord}]$ range in the capacitive vernier mode, the TCSC capacitor current $I_C$ is $I_L \leq I_C \leq X^{max}_{ord} I_L$ for all line currents $I_L$. The capacitor current (capacitor voltage) versus line current capability characteristic combines all the above constraints and is plotted in Figure 3.8.

The X-order versus line current can be derived using $X_{ord} = I_C / I_L$. First, the X-order control range is constrained to the $[1,\ X^{max}_{ord}]$ range in the capacitive vernier. Additional constraints result from the capacitor current (capacitor voltage) ratings

- $X_{ord} \leq I^c_{rat} / I_L$ for continuous loading,
- $X_{ord} \leq 1.35 I^c_{rat} / I_L$ for 30-minute temporary overload,
- $X_{ord} \leq 2 I^c_{rat} / I_L$ for transient 10-second overload.

There are several advantages of a multi-module TCSC implementation [20, 22]. Assume that a TCSC consist of $N$ modules with reactances of each capacitor bank $X^i_C$, and that each module operates with its own X-order $X^i_{ord}$. Then, the X-order of the entire TCSC unit is

$$X_{ord} = \sum_{i=1}^{N} X^i_{ord} X^i_C / \sum_{i=1} X^i_C.$$

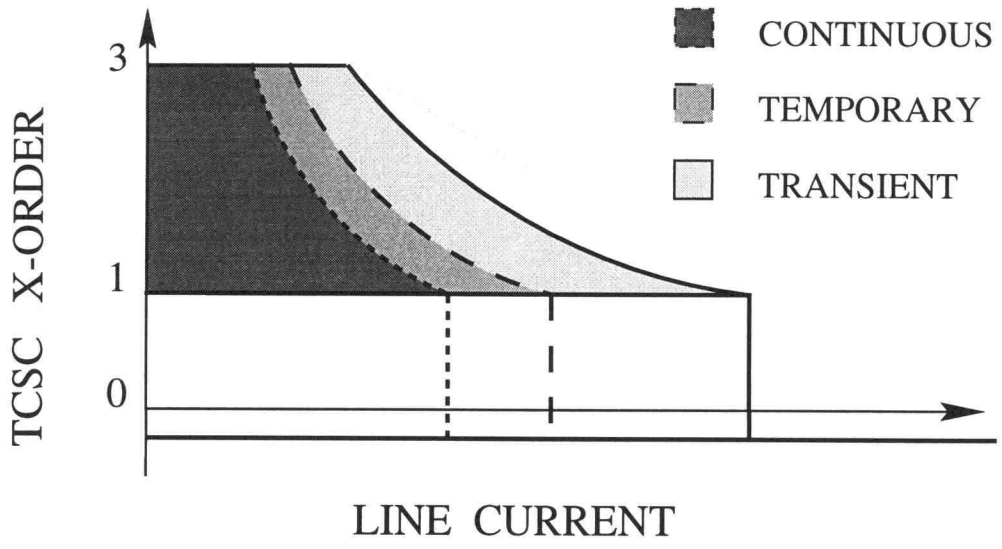


FIGURE 3.9. TCSC capability characteristics: TCSC X-order vs. line current

Typically, from four to six modules are suggested [20, 22].

When considering TCSC applications, additional constrains on the TCSC X-order can be added beyond those resulting from device ratings. For example, if there is a SSR concern, the TCSC operation can be restricted only to some vernier regions. These constraints should be added depending on a particular application.

### 3.5. Powerflow Model and Control Modes

A variable-reactance model is used to represent the TCSC in a powerflow program. The TCSC appears in the transmission system equations as a branch with controlled reactance: $X_{net} = X_{ord}X_C$, where $X_{ord}$ is the controlled variable. The current in the TCSC branch (line current) is:

$$\bar{I}_L = j\,\frac{\bar{E}_p - \bar{E}_q}{X_{ord}X_C},$$

where $\bar{E}_p$ and $\bar{E}_q$ are bus voltages at the ends of the TCSC branch.

Active power transfer through the TCSC branch is

$$P_{pq} = \frac{E_p E_q}{X_{ord} X_C} \sin(\delta_p - \delta_q),$$

and reactive power generated by the device and injected in the *p-th* node is:

$$Q_{pq} = \frac{(E_p)^2}{X_{ord} X_C} - \frac{E_p E_q}{X_{ord} X_C} \cos(\delta_p - \delta_q).$$

Within the allowed X-order capabilities various controls can be implemented. Since the TCSC has only one controlled variable $X_{ord}$, only one control can be performed at a time.

**Active Power Control**

The $X_{ord}$ is selected to keep the power transfer at the specified set-point $P_{SET}$. An equation representing this constraint should be added:

$$P_{pq}(\ E_p, E_q, \delta_p, \delta_q, X_{ord}\ ) = P_{SET}.$$

Similarly, power transfer can be controlled at remote lines.

**Line Current Control**

Controlled line current mode can be used:

$$I_L(\ E_p, E_q, \delta_p, \delta_q, X_{ord}\ ) = I_{SET}.$$

**Capacitor Voltage Control**

During the outages, it may be desirable to operate a TCSC at a temporary overload rating of TCSC capacitors. In this case, the X-order is controlled to keep the capacitor voltage at its temporary overload rating:

$$U_C = I_L(\ E_p, E_q, \delta_p, \delta_q, X_{ord}\ )\ \ X_{ord} X_C$$

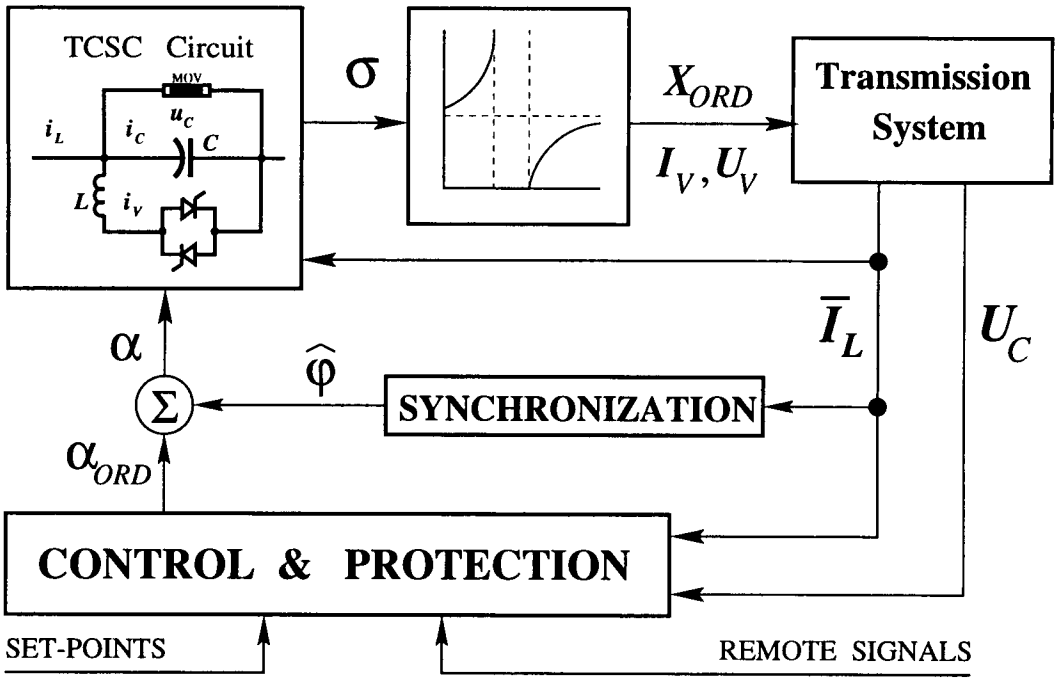


FIGURE 3.10. TCSC model for transient stability program

## 3.6. TCSC Model for Transient Stability Studies

Typical time steps used in transient stability studies are 1/2 and 1/4 of one electrical cycle. The TCSC thyristor firing occurs every 1/2 cycle. For all three models, the controlled variables (X-order, thyristor current, capacitor trapped voltage) are updated every 1/2 electrical cycle, which is consistent with the simulation time step. To determine the TCSC controlled variables, the set of differential equations is solved each half-cycle of stability simulations.

### 3.6.1. TCSC Model

The TCSC model diagram for the transient stability studies is shown in Figure 3.10. The model assumes a one-line TCSC representation. The TCSC circuit is

modeled by a set of differential equations representing the TCSC power circuit. The model inputs are the thyristor firing angle $\alpha$, and the line current $i_L = I_L \sin(\omega_0 t + \varphi)$. The magnitude $I_L$ and the phase $\varphi$ are updated at every step of the transmission network solution, and firing angle $\alpha_{ord}$ is computed by user-defined controls. The system state variables are the capacitor voltage $u_C$ and the thyristor (surge inductor) current $i_V$. The model output is the thyristor conduction angle $\sigma$.

The TCSC effective X-order is determined based on the present value of the conduction angle $\sigma$ using Figure 3.7. Then, depending on the used model, the TCSC net reactance $X_{net}$ (or thyristor current $I_V$, or capacitor trapped voltage $U_V$) is passed to the transmission network equations. MOV arrester can be represented with the transmission system.

The transmission network output is the line current $\bar{I}_L$ phasor, and the capacitor voltage $U_C$. These signals are used by a user-defined control and protection schemes to determine the firing angle set-point $\alpha_{ord}$ required to meet the specified control objectives.

Response of the synchronization circuits is also taken into account. Typically, thyristor firing is synchronized with the line current:

$$\hat{\varphi} = \mathcal{S}(\bar{I}),$$

where $\mathcal{S}$ is a model of a synchronization scheme. Thus, the effective firing angle $\alpha = \alpha_{ord} + \hat{\varphi}$.

Table 3.1 summarizes input information on the TCSC circuit parameters and ratings for a transient stability program.

| Input Name | Nom. | Units | Default |
|---|---|---|---|
| Capacitor | | | |
| Rated Current | $I^c_{rat}$ | A | |
| Temporary (30-min) overload | $I^c_{temp}$ | p.u. | 1.35 $I^c_{rat}$ |
| Transient (10-sec)overload | $I^c_{tran}$ | p.u. | 2 $I^c_{rat}$ |
| Reactance | $X_C$ | $\Omega$ | |
| Thyristor-Controlled Reactor | | | |
| Rated Current | $I^{th}_{rat}$ | A | |
| Surge Inductor Reactance | $X_L$ | $\Omega$ | |
| Minimum X-order | $X^{min}_{ord}$ | p.u. | -2.0 |
| Maximum X-order | $X^{max}_{ord}$ | p.u. | 3.0 |

TABLE 3.1. TCSC input data for transient stability studies

### 3.6.2. TCSC Model Initialization

TCSC X-order is used as a control variable in the powerflow studies. Powerflow studies determine the line current $\bar{I}_L(0)$ and the TCSC X-order set-point $X_{ord}(0)$. Based on the steady-state X-order, the firing angle $\alpha_{ord}(0)$ is determined. Thyristor firing is assumed to be synchronized perfectly, $\hat{\varphi}(0) = \varphi(0) = \arg[\ \bar{I}_L(0)\ ]$. Thus, the effective firing angle in steady-state is $\alpha(0) = \alpha_{ord}(0) + \hat{\varphi}(0)$.

To initialize the TCSC circuit, $u_C(0)$ and $i_V(0)$ have to be determined. The simplest procedure is to let the TCSC circuit run for several cycles until $u_C$ and $i_V$ settle at their steady-state waveforms. During this initialization run, the inputs to the TCSC circuit model are the firing angle $\alpha(0)$ and the line current $i_L = I_L(0)\sin(\ \theta + \varphi(0)\ )$. Set the initialization time to $\theta_i = -\varphi(0) - \pi/2 - 2\pi i$, where $i$

is the number of initialization cycles to run. Assuming that thyristors are blocked initially, set $u_C(t_i) = 0$, and $i_V(t_i) = 0$. Then, the simulation circuit is run till $\theta = 0$. At this time, $u_C(0), i_V(0)$ assume their initial values.

User-defined control and protection schemes are initialized based on the input-output relationships.

### 3.6.3. Model Performance Studies

The TCSC circuit is simulated using the EMTP, and firing angle control and all calculations are performed in Models similarly to those in a transient stability program.

**Step change in firing angle (Figure 3.11).**

The line current has constant magnitude and phase, when the firing angle changes according to Figure 3.11(a) from thyristor-blocked mode to the capacitive vernier mode. TCSC capacitor voltage is shown in Figure 3.11(b), and the thyristor conduction angle is shown in Figure 3.11(c). Based on the firing angle set-point, the TCSC X-order is computed using (3.1) and is shown in Figure 3.11(d) by the broken line. Based on the conduction angle, the TCSC X-order for stability studies is computed using (3.1)and is shown in Figure 3.11(d) by the solid line. The fundamental components of the line current and the capacitor voltage are obtained to compute the X-order. The X-order is identical to that computed by the stability model.

**Line current swings (Figure 3.12).**

The TCSC is operating in the capacitive vernier mode with constant firing angle, and the line current magnitude changes according to Figure 3.12(a) similarly to the line current swings. The TCSC capacitor voltage is shown in Figure 3.12(b), and the thyristor conduction angle is shown in Figure 3.12(c). Even when the firing angle

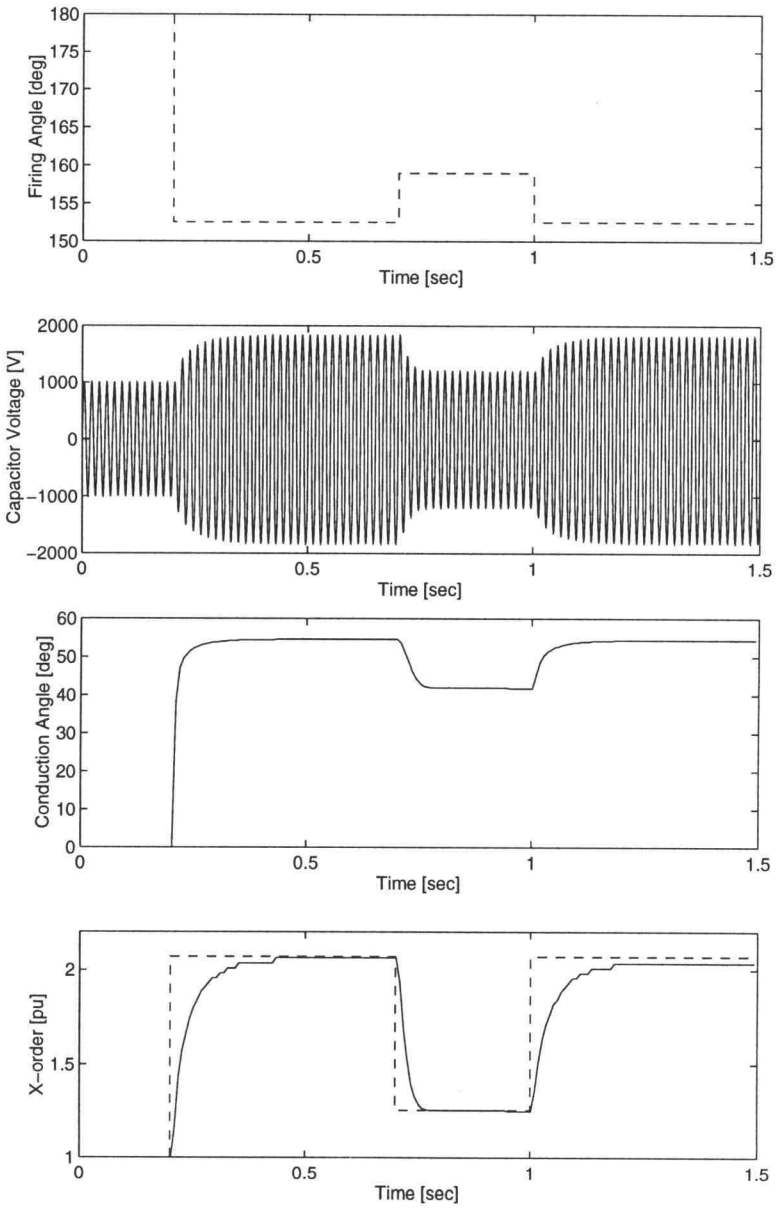


FIGURE 3.11. TCSC model performance

is constant, the thyristor conduction angle changes with the line current swings. The X-order set-point is shown in Figure 3.12(d) by the broken line. The solid line represents the X-order computed using (3.1) based on the conduction angles given in Figure 3.12(c). The dotted line represents the X-order computed from the fundamental components of the capacitor voltage and line current.

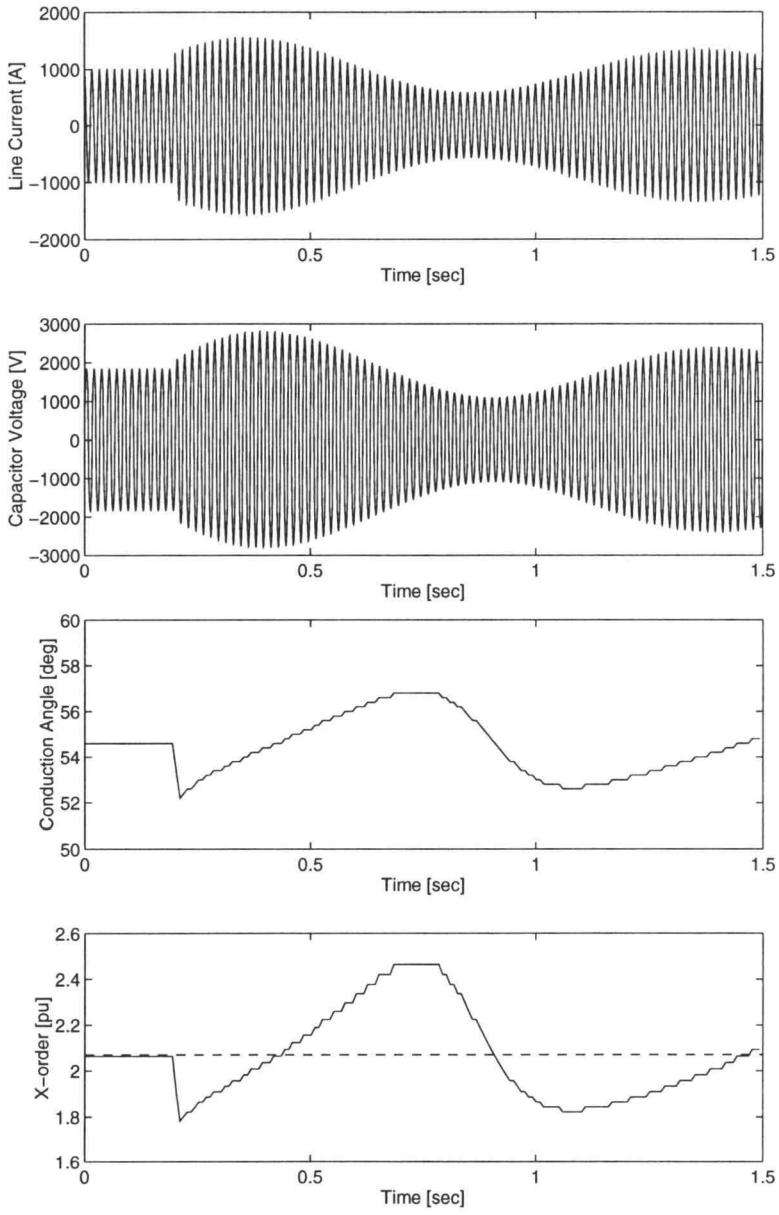


FIGURE 3.12. TCSC model performance

### 3.6.4. Model Limitations

The developed TCSC model is accurate. The model performance limitations result only from the transmission system representation in existing transient stability programs.

Existing transient stability programs use one-line representation of the transmission network, and model the transmission system by algebraic equations. This approach yields only positive sequence fundamental components of the line currents and bus voltages. This assumes that the current in the TCSC line is sinusoidal with magnitude and phase varying with power swings. Such an assumption is no longer valid when a severe disturbance (e.g. fault) occurs close to the TCSC location and the line current waveforms are distorted by harmonics and natural frequencies. Distorted current waveforms can affect the TCSC commutation, and consequently the TCSC transient performance. Another limitation of the one-line transmission system representation relates to inability of modeling unbalanced conditions. Single-pole tripping is often used for clearing phase-to-ground faults [18, 37], which account the majority of faults in transmission system. The Bonneville Power Administration employs single-pole relaying with automatic reclosing on major 500kV lines. Reclosing time on 500kV lines is determined by the time required for the secondary arc extinction, and is typically about 30-40 cycles, which is the time frame of the first swing stability. It is becoming more common to have two EHV lines on the same right of way, for example both Garrison-Taft lines in Montana. Simultaneous phase-to-ground faults on both lines are not uncommon, for example, there were five simultaneous faults on the Ashe-Marion and Buckley-Marion BPA 500kV lines from April 1987 to August 1995 caused by lightning. Such simultaneous disturbances represent a threat to system stability, as it was in the case of simultaneous phase-to-ground faults on the Garrison-Taft lines. These disturbances represent credible contingencies, and must be considered in transient stability studies. The TCSCs in the remaining unfaulted lines have to be modeled properly, taking into account their time-overload capabilities. The only solution for these problems will be better modeling of transmission facilities.

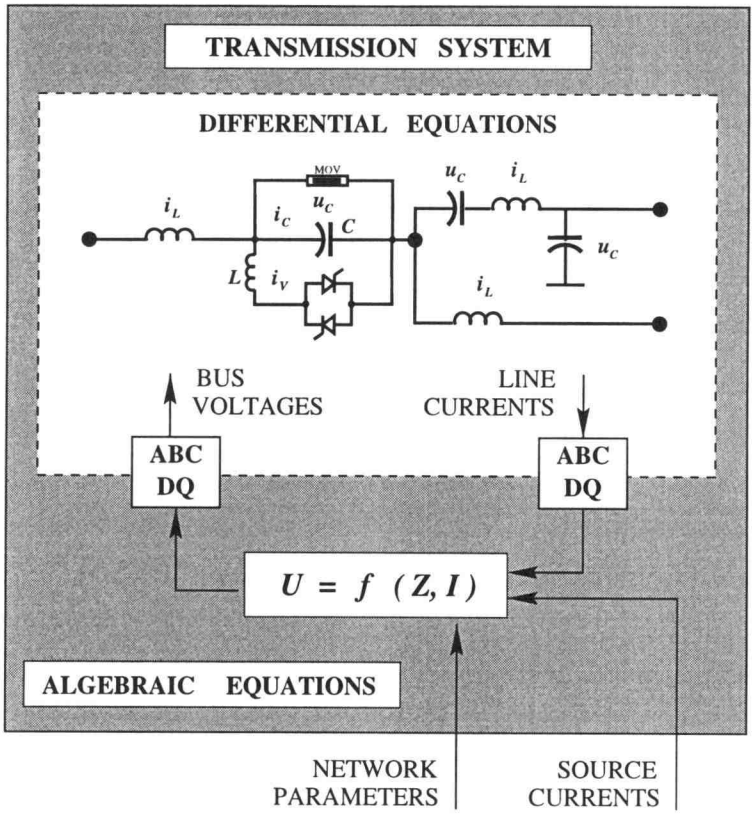


FIGURE 3.13. global approach for TCSC modeling in a transient stability program

## 3.7. Global Approach for TCSC Modeling for Transient Stability Studies

A global approach for the TCSC modeling for transient stability studies is illustrated in Figure 3.10.

A part of transmission network electrically close to the TCSC is represented in detail by differential equations (three-phase models). The rest of the transmission network is modeled traditionally by algebraic equations. Algebraic sub-model computes positive sequence bus voltages at each iteration step. The direct and quadrature voltage components are converted to ABC voltages by applying an inverse Park's transform from the synchronous DQO to the stationary ABC reference

frame. These voltages serve as inputs to the differential sub-model. The three-phase differential equations include those representing the TCSC power, control and protection circuits. The differential sub-network is solved using a very small time-step, necessary for adequate TCSC modeling. The output of the differential sub-model are line currents at the terminal nodes. The fundamental components of line currents are computed as follows. First, the Park's transform is applied to convert the line currents from the stationary ABC to the synchronous DQO reference frame. Direct and quadrature components of the line current are passed through a moving average one cycle filter to filter out the fundamental positive sequence component. The line current phasor is passed to the algebraic sub-network.

This modeling approach allows to represent effects of line current distortions and sever unbalanced conditions on the TCSC performance, and ultimately to perform correct determination of the TCSC impact on transient angle stability.

# 4. MODELING SYNCHRONOUS VOLTAGE SOURCE IN PLANNING STUDIES

Voltage stability is one of the major problems in developed transmission systems [17, 26, 27]. Various reactive power compensators can be employed to enhance voltage stability, and a Synchronous Voltage Source (SVS) is one of them [7, 8, 26, 27]. The SVS has control capabilities and dynamic response superior to those of conventional reactive power compensators [7, 9]. To evaluate the SVS applicability to present and future projects, the device has to be represented appropriately in planning studies. This chapter addresses issues of the SVS modeling for time-domain studies.

## 4.1. SVS Operating Principles

A block-diagram of the Synchronous Voltage Source (SVS) is depicted in Figure 4.1. The DC voltage source supplies voltage to a power converter array. The DC batteries and DC capacitors can be used as DC voltage sources. By controlling current flow at the DC bus, the DC source can either supply or absorb active power, and the power converter can operate as inverter or rectifier respectively. The converter array typically consists of several power conversion modules (PCMs). PCMs include basic six-pulse converters, where gate-turn-off (GTO) thyristors are used as power switches. Typically, several thyristors are connected in series to form a valve. The converter output voltages are combined electro-magnetically by means of a coupling transformer array to form a multi-pulse "sinusoidal" voltage. The secondaries of the transformer array are connected to the AC transmission

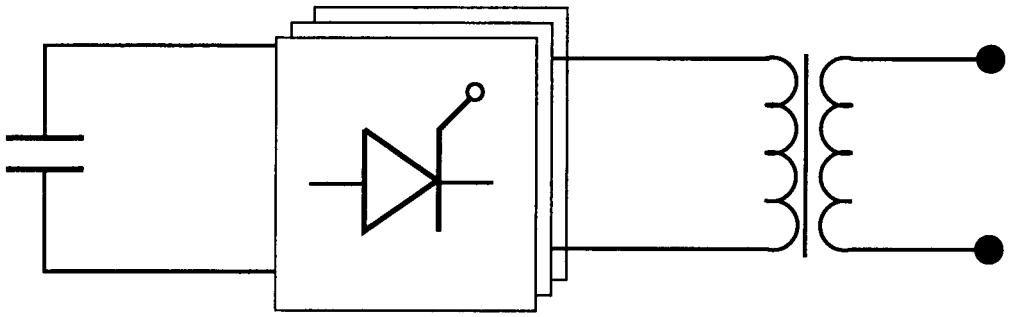


FIGURE 4.1. Synchronous Voltage Source block diagram

system. There is a circuit breaker which allows device disconnection from the AC transmission system.

Coupling transformers use harmonic neutralization techniques [8, 29], so that only $Pk \pm 1$ $(k = 1, 2, \ldots)$ harmonics are present in $P$-pulse waveform (typically $P = 6n$, $n = 1, 2, \ldots$). Both, power converter and coupling transformer can be implemented by a variety of circuits. Although the designs can be significantly different, the converter output voltage waveforms and DC currents are essentially the same.

The SVS can be connected either in shunt or in series with the transmission line. Shunt-connected SVS are the Battery Energy Storage (BES)-device [10] and the Static Condenser (Statcon) [7, 9]. The Statcon uses only capacitors as a DC voltage source, while the BES-device has also DC batteries. The series-connected SVS are the Static Synchronous Series Compensators (SSSCs) [8].

### 4.1.1. Example of the SVS Design

An example of the power converter design [10] is shown in Figures 4.2 and 4.3. The converter consists of three identical PCMs, each is labeled as "O DEG," "20 DEG," "40 DEG" to indicate their phase displacement of gating times with respect to the reference. Each PCM consists of two basic six-pulse converters, the first is leading and the second is retarded. The GTO-thyristors are conducting for $180^0$ at 60 Hz, and GTO-thyristor gatings are displaced by $120^0$ within each six-pulse converter. Nine single-phase transformers are used to connect converters to a utility AC bus. The transformer primaries are connected between the corresponding phases of the leading and retarded converters. The transformer secondaries are zig-zag connected and provide phase-shift necessary to form an 18-pulse waveform. The transformer turn ratios are selected to eliminate harmonics lower than 17-th from the line-to-line voltage. Transformers T1A, T1B, and T1C are identical, each having only one secondary with turns ratio: $N_0 = K \cos 30^0$. Transformers T2A, T2B, T2C, T3A, T3B, and T3C are also identical, each has two secondaries, with turn ratios $N_1 = K \cos 50^0$ $N_2 = K \cos 70^0$. In Figure 4.3, secondaries of transformers with $N_0$ ratio are depicted with four coils, secondaries of transformers with $N_1$ ratio are shown with three coils, and secondaries of transformers with $N_2$ ratio are shown with two coils. The angular positions of the transformer primaries and secondaries represents the relative phase shift of the voltage in that winding with respect to the reference. Capacitors can be used at the AC-bus to provide filtering of higher-order harmonics.

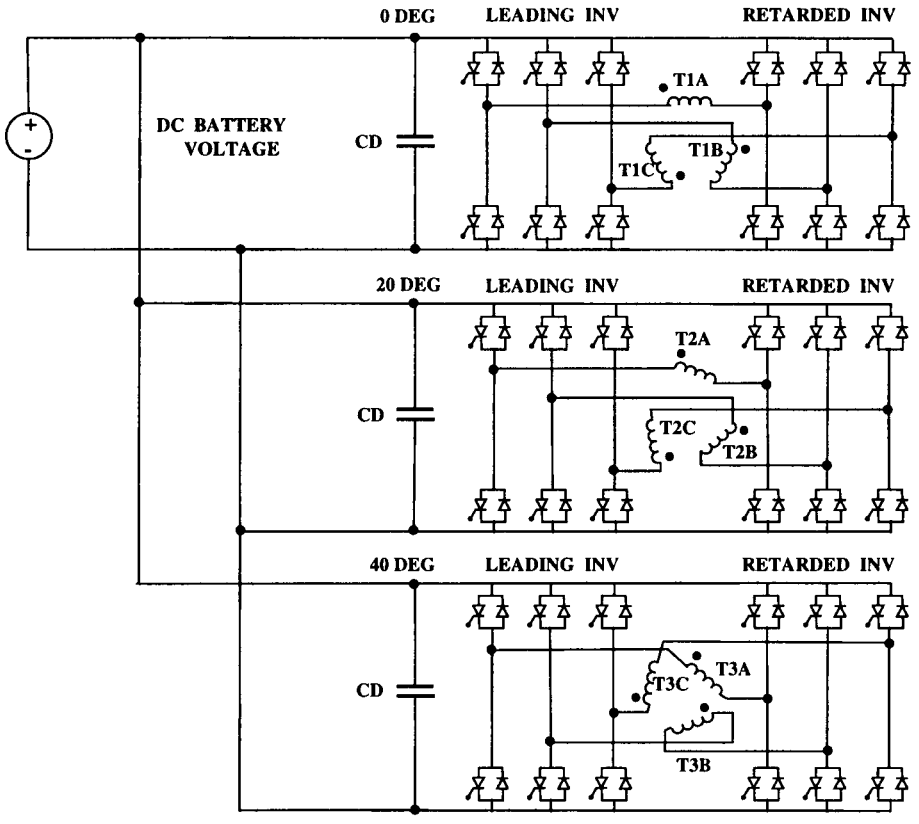


FIGURE 4.2. Synchronous Voltage Source, DC bus

### 4.1.2. Converter Controls

There are two levels of the converter controls: internal and external. The internal control provides gating signals to the thyristor valves in order to form a desired converter voltage waveform. The external controller determines parameters of the synthesized converter voltage (magnitude and phase of the fundamental component) required to meet specified performance objectives. These parameters are translated into thyristor firing angles and passed to the internal controls. Controllability of the synthesized voltage magnitude and phase is discussed bellow.

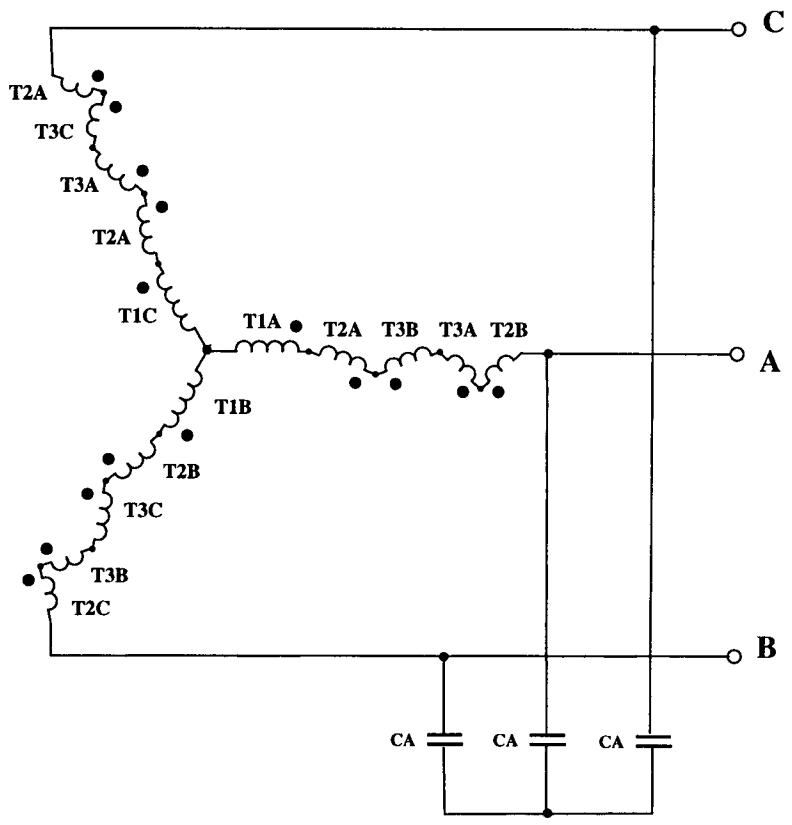


FIGURE 4.3. Synchronous Voltage Source, AC bus

### Voltage Magnitude Controllability

The fundamental component of the converter voltage magnitude $V_{CV}$ (line-to-line value) is proportional to the DC-bus voltage $E_{DC}$. Thus, the converter voltage magnitude can be controlled by the DC source voltage. This method is effective only for a Statcon, because battery voltage changes very slowly. The rate of change of the DC voltage depends on the DC capacitor size. The smaller capacitance, the faster response is, however at the expense of larger voltage ripples. For a fixed DC voltage, the converter voltage magnitude can be controlled also by a zero-dwell period $\beta$ in a PCM output voltage waveform [10, 29]. Although controls of $\beta$ can be different

for various converter implementations, the resulting effect on the converter voltage is the same

$$V_{CV} = K_V E_{DC} \cos(\beta/2), \tag{4.1}$$

where $K_V$ is the coefficient representing the fundamental component in a multi-pulse waveform, rms values. $K_V$ also includes the coupling transformer ratio.

**Voltage Phase Controllability**

The phase angle $\gamma$ is the angle between fundamental components of the converter voltage $\bar{V}_{CV}$ and the AC-bus voltage $\bar{V}_{AC}$. The angle $\gamma$ is called "power angle," since it determines the active power exchange in the converter [10]. Both, magnitude and phase of the synthesized converter voltage can be controlled independently.

For a Statcon, power angle control has indirect effect on the converter voltage magnitude. Since angle $\gamma$ controls active power exchange in the converter, it controls charge and discharge of the DC capacitors, and consequently the DC-bus voltage $E_{DC}$, and ultimately the converter voltage magnitude $V_{CV}$ according to (4.1).

Internal controls provide gating signals for thyristor valves. The thyristor firing is synchronized with the AC-bus voltage. Synchronizing circuit output serves as a reference for the thyristor firing. Each gating sequence is advanced by the power angle $\gamma$ with respect to the reference. Within a PCM gating sequence, thyristor firing of complementary GTOs can be displaced by angle $\beta$ to introduce a zero-voltage dwell.

## 4.2. EMTP Model

The modeled SVS device is rated at 12.5kV (transmission side) voltage and 10MVA power. The nominal DC-bus voltage is 2.5 kV, and the DC capacitors are

sized at 100$\mu$F. The 18-pulse converter is modeled according to [10]. The GTO-thyristors are represented by type-11 TACS-controlled switches. Small resistances are put in series with the switches to represent power losses in the converter. Snubber RC circuits are modeled in parallel with the thyristor switches. The transformer array consists of single-phase transformers, where transformer ratios are selected according to [10]. Transformer secondaries are zig-zag connected. Transformer ratios and winding connections are arranged to provide neutralization of harmonics less than 17th in the secondary line-to-line voltage [10].

The utility voltage and the converter currents are passed to Models (ATP language for control implementation) and used for both, internal and external controls. Synchronization schemes and firing angle logic are implemented using Models. The output of Models is the status of GTO switches.

## 4.3. SVS Representation at the Fundamental Frequency

### 4.3.1. Representation of Shunt-Connected SVS at the Fundamental Frequency

The representation of a shunt-connected SVS at the fundamental frequency is shown in Figure 4.4. The shunt-connected SVS interacts with the transmission network through the AC-bus voltage $\bar{V}_{AC}$ (line-to-line value).

**DC Source.**

The DC voltage source is represented by voltage $E_{DC}$ and current $I_{DC}$. The DC power output is

$$P_{DC} = E_{DC} I_{DC}. \tag{4.2}$$

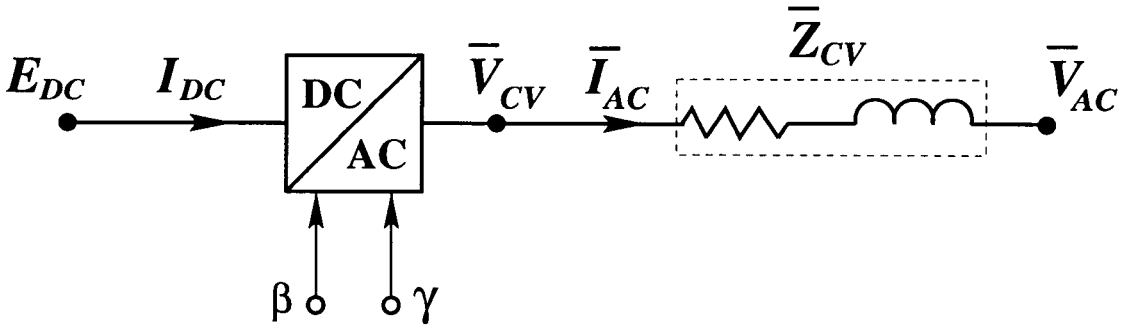


FIGURE 4.4. Shunt-Connected SVS representation at the fundamental frequency

**Coupling Transformer.**

The coupling transformer array is represented by an equivalent impedance $\bar{Z}_{CV} = R_{CV} + jX_{CV}$.

For the shunt-connected SVS, the AC current (phase value) is

$$\bar{I}_{AC} = \frac{1}{\sqrt{3}} \frac{\bar{V}_{CV} - \bar{V}_{AC}}{\bar{Z}_{CV}}. \tag{4.3}$$

**Power Converter.**

For a given DC source voltage $E_{DC}$, the converter output voltage magnitude $V_{CV}$ can be computed according to (4.1), and is controlled by angle $\beta$. The power angle $\gamma = \delta_{CV} - \delta_{AC}$, where $\delta_{CV}$ is the converter voltage phase and $\delta_{AC}$ is the phase of the AC-bus voltage $\bar{V}_{AC}$.

The converter active power is

$$P_{CV} = \frac{V_{CV}\, V_{AC}}{Z_{CV}} \sin(\gamma - \alpha) + \frac{V_{CV}^2}{Z_{CV}} \sin\alpha = \sqrt{3}\, V_{CV}\, I_{AC} \cos\varphi \tag{4.4}$$

where $\alpha$ is the conduction angle of impedance $\bar{Z}_{CV}$, and $\varphi$ is the angle between converter voltage and AC current.

The active power exchange in converter is

$$P_{CV} = P_{DC}. \tag{4.5}$$

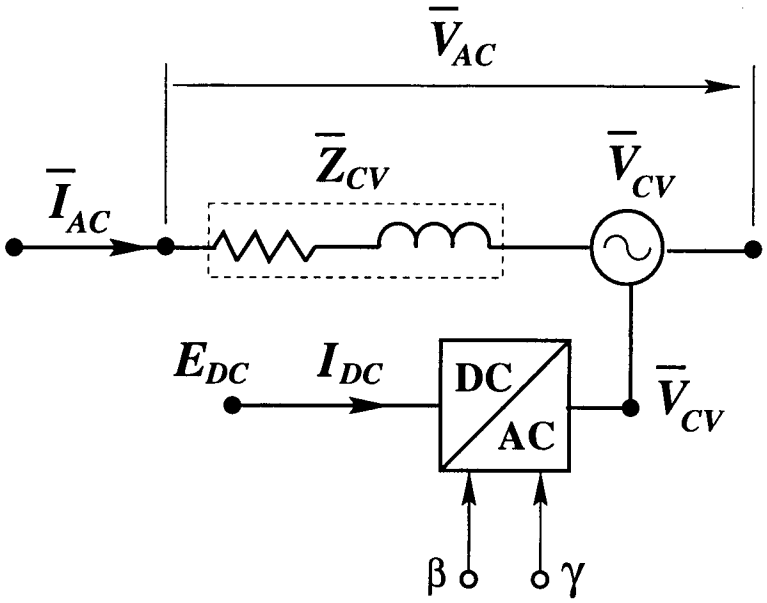


FIGURE 4.5. Series-Connected SVS representation at the fundamental frequency

**Transmission Network.**

Active and reactive power on the AC side are

$$P_{AC} = \frac{V_{CV}\, V_{AC}}{Z_{CV}} \sin(\gamma + \alpha) - \frac{V_{AC}^2}{Z_{CV}} \sin \alpha, \tag{4.6}$$

and

$$Q_{AC} = \frac{V_{CV}\, V_{AC}}{Z_{CV}} \cos(\gamma + \alpha) - \frac{V_{AC}^2}{Z_{CV}} \cos \alpha, \tag{4.7}$$

respectively.

### 4.3.2. Representation of Shunt-Connected SVS at the Fundamental Frequency

The diagram of a series-connected SVS at the fundamental frequency is shown in Figure 4.5. The series-connected SVS interacts with transmission network through the AC-bus current $\bar{I}_{AC}$ (phase value).

The DC-bus equations and coupling transformer representations are identical. For a series connected SVS, the voltage (phase value) at the coupling transformer secondary is

$$\bar{V}_{AC} = \bar{V}_{CV} - \bar{Z}_{CV}\ \bar{I}_{AC}. \tag{4.8}$$

The converter active power is given by

$$P_{CV} = 3V_{CV}\ I_{AC} \cos\varphi. \tag{4.9}$$

## 4.4. Synchronous Voltage Source Ratings and Capability Characteristics

To represent the SVS appropriately in planning studies, its capability characteristics should be derived based on the device ratings.

### 4.4.1. SVS Ratings

The SVS equipment ratings are determined by those of its components: DC voltage source, power converter, and coupling transformers.

**DC voltage source**

The DC voltage source is characterized by its voltage and current ratings. The DC-bus voltage $E_{DC}$ should not exceed the voltage rating of the DC voltage source, i.e. $E_{DC} \leq E_{DC}^{max}$. Overvoltage arresters can be used in parallel with the voltage source to keep voltage $E_{DC}$ below the protective level. For BES devices, there is also a constraint on how low the DC battery can be discharged, $E_{DC} \geq E_{DC}^{min}$. The DC voltage has to be constantly above a certain level to avoid thyristor firing failure due to low voltage conditions.

DC current ratings determine how fast the voltage source can be charged and discharged, $I_{DC}^{min} \leq I_{DC} \leq I_{DC}^{max}$. Typically, DC batteries and capacitors are protected by the overcurrent fuses.

**Power Converter Valves.**

Power converter valves are characterized by their current and voltage ratings. The thyristor valves are composed of several GTO-thyristors connected in series, and the voltage rating of the valve is the sum of rated voltages of individual thyristors in the valve minus a derating factor. Typically, a redundant thyristor is added to the valve for reliability reasons [10, 9].

The valve current ratings include both, instantaneous and RMS currents. The RMS current ratings are constrained by the device thermal capabilities and depend on the design of GTO-thyristor heat sinks and their cooling systems. The valve has short time-overcurrent capabilities, typically up to 25% for several seconds [9]. The RMS current ratings translate in restrictions on the converter currents on the AC side: $I_{AC} \leq I_{rat}$ for continuous operation, and $I_{AC} \leq I_{tran}$ for 10-second transient overload.

Peak current ratings relate to the device turn-off capabilities and represent the maximum instantaneous turn-off current. Instantaneous overcurrent protection is built in the firing angle control logic [10]. When the valve instantaneous current reaches the protection level, the thyristors are blocked.

**Coupling Transformer**

The coupling transformer is characterized by its voltage and current ratings. Voltages at transformer primaries and secondaries should not exceed their respective voltage ratings. Overvoltages can result in transformer saturation and overexcitation. Current ratings should account for harmonic distortion of transformer currents.

### 4.4.2. Operating Characteristics for the Shunt-Connected SVS

The SVS operating characteristic defines a region where the converter voltage phasor $\bar{V}_{CV}$ can reside depending on the operating conditions, and subject to the rating constraints. The operating conditions are determined by the AC-bus voltage $\bar{V}_{AC}$, and the DC-bus voltage $E_{DC}$. The SVS operating characteristics are shown in Figure 4.6 using the complex plane.

Given the converter RMS current ratings, the magnitude of the maximum voltage drop across impedance $Z_{CV}$ is $\Delta V_{rat} = \sqrt{3} I_{rat} Z_{CV}$ for continuous loading, and $\Delta V_{tran} = \sqrt{3} I_{tran} Z_{CV}$ for transient overload. The phasor $\bar{V}_{CV}$ should stay within a circle centered at the end of phasor $\bar{V}_{AC}$ and of radius $\Delta V$. The magnitude of the current generated by the SVS is independent on the AC-bus voltage; the SVS current versus terminal voltage characteristics are presented in [7–9].

Given DC voltage $E_{DC}$, the maximum magnitude of the converter voltage $\bar{V}_{CV}$ is $V_{CV}^{max} = K_V E_{DC}$. The phasor $\bar{V}_{CV}$ should stay within a circle centered at the origin and of radius $V_{CV}^{max}$. If there is an upper limit on the angle $\beta \leq \beta^{max}$, the converter voltage $\bar{V}_{CV}$ should stay outside a circle centered at origin and of a radius $V_{CV}^{min} = K_V E_{DC} \cos(\beta^{max}/2)$.

The DC-bus current ratings result in constraints on active power exchange in the converter: $E_{DC} I_{DC}^{min} \leq P_{CV} \leq E_{DC} I_{DC}^{max}$. Proper device ratings should be selected to ensure sufficient operating region.

## 4.5. Powerflow Model and Control Modes

In this section, only shunt-connected SVS is considered.

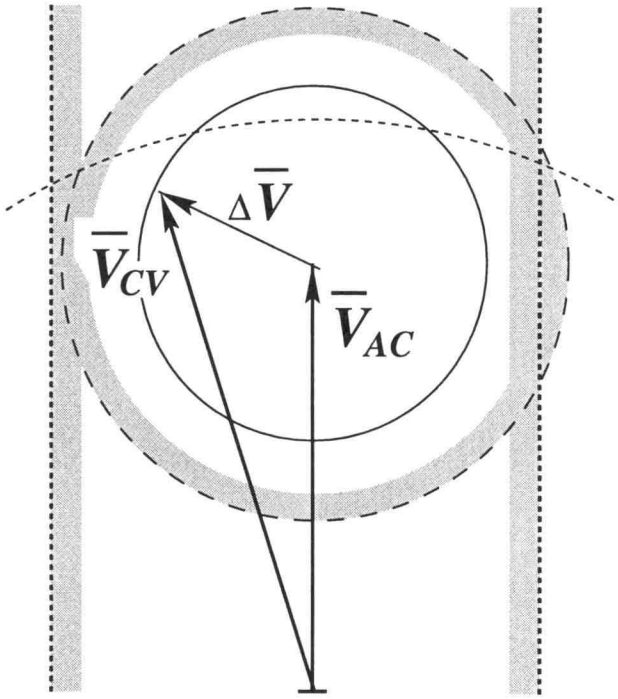


FIGURE 4.6. SVS control capability characteristics

### 4.5.1. Powerflow Model

Existing powerflow programs do not include specific SVS models. In the BPA Powerflow program [30], a G(generator)-type bus is most appropriate. At this bus, the active power is scheduled and the reactive power can be controlled within specified limits to keep the voltage at either local or remote bus at a given set-point. Since the G-bus has reactive power limits independent of the terminal voltage, modeling errors can be introduced when representing the device at low voltages at its capacitive current limit. This is illustrated in Figure 4.7(A). The modeled VAR control range at low voltages is larger than that of a Statcon. The solution to the problem is to model the Statcon as a G-bus with a constant current load. The current load is set to be equal to the Statcon capacitive current limit, while the VAR limits of the G-bus are set only for the inductive region from 0

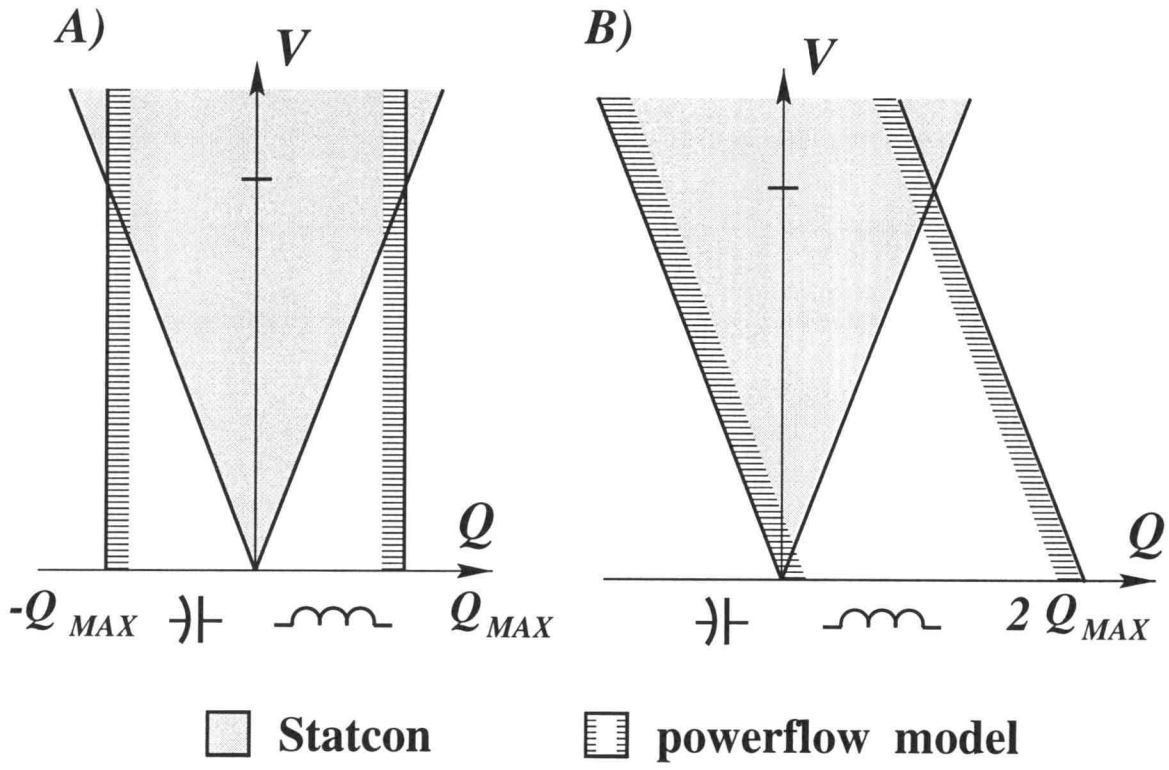


FIGURE 4.7. Statcon representation in powerflow programs

to twice VAR rating. This modeling approach is illustrated in Figure 4.7(B). The capacitive current limit is represented correctly by this model, but not inductive.

A detailed SVS model represents the device by a controllable voltage $\bar{V}_{CV}$. The model includes the device operating characteristics, and is implemented as a Matlab function. Matlab language is used by the Power Systems Toolbox [31]. This toolbox is a very useful tool for studies of medium and small scale systems, and Matlab language provides excellent environment for modeling various user-defined dynamic elements and controls.

For a BES device, the DC battery voltage is constant in powerflow studies. Thus, the BES device has two independently controllable variables: converter voltage magnitude and phase. Two control modes can be implemented independently

and simultaneously, subject to the device control capabilities. There may be operational constraints on active power exchange in the converter $P_{CV}$, depending on the DC battery charge conditions.

For a Statcon, the DC-bus time constant (DC capacitance) is significantly less than a time frame of powerflow studies. To keep the DC capacitor voltage at a controlled value, the active power exchange in the converter has to be zero, i.e. $P_{CV} = 0$. This condition eliminates one independent control variable, and consequently only one control mode can be implemented at a time.

### 4.5.2. Powerflow Control Modes

The following powerflow control modes can be implemented using the SVS.

**Active Power Control.** This is the basic control mode for the BES device. The active power output is held at a given set-point $P_{SET}$:

$$P_{AC}(\bar{V}_{CV}, \bar{V}_{AC}) = P_{SET}.$$

This mode is not applicable for STATCON.

**Constant AC bus Voltage.** Either local or remote bus voltage is held at a given set-point $V_{SET}$ : $V_{AC} = V_{SET}$.

**Constant Current.** The AC output current is held at a given set-point $I_{SET}$ :

$$I_{AC}(\bar{V}_{CV}, \bar{V}_{AC}) = I_{SET}.$$

**Constant Power Factor.** Load power factor is held as a given set-point $\mathrm{PF}_{SET}$:

$$\mathrm{PF}(\bar{V}_{CV}, \bar{V}_{AC}) = \mathrm{PF}_{SET}.$$

The above modes are active only within the device operating characteristic shown in Figure 4.6.

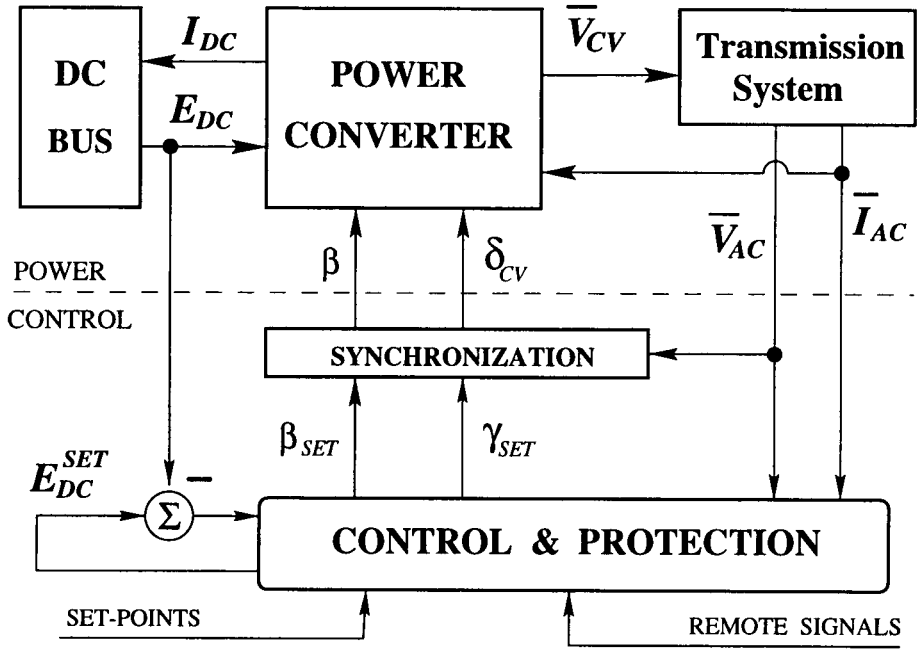


FIGURE 4.8. SVS model for stability studies

## 4.6. Model of Synchronous Voltage Source for Transient and Long-Term Stability Studies

The SVS model for transient stability studies is derived based on the device representation at the fundamental frequency as in Figures 4.4 and 4.5, and also includes protection, control, and synchronization circuits.

### 4.6.1. Detailed Stability Model

The block-diagram of the SVS stability model is shown in Figure 4.8. The upper part represents power circuits, while the lower part represents the controls.

**DC bus.**

The DC source is assumed to be charged initially to voltage $E_{DC}(0)$. The source

can be charged and discharged by the current $I_{DC}$. The DC source dynamics are represented by a first-order system

$$\tau_d \dot{E}_{DC} = -I_{DC}, \tag{4.10}$$

where $\tau_d$ is a charging time constant.

For a BES device, $\tau_d$ is very large, such that the DC battery voltage can be assumed constant in the transient stability studies. For a Statcon, $\tau_d$ equals to the capacitance of the DC capacitors. An overvoltage arrester can be used in parallel with the voltage source to keep the DC source voltage $E_{DC}$ below the protective level $E_{DC}^{max}$. The arrester can be represented as a dynamic limiter on the capacitor voltage.

**DC voltage control**

For a Statcon, the converter voltage magnitude is controlled by the DC-bus voltage (4.1), and consequently the DC voltage control is an important part of a Statcon stability model. Measured DC voltage is pre-filtered and subtracted from a set-point $E_{DC}^{set}$, and the error signal is fed to the controller. The voltage reference is determined by user-defined controls, otherwise is held at its steady-state value. The controller output translates into the power angle set-point

$$\gamma_{SET} = \mathcal{F}(E_{DC}^{set} - E_{DC}),$$

where $\mathcal{F}$ represents a dynamic control function. The power angle determines the active power exchange in the converter, and consequently the DC current flow, and the DC capacitor voltage.

**Power Converter.**

The power converter is represented by algebraic equation (4.1) for voltage synthesis, and equations (4.2,4.4,4.5) for power conversion. The angles $\beta$ and $\gamma$ are updated at every step of the transmission network solution.

**Synchronization.**

Imperfect synchronization during transient swings should also be taken into account in the stability model. The AC-bus voltage $\bar{V}_{AC}$ phasor is used as an input to the synchronization circuit. The synchronization circuit estimates the phase of the AC voltage

$$\hat{\delta}_{AC} = \mathcal{S}(\bar{V}_{AC}),$$

where $\mathcal{S}$ represents a model of a synchronization circuit. Values of $\bar{V}_{AC}$ are updated after each network solution step. The phase angle of the converter voltage is $\delta_{CV} = \gamma_{SET} + \hat{\delta}_{AC}$. The actual power angle is $\gamma = \delta_{CV} - \delta_{AC} = \gamma_{SET} + (\hat{\delta}_{AC} - \delta_{AC})$. Angle $\beta$ is not affected by the synchronization errors, $\beta = \beta_{SET}$.

**Control.**

Various user-defined controls can be implemented using this model to achieve full utilization of the device control capabilities [26]. Local voltages and currents, DC voltage, as well as remote signals can be used as controller inputs. The controller determines magnitude and phase of the converter voltage which are required to meet the control objectives. This desired voltage should stay within the operating capabilities of the device, Figure 4.6. The desired converter voltage is translated into set-points $\beta_{SET}$, $\gamma_{SET}$, and $E_{DC}^{set}$.

The detailed model is implemented as a Matlab function. This model is to be used mainly for transient voltage stability studies as well as for design and performance evaluation of user-defined controls. Transient voltage stability is associated in many cases with behavior of dynamic loads such as induction motors. In such studies, systems under consideration (e.g. industrial plant, sub-transmission system) are of medium size, which is consistent with Matlab simulation capabilities.

### 4.6.2. Stability Model Initialization

The transient stability model is initialized based on powerflow results. The initialization should be performed for all dynamical elements of the model: DC bus, voltage and synchronization controls, and user-defined controls. Powerflow studies determine AC-bus voltage $\bar{V}_{AC}$ and converter voltage $\bar{V}_{CV}$ at $t = 0$.

1. The steady-state voltage $E_{DC}(0)$ is determined first. Unless specified explicitly, the worst-case voltage $E_{DC}(0)$ is assumed, $E_{DC}(0) = V_{CV}/K_V$ (using (4.1) with $\beta = 0$).

2. In steady-state, the converter firing is synchronized perfectly with AC-bus voltage, $\hat{\delta}_{AC}(0) = \delta_{AC}(0)$. Then, the synchronization circuit is initialized based on the known input and output. Knowing the converter voltage phase $\delta_{CV}(0)$, the power angle set-point can be determined $\gamma_{SET}(0) = \delta_{CV}(0) - \hat{\delta}_{AC}(0)$.

3. For a Statcon, the DC voltage controller can be initialized based on known DC-bus voltage $E_{DC}(0)$ (input) and power angle set-point $\gamma_{SET}(0)$ (output). The DC voltage set-point $E_{DC}^{set}$ is also determined at this step.

4. Finally, the user-defined controls can be initialized using input (bus voltage, converter current, remote signals) and output (angles $\beta_{SET}$ and $\gamma_{SET}$) signals.

### 4.6.3. Simplified Models

Simplified models of the SVS can be used depending of the study purpose. First simplification is achieved by assuming perfect synchronization, $\hat{\delta}_{AC} = \delta_{AC}$. For a Statcon, the DC-bus dynamics and DC voltage controls can be approximated by a lower-order equivalent system

$$E_{DC} = \mathcal{G}(E_{DC}^{set}),$$

where $\mathcal{G}$ is a dynamic system. This assumes that the controller response is sufficiently fast to keep the DC voltage at a controlled value. In this case, the SVS is represented as a voltage source with controllable magnitude $V_{CV}(E_{DC})$ and phase subject to the constraint $P_{CV} = 0$.

## 4.7. Model Validation: A Case Study

The stability model has to represent correctly the fundamental components of the AC-bus voltage and the compensator current in the frequency range of interest [28]. For transient voltage stability studies, the frequency range of interest can be up to 5Hz.

The model validation studies are performed for a system depicted in Figure 4.9. First, the system is modeled using EMTP. The system rated voltage is 12.5kV. Transmission lines are modeled by R-L circuits and the load is assumed to be resistive. The system is fed by a sinusoidal AC-voltage source at bus A. The SVS (power, synchronization and control circuits) is modeled in detail as described in section 4.1.1. The fundamental components of voltage and current waveforms are computed by a phasor measurement algorithm, which includes signal transformation from a stationary ABC reference frame to a synchronous DQO reference frame and post-filtering by a moving-average filter over two electrical cycles.

The system is modeled using Matlab. The transmission network is represented by algebraic equations, and the SVS is modeled by a detailed model. All external controls are identical to those used in the EMTP model. For the purpose of this study, no user-defined controls are modeled so as not to include their effects on the model performance. Thus, all presented responses are open-loop. To account for delays in phasor computations in EMTP, phasors computed by the sta-

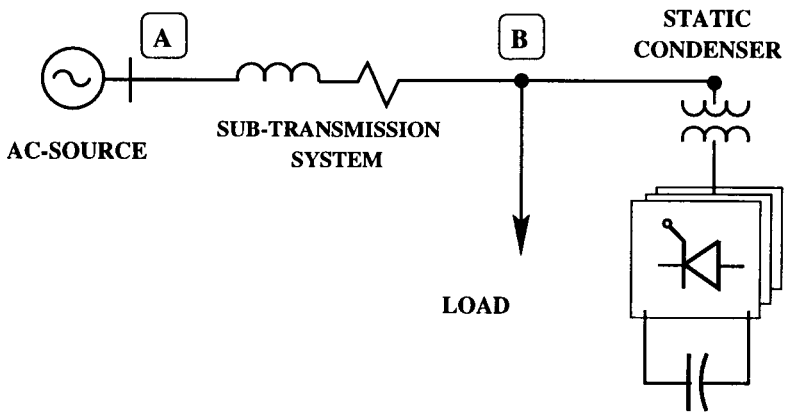


FIGURE 4.9. System used for SVS model validation studies

bility program are passed through a two-cycle moving-average filter. The simulation step used in stability studies is 1/720 sec to be consistent with sampling rates of synchronization and DC voltage controllers used in the EMTP model. A simplified model is also considered. The equivalent DC system response to a set-point $E_{DC}^{set}$ change is approximated by a discrete finite impulse response system. The active power balance equation, $P_{CV} = 0$, is added to algebraic equations representing the transmission network.

A BES-device is considered first. The DC-bus voltage is constant at 1.7 kV. The following tests are performed:

1. Step changes in converter angle $\beta$ from $30^o$ to $15^o$ and back to $30^o$.
2. Step changes in converter angle $\gamma$ from $1^o$ to $2^o$ and back to $1^o$.

The results are shown in Figure 4.10. The top plot shows angle $\beta$(solid line) and $\gamma$(broken line) set-points, $\gamma$ is multiplied by a factor of 10 for better visualization. The second plot shows ac-bus voltage responses (solid line - EMTP, broken line - stability). The bottom plot shows active power injected in the AC-bus by the BES-device (solid line - EMTP, broken line - stability model). There is a very good

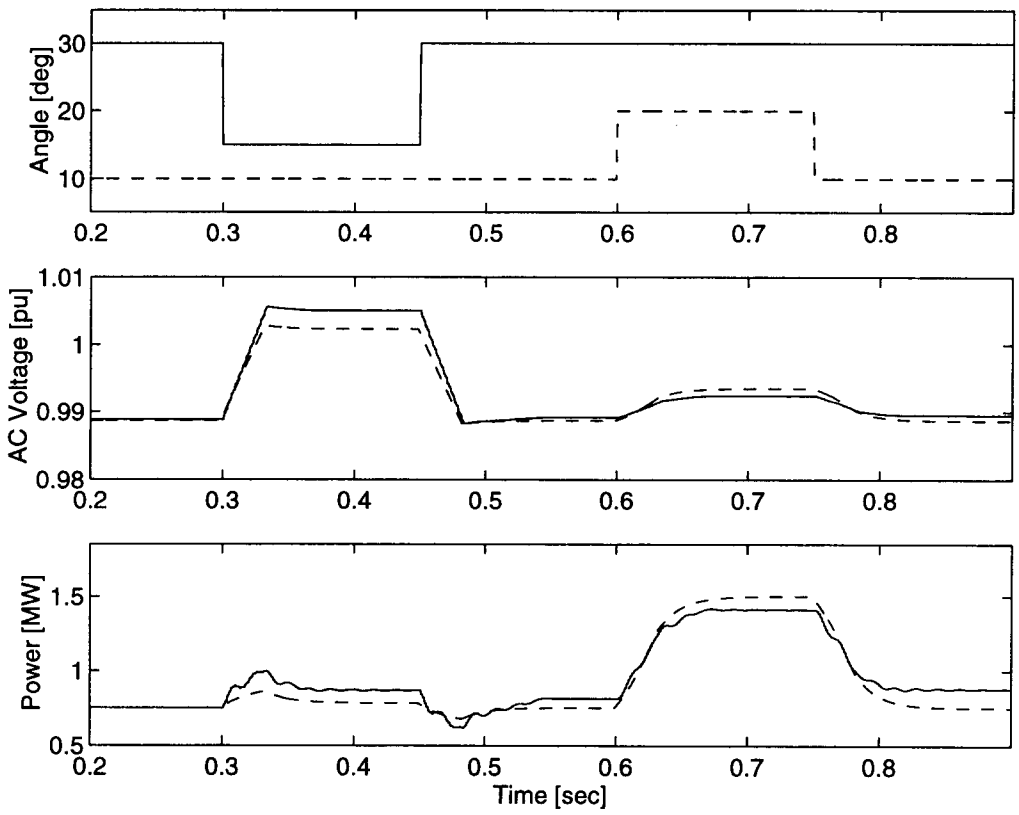


FIGURE 4.10. SVS model validation: BES-device responses

correlation between EMTP and stability model traces. In both cases, the delay in response is caused mainly by the data post-filtering and measurement delay of the transducers.

A Statcon is considered next. The test is performed for a step change in the DC voltage set-point from 1700V to 1800V and back. The results are shown in Figure 4.11. The solid lines show the EMTP-model response, the broken lines represent response of the detailed stability model and the dotted lines represent response of the simplified stability model. The first plot shows DC voltages, the second plot shows AC-bus voltages, and the bottom plot shows the reactive component of the AC current injected by the Statcon. There is a good agreement between all three models.

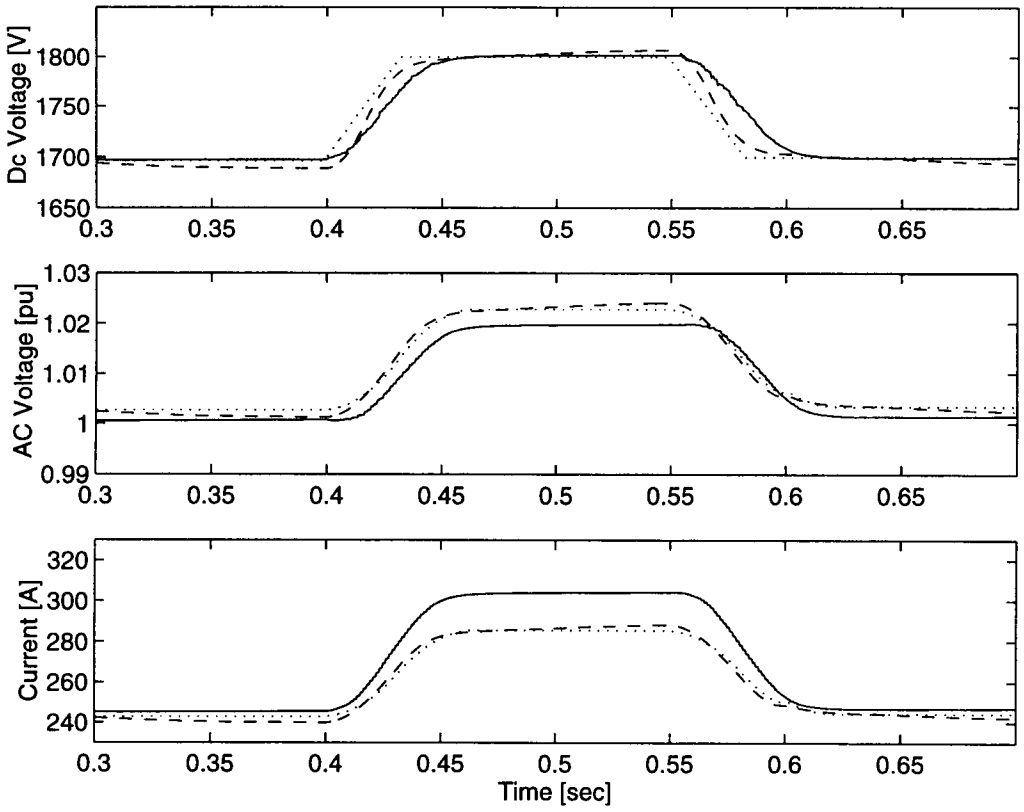


FIGURE 4.11. SVS model validation: Statcon responses

## 4.8. Conclusions

This chapter presents the SVS models for EMTP, powerflow, and transient stability studies. These models allow a power transmission engineer to evaluate the SVS performance adequately and to determine the device benefits in present and future planning projects. The developed models can be also interfaced with various user-defined controls, thus providing a tool for testing the controller effect on the device dynamic performance.

# 5. APPLICATION STUDY FOR RATING AND SIZING CONTROLLED AND CONVENTIONAL SERIES COMPENSATION

In this chapter, a procedure for planning for controlled series compensators is presented [32]. The Montana 500kV transmission system is used to illustrate the established methodology.

## 5.1. Study Objective

### 5.1.1. System Description

Figure 5.1 depicts a one-line diagram of the Montana 500kV transmission system and the underlying 230kV transmission network. This transmission system is described in detail in [34]. The power flows from the East (Colstrip) to the West (Taft, Eastern BPA area). The eastern Montana system is represented with four coal-fired thermal units at Colstrip having a total generating capacity of 2272MW (generators #1 and #2 of 358MW, generators #3 and #4 of 778MW) and a 200MW back-to-back DC link at Miles City. Power station auxiliaries at Colstrip consume 170MW of the generated power, and the net station output is about 2100MW. Upgrades of the Colstrip turbines are being considered by the participants as one means available to serve increased generation demands. The Miles City DC link adds 200MW to the generation capacities in Eastern Montana.

The Montana intertie consists of three 500kV sections: Colstrip-Broadview, Broadview-Garrison, and Garrison-Taft, each having two parallel circuits equipped with fixed series capacitors compensating approximately 35% of the corresponding

line reactance. Table 5.1 gives information on the line distances and reactances, as well as the series compensator sizes and ratings.

| | Colstrip-Broadview | Broadview-Garrison | Garrison-Taft |
|---|---|---|---|
| Transmission Lines | | | |
| Length | 185 km | 362 km | 257 km |
| Reactance | 56.0 Ω | 112.83 Ω | 84.38 Ω |
| Series Compensation | | | |
| Rated Current | 2000 A | 2000 A | 1090 A |
| Reactance | 19.6 Ω | 39.5 Ω | 26.35 Ω |
| Percentage | 35.0 % | 35.0 % | 31.2 % |

TABLE 5.1. Montana 500kV transmission system

To absorb the reactive power generated by the long 500kV transmission lines, fixed line reactors are installed on the Colstrip-Broadview and Broadview-Garrison lines and switched reactors are installed at Garrison and Taft buses. The Montana transmission system is currently rated for 2200MW power transfer as measured in the west-of-Garrison cutplane, with the potential of increasing its power loading to 3000MW by adding new facilities and uprating existing equipment [34].

### 5.1.2. Study Objective and Assumptions

For this study, it is assumed that there is a need to increase the Montana intertie loading to a level between 2200MW and 3000MW with an ultimate loading of 3000 MW. To accommodate this increase in power transfer, the 500kV transmission system will have to be upgraded. Series compensation represents an economically

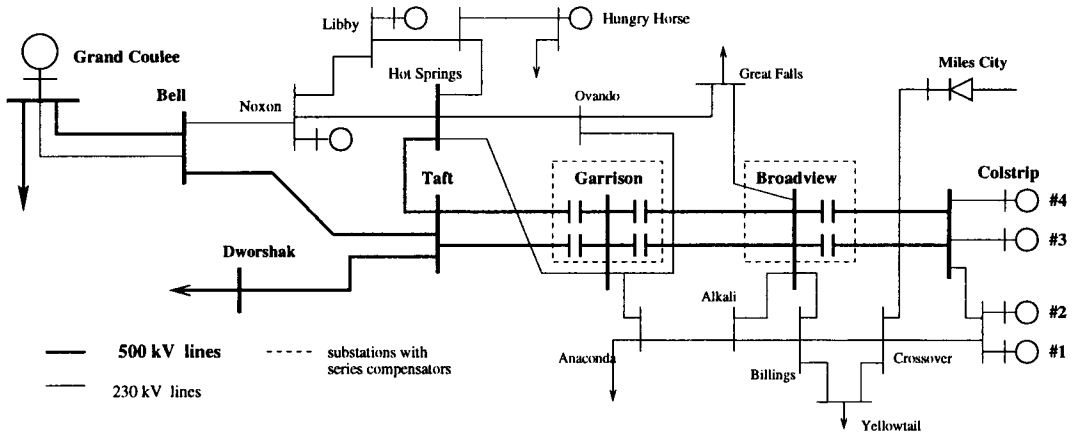


FIGURE 5.1. One-line diagram of Montana 500kV transmission system

attractive way to increase the transfer capability of long transmission lines, and is considered in this study.

The present fixed series compensation on the Montana 500kV transmission is approximately 35%. This is the system limit for conventional series capacitors without incurring subsynchronous resonance (SSR) at the Colstrip generation units [33]. Additional series compensation has to be provided by the series compensators neutral to the SSR effects. Thyrsitor-Controlled Series Compensators have characteristics in the sub-synchronous range essentially different from those of conventional fixed capacitors, and can be mitigate the SSR effects when operating in the vernier mode [33, 35, 36]. This work also can be applied to the Static Synchronous Series Compensators (SSSC) [6, 8]. Since the SSSC provides series compensation by voltage insertion at synchronous frequency only, the device is expected to be neutral to the SSR effects.

To avoid voltage reduction as the system loading is increased, shunt compensation is also reviewed. Switched reactors are installed presently at Garrison and Taft buses, and line reactors are installed on Broadview-Garrison and Colstrip-

Broadview lines. Besides maintaining a desired voltage profile, the line reactors at Broadview-Garrison are used with single-phase tripping for secondary arc extinction [37]. The line reactors are assumed to stay at their present values, unless the secondary arc extinction method is changed (e.g. a high speed ground switching scheme used at the Garrison-Taft line). To provide needed reactive power support in the system as its loading increases, bus connected shunt capacitors are considered. To utilize the time-overload characteristics of shunt capacitors, a Capacitor Series Group Shortening Scheme (CAPS) can be employed to increase capacitor reactive power output during outages and transients [38].

In this study, we consider only the transmission system between Colstrip and Taft. Higher system loadings also require transmission reinforcement west of Taft. A 500kV line from Bell to Grand Coulee is assumed to be added. In addition, series compensation is represented in the Taft-Dworshak and Taft-Bell lines.

## 5.2. Steps to Rate and Size Series Compensation

The base 2200MW power transfer capability of the Montana transmission system has been already established. In this study, the intertie power transfer capability is increased by uprating existing series capacitors and adding new series and shunt compensators as required. The following steps are taken to determine the compensation requirements:

1. Powerflow studies are conducted for the 3000MW loading to determine the minimum net series compensation which meets steady-state stability and powerflow requirements. Required shunt compensation is also determined. Line currents are determined for normal and outage conditions.

2. The sub-synchronous resonance studies are performed to determine series compensator designs neutral to the SSR conditions. The series compensation share between fixed and TCSC capacitors as well as the required TCSC X-order are determined using results of the SSR studies.

3. Fixed and TCSC capacitors are rated and sized initially based on results of the powerflow studies. TCSC control capabilities are derived for normal and outage conditions. SSSC ratings are also considered, and a comparison between the TCSC and SSSC designs is performed.

4. Transient stability studies are performed to determine whether the design meets transient stability requirements and any further revision of the equipment ratings and compensation requirements is needed.

5. The compensation requirements are determined first for the maximum expected power transfer (3000MW). Then, equipment installation and uprate sequences are developed as a function of the system loading.

## 5.3. Powerflow Studies

A two-circuit transmission section equipped with series compensation units is shown in Figure 5.2. Step-down power transformers connect the system to an underlying lower-voltage network. This circuit topology corresponds to that of each of the Montana intertie sections.

The terms "normal" and "outage" in this work refer to conditions of a transmission section depicted in Figure 5.2. Normal operation denotes conditions when both parallel lines are in service. Outage refers to the condition when only one line

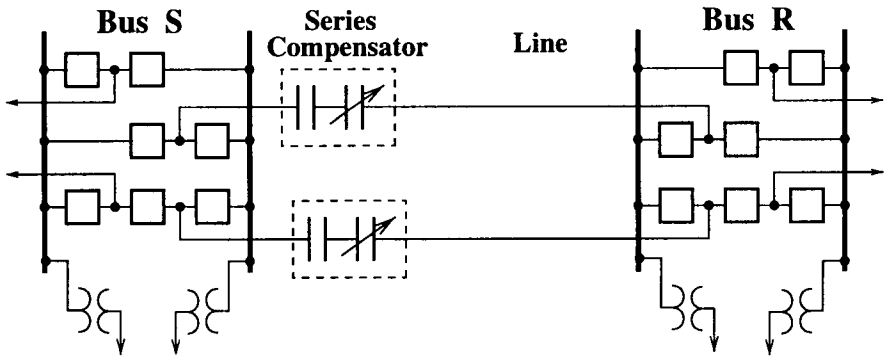


FIGURE 5.2. One-line diagram of a transmission section

is in service, and the parallel line is open. The following notations stand for various line currents:

$I_L$ : line current

$I_{nor}$ : maximum normal steady-state line current

$I_{ot}$ : maximum outage steady-state line current

$I_{sw}$ : maximum swing line current.

The maximum swing line current occurs during transient conditions with a parallel line outage. The current values (rms Amps) depend on the scheduled power loading of the transmission section.

### 5.3.1. Steady-State Stability and Powerflow Requirements

The uprated transmission system should meet the following requirements:

- Steady-state (angle and voltage) stability. A stable steady-state equilibrium must exist for all credible contingencies under consideration.

- Voltages at the section terminals should be kept within the governing limits ($500 - 550$kV for 500kV system) in both normal and outage conditions.

- System loading
  - During normal conditions, the system facilities should be loaded within their continuous capabilities with the power loading at the maximum scheduled level.
  - During outage conditions, the system can be operated within temporary overload limits of the equipment for up to 30 minutes.
  - If an outage is sustained for over 30 minutes, the system loading should be reduced, such that it is again loaded within its continuous capabilities.
- Loadings under normal and outage conditions on the underlying lower voltage system will not be increased over present loadings with a total west of Garrison schedule of 2200MW.

Criteria used in powerflow studies is illustrated in Figure 5.3. As the transmission section loading increases ($P_{total}$), the series compensation at 500kV lines and the shunt compensation at 500kV buses are also increased, such that the phase angle between voltages at sending and receiving terminals is kept at the same value, and the bus voltage magnitudes stay within the reliability limits. These criteria have to be met for both, normal and outage conditions, realizing that angles can be different for each. By meeting these criteria, the following is ensured:

- steady-state stability at higher power transfers
- increase in power transfer will occur primarily at 500kV path, and consequently there will be no addition powerflow in the underlying system
- only 500kV equipment has to be uprated.

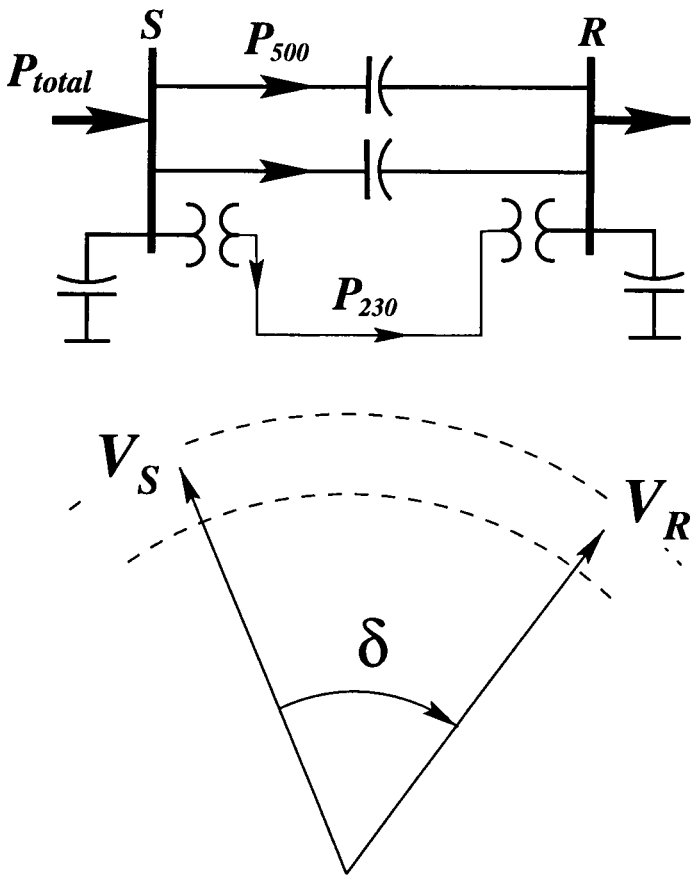


FIGURE 5.3. Powerflow criteria

### 5.3.2. Powerflow Studies of the Montana Intertie

The analysis in this paper uses as a base transient stability and powerflow results for the 2200MW transfer level. Table 5.2 gives information on the normal and outage intertie angles at this loading.

For the Garrison-Taft line, the series capacitors are not required for the outage condition and therefore are rated only for normal system current. Because the outage line current $I_{ot}$ exceeds the 30-minute overload capability, the series capacitors are bypassed. For the remaining two sections, the series capacitor ratings are adequate for both normal and 30-minute overload requirements.

| | Colstrip-Broadview | Broadview-Garrison | Garrison-Taft |
|---|---|---|---|
| Normal | $7.5^o$ | $15.8^o$ | $12.3^o$ |
| 30min Outage | $14.6^o$ | $29.8^o$ | $27.3^o$ |

TABLE 5.2. Montana intertie angles at the base 2200MW loading

As the line transfer capability is increased above 2200MW, there may be a need to uprate existing series capacitors to new loading conditions. It can be done by adding capacitor cans in parallel to the existing racks. This in turn reduces the overall compensator reactance according to:

$$X_C^{up} \times I_{rat}^{up} = X_C^{pr} \times I_{rat}^{pr}, \tag{5.1}$$

where $I_{rat}^{pr}$, $I_{rat}^{up}$ are current ratings for present and uprated capacitors respectively, and $X_C^{pr}$ and $X_C^{up}$ are reactances of present and uprated capacitors respectively. On the Broadview-Garrison line, rack space is available to increase the current rating up to 3000A. This reduces the series compensation to 23.3%. A similar adjustment is possible for the capacitors at the Colstrip-Broadview line.

Powerflow studies are performed using the BPA Powerflow program. To represent higher transfers, the data file used for the 2200MW studies is modified by reducing generation in the Pacific Northwest area and adding a 820MW hypothetical fifth unit at Colstrip. As the Montana intertie transfer increases, the intertie section angles are held to the values given in Table 5.2, and the system voltages are maintained within the allowed reliability levels.

Resulting steady-state line currents and series compensation required to meet the angle constraints are given in Table 5.3. Here the line currents obtained in

powerflow studies are rounded up, and a 200A design margin is added. The Miles City DC link is tripped by remedial actions during outages of the intertie lines west of Broadview. Because of large overvoltages on the line side of the Garrison East series compensator during Broadview-Garrison outages, the series compensation for this line is divided between the two ends by installing the new capacitor bank at the Broadview end. Figure 5.4 shows resulting series compensator installations.

| | Colstrip-Broadview | Broadview-Garrison | Garrison-Taft |
|---|---|---|---|
| Line Current, Amp | | | |
| Normal | 1800 | 1850 | 1850 |
| 30min Outage | 3150 | 3150 | 2750 |
| Series Compensation, percent | | | |
| Normal | 54.7 | 52.4 | 52.4 |
| 30min Outage | 53.9 | 51.2 | 34.8 |

TABLE 5.3. Required series compensation and line currents at 3000MW loading

If an outage exceeds 30 minutes, generation is reduced at Colstrip such that the system is loaded within its continuous capabilities. The sustained outage reduction level is easily determined using the powerflow program.

### 5.3.3. Series Compensation Requirements

Based on Table 5.3, the series compensation requirements can be specified for each intertie section. As mentioned before, the amount of fixed compensation in each line is not allowed to exceed 35%. For the conventional capacitors, the continuous current rating is selected to be the larger of either the normal line current or the

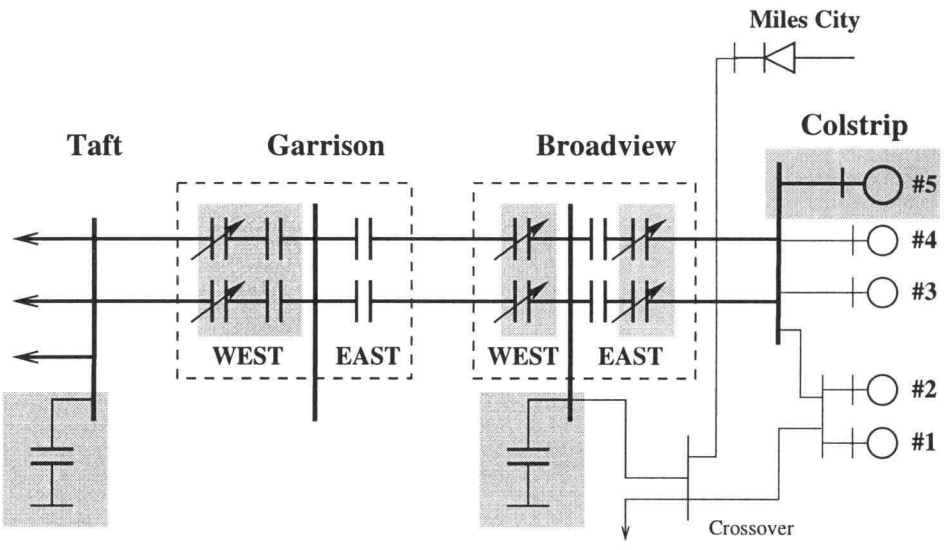


FIGURE 5.4. Equipment additions at 3000MW loading

outage current divided by 1.35 (a typical value for 30-minute overload capacitor current [22]).

**Colstrip-Broadview**

Based on Table 5.3, a continuous current rating of 2400A (max{1800A, 3150A/1.35} rounded up ) is chosen. This exceeds a previous current rating 2000A of the present fixed capacitors in the line. By filling in the racks of the existing Broadview East bank, the compensation percentage is reduced from 35.0% to 29.2% according to equation (5.1). The balance of the requirement is met by a TCSC. The TCSC may be located at the Broadview end of the line with the fixed capacitor bank.

**Broadview-Garrison**

Based on Table 5.3, a continuous current rating of 2400A is required for fixed capacitors. By filling in the racks of the existing Garrison East bank, the compensation percentage is reduced from 35.0% to 29.2%. The balance of the requirement is met by a TCSC. To provide a better voltage profile, the TCSC should be located at the Broadview end of the line (Broadview West terminal).

### Garrison-Taft

This case is different from those presented above. As noted in Table 5.3, only 34.8% compensation is needed for the outage conditions. Since the existing series capacitors are rated at 1090A only, it may be most economical to salvage this bank for use somewhere else in the BPA system and to install a new 34.8% compensation bank rated at 2100A (max{1850A, 2750A/1.35} rounded up ). Thus, the new fixed capacitor entirely meets outage compensation requirements. Since the total normal compensation must be 52.4%, a TCSC is installed to make up the difference of 17.6% rated for normal current only (1850A).

Table 5.4 shows the resulting compensation requirements for each line based on powerflow studies. The compensation percentage and ohms are net values affecting each line.

| | Colstrip-Broadview | Broadview-Garrison | Garrison-Taft |
|---|---|---|---|
| Series Compensation Percentage | | | |
| Conv. caps | 29.2 | 29.2 | 34.8 |
| TCSC Normal | 25.5 | 23.2 | 17.6 |
| TCSC Outage | 24.7 | 22.0 | 0 |
| Series Compensation Ohms | | | |
| Conv. caps | 16.35 | 32.95 | 29.37 |
| TCSC Normal | 14.28 | 26.18 | 14.85 |
| TCSC Outage | 13.83 | 24.82 | 0 |

TABLE 5.4. Net compensation requirements for conventional and TCSC capacitors

### 5.3.4. Shunt Compensation Requirements

Powerflow studies also determined shunt compensation requirements. Table 5.5 shows the new bus-connected shunt capacitors and the present bus-connected switched shunt reactors in the system.

| Shunt | Taft | Garrison | Broadview |
|---|---|---|---|
| Capacitors | 300+180 | 300+180 | 300 |
| Reactors | 225 | 3×225 | 0 |

TABLE 5.5. Present shunt reactor and new shunt capacitor installations, MVAr ratings are at 550kV

Shunt capacitor requirements may be reduced if the line-connected shunt reactors (225 MVA at each end of Broadview-Garrison lines) are switched off for disturbance and outage conditions. Powerflow studies are conducted to investigate this option. All four reactors are equipped with circuit-breakers. For the Colstrip-Broadview single line outage, both reactors at the Broadview end of the Broadview-Garrison lines are tripped. For the Broadview-Garrison single line outage, the reactors are tripped at both ends of the remaining line. For the Garrison-Taft single line outage, both reactors at the Garrison end of the Broadview-Garrison lines are tripped. This reduces shunt compensation requirements to a 180 MVAr bank at Broadview and to a 300 MVAr bank at Taft, used for normal and outage conditions. The shunt capacitor banks can be equipped with CAPS to increase the reactive power output during outages by a better use of capacitor time-overvoltage capabilities.

New equipment installations at the 3000MW loading are shown in Figure 5.4 by shadowed boxes.

## 5.4. Sub-Synchronous Resonance Studies

Sub-Synchronous Resonance studies are conducted to determine the SSR immune series compensator designs. The SSR studies are performed using EMTP. The Montana system is modeled as depicted in Figure 5.5. Colstrip generators are represented in great detail, including multi-mass shaft representation, with generator parameters given in [33]. 500kV transmission facilities (lines, series capacitors, shunt reactors, transformers) are modeled in detail from Colstrip to Taft, and the underlying 230kV system is represented by equivalent circuits to match powerflow conditions.

A comprehensive analytical study of the SSR performance in the system is reported in [33]. The analytical study determined that the sub-synchronous modes of concern are 18.2 and 20.6 Hz mechanical shaft modes of Colstrip units #3 and #4. These frequencies are most observable at the high-pressure turbine end of the shaft, and therefore this speed is used for comparison of the SSR performance. The Power System Identification Toolbox in Matlab is employed to determine modal damping ratios using Prony analysis.

The considered disturbance is tripping the Miles City DC link. First, the system is simulated under the present 2200MW loading conditions. The present 35% series compensation level is safe from the SSR standpoint, as indicated in Figure 5.6(A). These waveforms serve as a reference for the SSR study.

Next, the system is simulated under the 3000MW loading. Since the bus angles at the 3000MW loading are the same as those at the 2200MW (because of the powerflow criteria used), only the series and shunt compensation of the 500kV circuits is adjusted in the EMTP data case. Also, generator #5 is added at Colstrip, identical to the existing units #3 and #4.

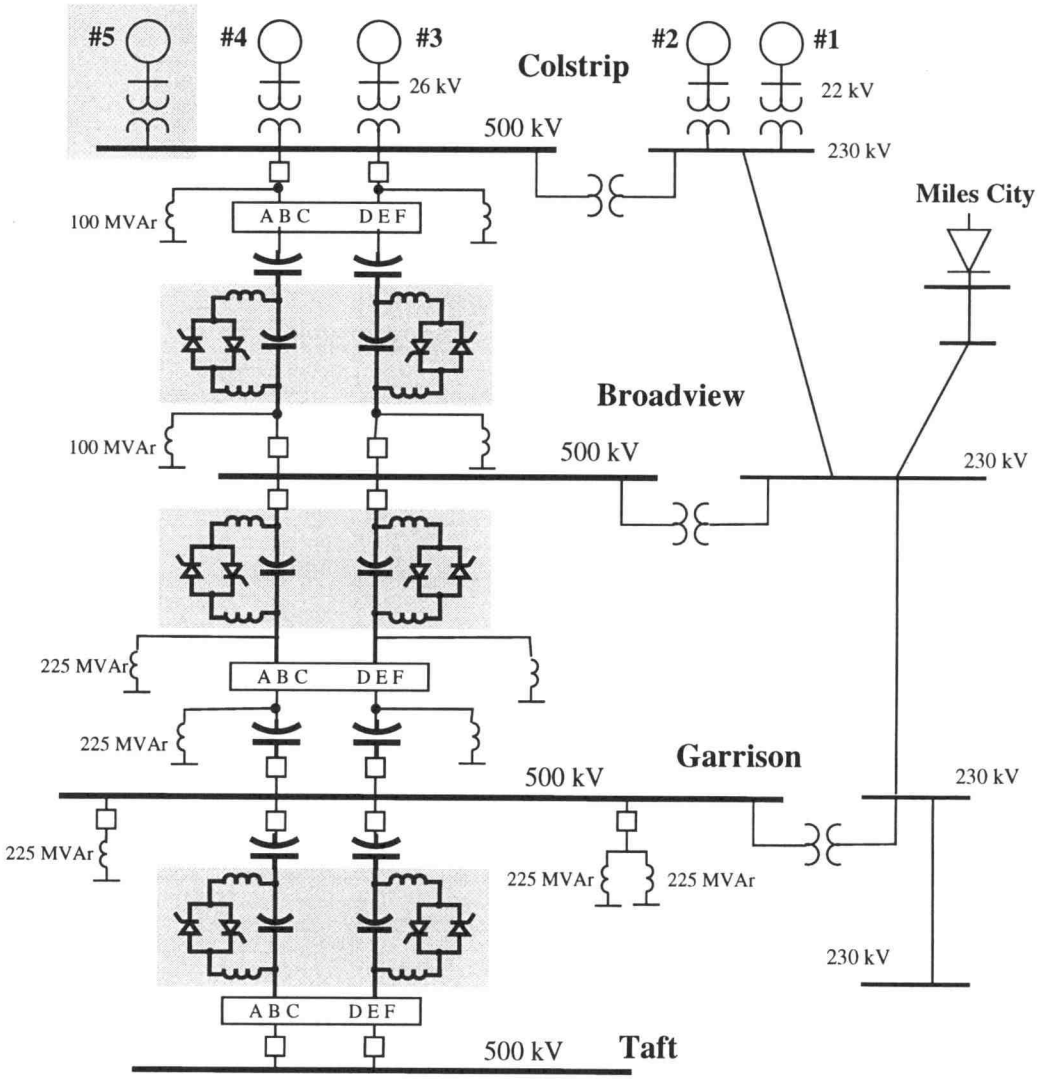


FIGURE 5.5. EMTP model of Montana system

The following series compensator designs are considered:

*Design 1:* The entire series compensation is fixed at the values given in Table 5.3. The SSR is evident, as follows from Figure 5.6(B). The resonant mode is 20.6Hz.

*Design 2:* The series compensation is a combination of fixed and TCSC capacitors, as shown in Figure 5.7. The dashed box encloses capacitors that are presently

installed in the line. For the Colstrip-Broadview and Broadview-Garrison lines, capacitors in parallel are added to uprate the existing ones. For the Garrison-Taft lines, new fixed capacitors are installed in place of present low-rated capacitors. The reminder of the series compensation requirement is made up by TCSCs. The series compensation share between fixed and controlled compensation is given in Table 5.5. The TCSC power circuits are similar to those used at the Kayenta TCSC. The TCSCs are gated at a constant firing angle $155^o$. Figure 5.6(C) demonstrates that the TCSC detunes the resonant frequency and provides excellent damping of the SSR modes.

*Design 3:* The series compensation is a combination of fixed capacitors and SSSC, as shown in Figure 5.8. The dashed box encloses fixed capacitors that are presently installed in the line. For the Colstrip-Broadview and Broadview-Garrison lines, the most economical solution is to add conventional capacitors to increase the overall fixed compensation from 29.2% to 35% (SSR limit for the fixed compensation). Added fixed capacitors are rated at 2400 Amps. For the Garrison-Taft line, new fixed capacitors are installed in place of present low-rated capacitors. The balance of the compensation requirement (5.3) is made up the SSSC. The SSSC is represented in EMTP as a type-60 controllable voltage source connected in series with the line via a coupling transformer. The SSSC is modeled as an ideal voltage source in quadrature with the line current. Figure 5.6(D) demonstrates that the SSSC is neutral to the SSR effects. This is explained by the fact that the SSSC is modeled as an ideal voltage source with zero impedance.

The studies demonstrate if the series compensation is increased only by conventional fixed capacitors, the SSR will occur. At the same time, controlled compensation such as the TCSC operating in vernier mode and the SSSC are shown to be neutral to the SSR conditions. Next, the TCSC and SSSC ratings and size

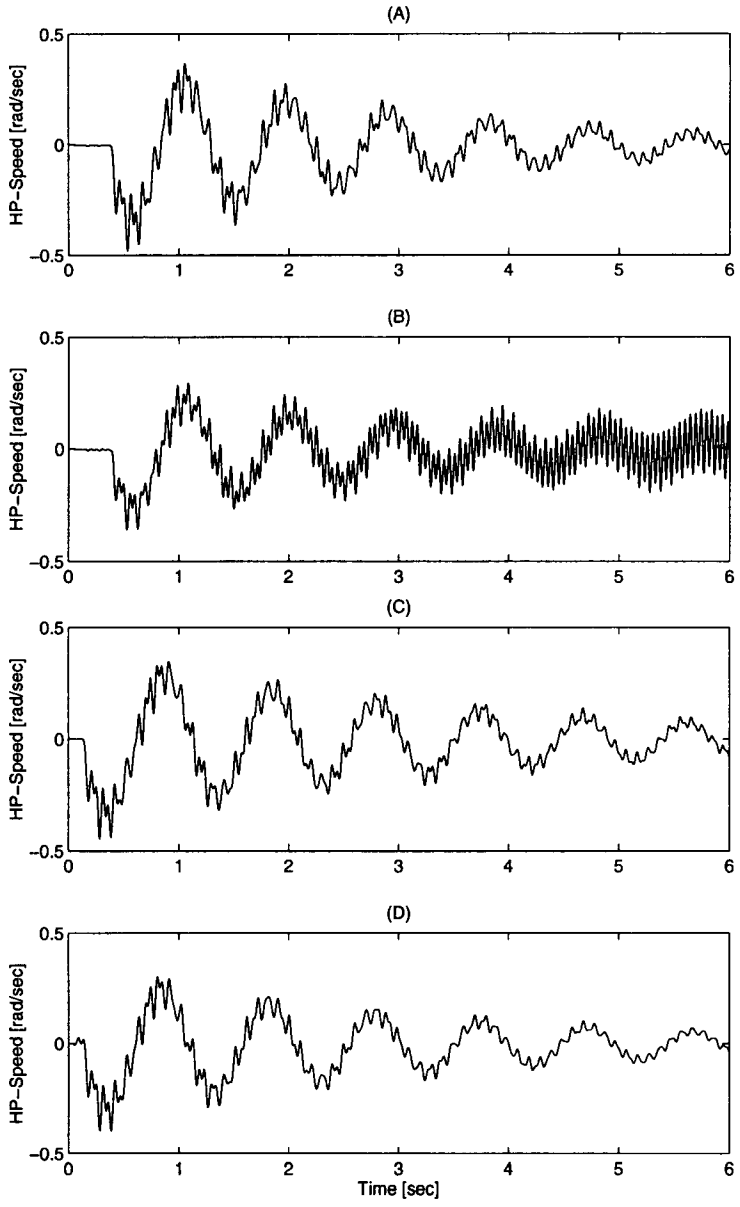


FIGURE 5.6. Speed of the high-pressure turbine end of Colstrip generator #3

will be determined, and the design with the most economical MVA ratings will be selected.

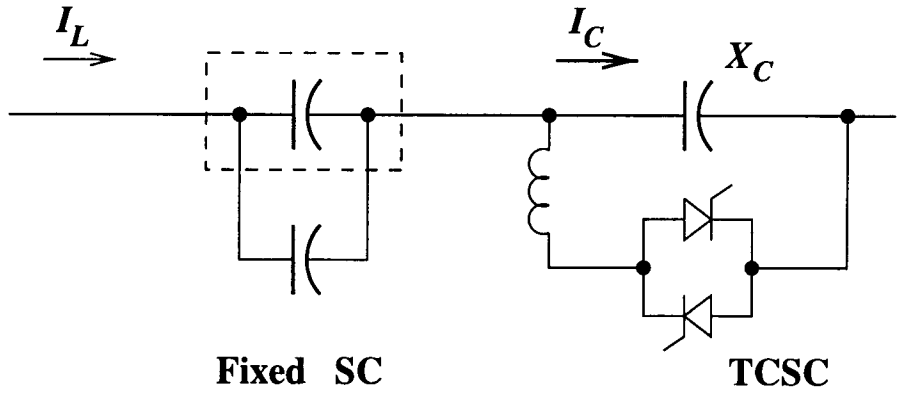


FIGURE 5.7. Series compensation unit, TCSC design

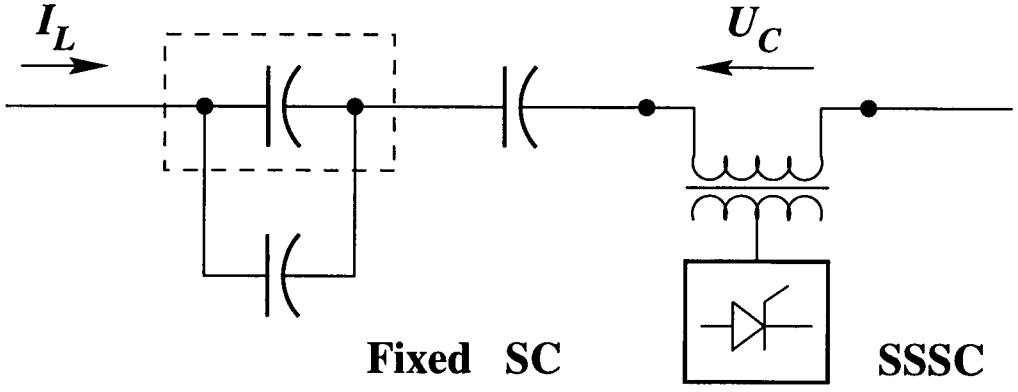


FIGURE 5.8. Series compensation unit, SSSC design

## 5.5. TCSC Ratings and Sizing

For the TCSC design, each series-compensation unit consists of both conventional fixed and thyristor-controlled capacitors, as shown in Figure 5.7. Both, fixed capacitors and TCSCs can be implemented in a multi-module structure [5, 22].

The powerflow studies give: (i)the current loading for normal and outage conditions (Table 5.3), and (ii) the TCSC net ohms required to meet the specified powerflow requirements (Table 5.5). Using results of the powerflow studies, it is

now possible to perform initial rating and sizing of the TCSC capacitor bank. Once this is done the design has to be checked to ensure that no additional requirements result from transient stability studies.

### 5.5.1. Rated Current

The rated current $I^c_{rat}$ of the TCSC capacitor bank has to meet the following requirements, recognizing that $X_{ord}$ could be chosen to be different for each case:

1. For normal steady-state conditions, the capacitor current $I_C = X_{ord}\ I_{nor}$ should stay within the continuous capabilities of the capacitors; $X_{ord}\ I_{nor} \leq I^c_{rat}$.

2. For 30-minute outage conditions, the capacitor current $I_C = X_{ord}\ I_{ot}$ should stay within the temporary 30-minute overload capabilities of the device; $X_{ord}\ I_{ot} \leq I_{temp} = 1.35\ I^c_{rat}$.

Conditions 1-2 can be expressed in terms of the rated current $I^c_{rat}$, and combined in the following inequality:

$$I^c_{rat} \geq \max\{X^{nor}_{ord}\ I_{nor};\ X^{ot}_{ord}\ I_{ot}/1.35;\ \} \tag{5.2}$$

where $X^{nor}_{ord}, X^{ot}_{ord}$ are minimum TCSC X-orders required for normal and outage conditions respectively.

For outage conditions, it is assumed initially that the TCSC X-order is needed only for the SSR avoidance, and that the X-order of at least $X_{ord} = 1.1$ is required ($X^{ot}_{ord} = 1.1$ ). For normal conditions, an additional reactance control margin of 15% is allowed for a limited power modulation control [22, 20], which results in the minimum required $X^{nor}_{ord} = 1.1\ (1.15) = 1.26$. This also provides a margin for a loop

flow control. An equation for rating conventional series capacitors is similar to (5.2), except X-orders are set to 1.0 since $I_L = I_C$.

TCSC rated currents are computed according to (5.2) using results of powerflow studies presented in Table 5.3. Since the Garrison West TCSCs are bypassed during outages, their rated current is computed for the normal conditions only. For the remaining TCSCs, the rated currents must be adequate for both normal and outage conditions. Current ratings and ohmic size (determined in the next section) of conventional and TCSC capacitors are given in Table 5.6. The values are amps and ohms of the capacitor banks only.

| Capacitor Bank | Type | Amps | Ohms | MVAr |
|---|---|---|---|---|
| Broadview East | Conv(Uprated) | 2400 | 16.35 | 283 |
| Broadview East | TCSC | 2600 | 12.57 | 255 |
| Broadview West | TCSC | 2600 | 22.56 | 458 |
| Garrison East | Conv(Uprated) | 2400 | 32.95 | 570 |
| Garrison West | Conv | 2100 | 29.37 | 389 |
| Garrison West | TCSC | 2350 | 13.5 | 224 |

TABLE 5.6. Series capacitor bank ratings and ohms

### 5.5.2. TCSC Control Capability Characteristic

Based on the TCSC capacitor rated current, the device control capability characteristic are derived for the capacitive vernier mode. TCSC X-order versus line current characteristics are shown in Figure 5.9 for the Colstrip-Broadview TCSC. The solid line shows continuous capability characteristic, and the broken line represents temporary (30-minute) overload capability characteristic. The TCSC X-order

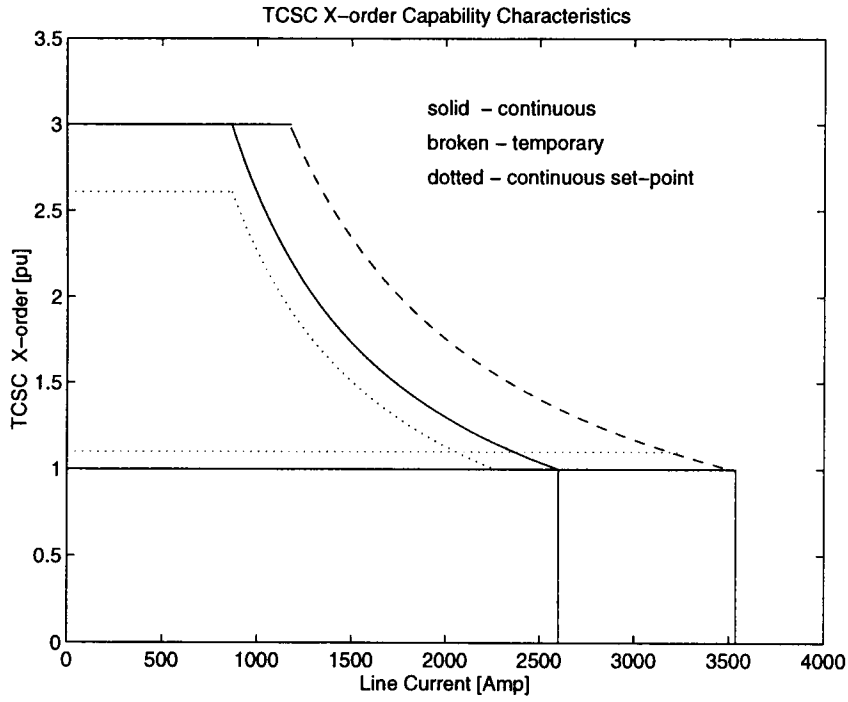


FIGURE 5.9. TCSC X-order capability characteristics: continuous and 30-minute overload

should stay within the continuous operating region during the normal conditions, and can rise to the 30-minute overload region during outages. To account for the 15% margin allowed for modulation and powerflow controls, the X-order set-point during the normal conditions is constrained to a smaller region shown by dotted line. To meet the SSR requirement, the X-order should be greater than 1.1, $X_{ord} \geq 1.1$.

For a given line current, the X-order control range can be determined using Figure 5.9. Knowing the line currents at the 3000MW loading ( Table 5.3), the TCSC control range is determined for normal and outage conditions, and presented in Table 5.7. Two numbers are specified for the normal continuous conditions: the first one is the total X-order range including the margin for modulation and loop flow controls, and the second number is the X-order set-point.

| TCSC | Continuous | 30-min Overload | |
|---|---|---|---|
| Capacitors | Normal | Normal | Outage |
| Broadview East | 1.44/1.25 | 1.95 | 1.10 |
| Broadview West | 1.40/1.22 | 1.89 | 1.10 |
| Garrison West | 1.26/1.10 | 1.70 | Bypassed |

TABLE 5.7. X-order control range at 3000MW loading

### 5.5.3. TCSC Capacitor Bank Sizing

Based on the minimum required TCSC net reactances given in Table 5.4 and the available TCSC X-orders in Table 5.7, the reactance $X_C$ of TCSC capacitors can be determined. $X_C$ should be such that with available X-orders the TCSC net reactances $X_{net} = X_{ord}X_C$ meet the net compensation requirements given in Table 5.4 for normal and outage conditions. X-orders can be different for normal and outage conditions, and should stay within the respective control ranges given in Table 5.7.

Let us illustrate the sizing procedure using the Broadview East TCSC as an example. The minimum TCSC net reactance required for outage conditions is 13.83Ω (Table 5.4). The X-order for outage conditions is 1.1 (Table 5.7). Then, the reactance $X_C$ of TCSC capacitors should be at least $X_C = 12.57\Omega = 13.83/1.1$. A smaller ohmic value requires a larger X-order and also increases the device current rating. The minimum TCSC net reactance required for normal conditions is 14.28Ω. The X-order set-point of $1.14 = 14.28\Omega/X_C = 12.57\Omega$ is needed to meet this requirement. This X-order is within the TCSC control range from 1.1 to 1.25. Thus, $X_C = 12.57$ is selected as the reactance of Broadview East TCSC capacitors.

Reactances of other TCSC capacitors are determined similarly, and are given in Table 5.6. TCSC capacitor MVAr ratings are computed based on the current ratings and the ohmic size, and presented in Table 5.6. This sizing and rating procedure allows to select the TCSC capacitor bank with the most economical MVAr ratings.

## 5.6. Solid-State Series Compensation Ratings

For the SSSC design, each series-compensation unit consists of conventional fixed capacitors and SSSC units, as shown in Figure 5.8. The SSSC sizing and rating is performed initially based on the powerflow requirements determined in section (5.3).

Table 5.8 presents line currents and SSSC voltages during normal and outage conditions.

| Section | Colstrip-Broadview | Broadview-Garrison | Garrison-Taft |
|---|---|---|---|
| Line Current, Amp | | | |
| Normal | 1800 | 1850 | 1850 |
| Outage | 3150 | 3150 | 2750 |
| Compensation Voltage, V | | | |
| SSSC | Broadv.East | Broadv.West | Garr.West |
| Normal | 19,900 | 36,350 | 27,480 |
| Outage | 33,350 | 57,600 | 0 |

TABLE 5.8. Line currents and SSSC voltages

Unlike the TCSC, the SSSC does not have 30-minute overcurrent and overvoltage capabilities, hence, the device continuous ratings should meet both, normal and outage powerflow requirements.

Table 5.9 gives the SSSC current, voltage and MVAr ratings. Currents and voltages are given per phase, and MVArs are for three-phases.

| Compensator | Type | Amps | Volts | MVAr |
|---|---|---|---|---|
| Broadview East | SSSC | 3150 | 33,350 | 316 |
| Broadview West | SSSC | 3150 | 57,600 | 545 |
| Garrison West | SSSC | 2600 | 27,480 | 215 |

TABLE 5.9. SSSC ratings

Table 5.10 gives the fixed capacitor ratings for the SSSC design.

| Capacitor Bank | Type | Amps | Ohms | MVAr |
|---|---|---|---|---|
| Broadview East | Conv(Uprated) | 2400 | 16.35 | 283 |
| Broadview East | Conv(Added) | 2400 | 3.25 | 56 |
| Broadview West | Conv(Added) | 2400 | 6.55 | 113 |
| Garrison East | Conv(Uprated) | 2400 | 32.95 | 570 |
| Garrison West | Conv | 2100 | 29.37 | 389 |

TABLE 5.10. Series capacitor bank ratings and ohms, SSSC design

Comparison of the TCSC (Table 5.6 ) and SSSC (Table 5.9 and 5.10) designs shows that the latter requires additional 169 MVA of fixed compensation and 139 MVA of controlled compensation. Assuming similar price for TCSC and SSSC, the TCSC design is more economical. Also, the TCSC has several advantages over

the SSSC from transient stability viewpoint. The TCSC capacitors have significant transient overvoltage and overcurrent capabilities, while the GTO-based devices only have moderate transient overcurrent ratings. The TCSC is a single-phase device, while the SSSC is a three-phase device, exchanging active power among three phases to keep DC-bus voltage constant. In the considered system, Broadview-Garrison and Garrison-Taft lines use single-pole tripping for single phase-to-ground faults, and the SSSC performance can be significantly reduced during such severe unbalanced conditions. Thus, the TCSC design is chosen in this study.

## 5.7. Transient Stability Studies

Finally, the design is tested under transient conditions to determine whether the TCSC current ratings are adequate for maximum swing currents and the TCSC ohms meet compensation requirements for transient stability.

The system has to meet the following stability requirements:

- First swing stability. The stability margin should be the same or exceed that in the present system.
- Transient swings should have positive damping.
- Equipment should be loaded within its transient overload capabilities.
- For the first contingency disturbance, bus voltages should meet the WSCC reliability criteria: the maximum voltage dip is 25%, not exceeding 20% for more than 20 cycles.

System planning studies use a concept of a "three-phase fault umbrella," i.e. if the system can maintain stability following a severe three-phase fault, then it will

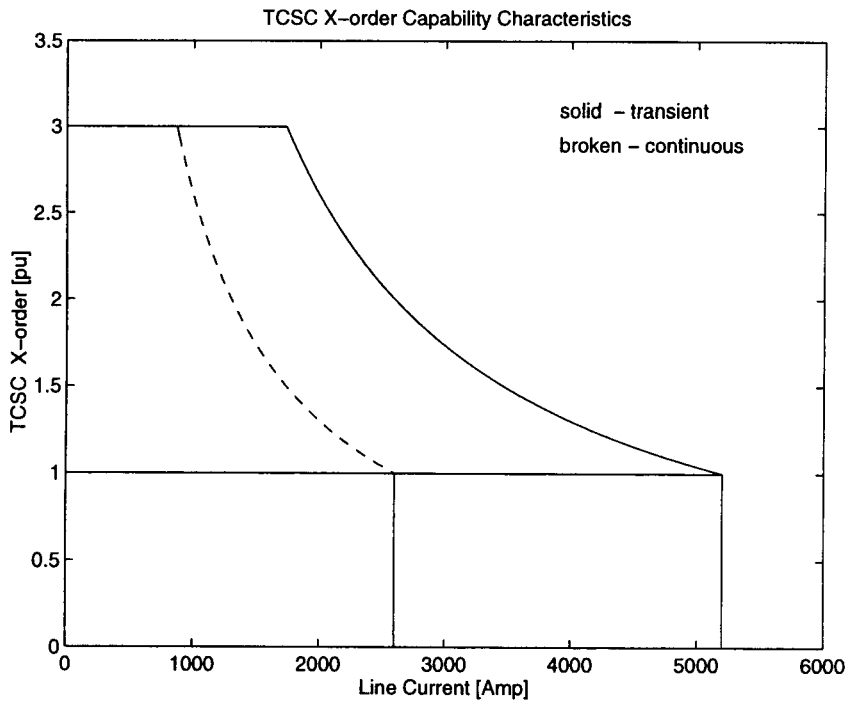


FIGURE 5.10. TCSC X-order transient overload capability characteristic

be stable for less severe disturbances, including the majority of multi-contingency disturbances. The considered single contingency disturbances include three-phase faults on the 500kV lines with normal 4 cycle clearing. The first swing stability margin requirement implies that no generation tripping is needed at Colstrip for stability reasons in addition to that tripped presently for the same faults. Thus, the remedial actions presently used at 2200MW loading are retained. Added remedial actions include insertion of bus-connected shunt capacitors for the post-disturbance voltage requirements, and tripping line-connected shunt reactors on the Brodaview-Garrison lines.

The TCSC X-order versus line current transient (10-second) overload capability characteristic is shown in Figure 5.10 by solid line for the Colstrip-Broadview TCSC. Dashed line represent continuous loading curve.

To utilize full transient overload capabilities of TCSC capacitors, the device should be equipped with a transient stability controller. An open-loop preprogrammed transient stability control is used here [5]. Following a fault clearing, the TCSC X-order is set to a pre-selected transient value, which has to stay within the device transient overload capabilities defined in Figure 5.10. After 10 seconds, X-order is reduced to stay within 30-minute overload characteristic (Figure 5.9, Table 5.7). This reduction is performed gradually to prevent adverse effects on stability.

The intertie section is called "disturbed," if one of the parallel 500kV lines at this section is open during transient swings. "Normal" refers to conditions when both lines are in service. There is a significant difference between line currents during disturbed and normal conditions and, consequently, different X-orders can be used to maximize utilization of the TCSC transient overload capabilities. Thus, TCSCs on the normal sections pick up the overall compensation burden from the TCSCs on the disturbed sections, thus improving the first swing stability.

Transient stability studies are performed using the BPA Transient Stability Program (TSP). The stability data file used for 2200MW loading studies is modified by adding the fifth unit at Colstrip. The stability data file includes description of the entire WSCC system, 4576 buses and 788 machines. The line currents are given in Table 5.11 for normal and disturbed conditions. These currents stay within the capacitor transient ratings determined from Table 5.6. The X-order set-points used in swing studies are determined using Figure 5.10, and are shown in Table 5.11.

**Garrison-Taft three-phase fault.** The three-phase fault is applied at the Garrison end of the Garrison-Taft line #1. Series capacitors at the faulted line are bypassed. The fault is cleared at the Garrison end at 3 cycles and at the Taft end at 4 cycles. The bus reactors at Garrison are tripped at 6.5 cycles, and the line reactors

| Section | Colstrip-Broadview | Broadview-Garrison | Garrison-Taft |
|---|---|---|---|
| Line Swing Current, Amp | | | |
| Normal | 2300 | 2300 | 2200 |
| Disturbed | 4200 | 4200 | 3700 |
| Transient X-order set-point, per unit | | | |
| TCSC | Broadv.East | Broadv.West | Garr.West |
| Normal | 2.25 | 2.25 | 1.90 |
| Disturbed | 1.23 | 1.23 | 1.13 |

TABLE 5.11. Line swing current and TCSC transient X-order set-points

(Garrison end only) on both Broadview-Garrison lines are tripped at 6.5 cycles. The Miles City DC link is tripped at 11 cycles. The TCSC X-order set-points are set to the transient values at 6 cycles.

Figure 5.11(a) shows transient rotor angle swings of the Colstrip and Western Montana hydro units with respect to the Grand Coulee. The system has sufficient first-swing stability margin and good natural damping; transient swings are stable and well-damped within 5 seconds. Figure 5.11(b) shows the intertie bus voltage swings. The intertie voltages stay within the WSCC reliability criteria limits.

**Broadview-Garrison three-phase fault.** This is the most severe intertie fault. The three-phase fault is applied at the Broadview end of the Broadview-Garrison line #1. TCSCs at the Broadview end are bypassed. The fault is cleared at the Broadview end at 3 cycles and at the Garrison end at 4 cycles. The bus reactors at Garrison are tripped at 6.5 cycles, and the line reactors in the remaining

Broadview-Garrison line #2 are tripped at 6.5 cycles at both ends. The Miles City DC link is tripped at 11 cycles. The TCSC X-order set-points are set to the transient values at 6 cycles.

Presently, the Colstrip unit #1 is tripped by remedial actions for this fault. Utilizing the TCSC transient overload capability increased the first swing stability margin so that tripping Colstrip #1 can be avoided for the first swing stability.

Figure 5.12(a) shows transient rotor angle swings of the Colstrip and Western Montana hydro units angle swings with respect to Grand Coulee. Figure 5.12(b) shows the intertie bus voltage swings.

## 5.8. Installation Sequence

A sequence of uprating existing series capacitors and of installing new fixed capacitors and TCSCs is developed as a function of the system loading. Powerflow studies are conducted for intertie loading from 2200MW to 3000MW in steps of 200MW. The net series compensation meeting powerflow requirements is determined for each power loading, for both normal and 30-minute outage conditions.

The TCSC installation may proceed in discrete steps. Generally, it is recommended to have from 4 to 6 TCSC modules [5, 22, 20]. The required compensation for 3000MW can be divided into 4 to 6 steps, and each module is added when it is required by increased power transfer. Each module is installed at the final full load rating to avoid retrofit of TCSC modules as loading increases. For the fixed capacitors, parallel cans can be filled in the racks as needed, and new segments can be added. Figures 5.13 and 5.14 can be used to determine the addition of discrete capacitor modules as loading increases.

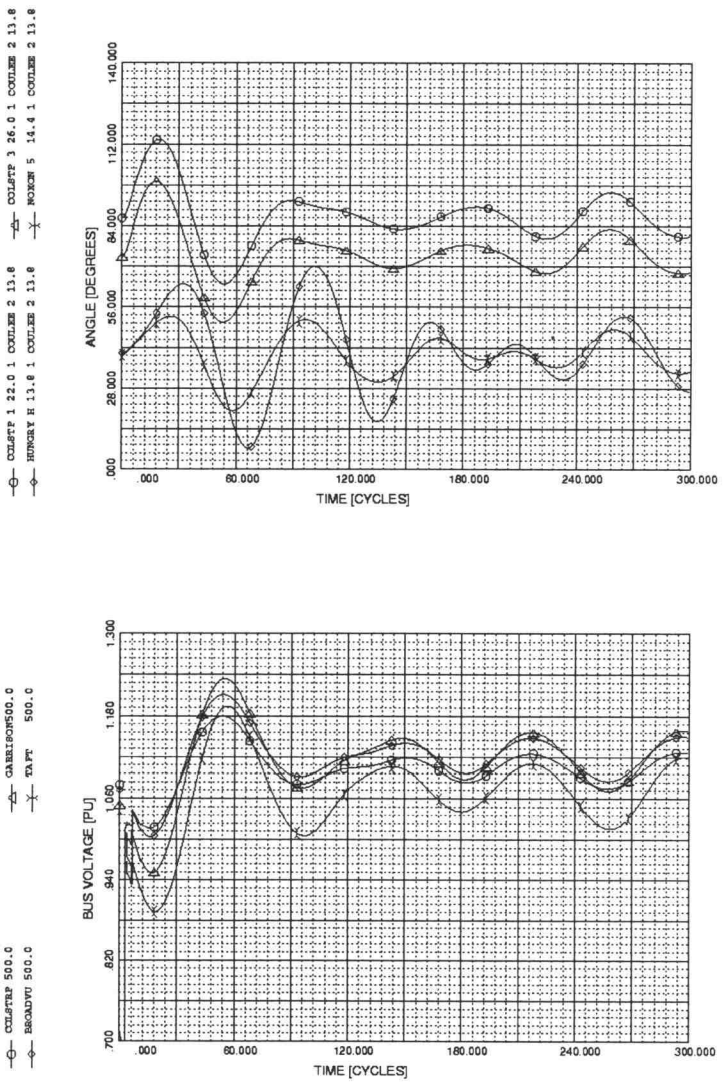


FIGURE 5.11. System transient following Garrison-Taft three-phase fault

### Colstrip-Broadview

The required series compensation as a function of the system loading is presented in Figure 5.13(a) for both normal and outage conditions. From powerflow studies for each transfer level, the normal and outage line currents are determined and used to compute the current ratings for the fixed capacitors. The rated current of uprated

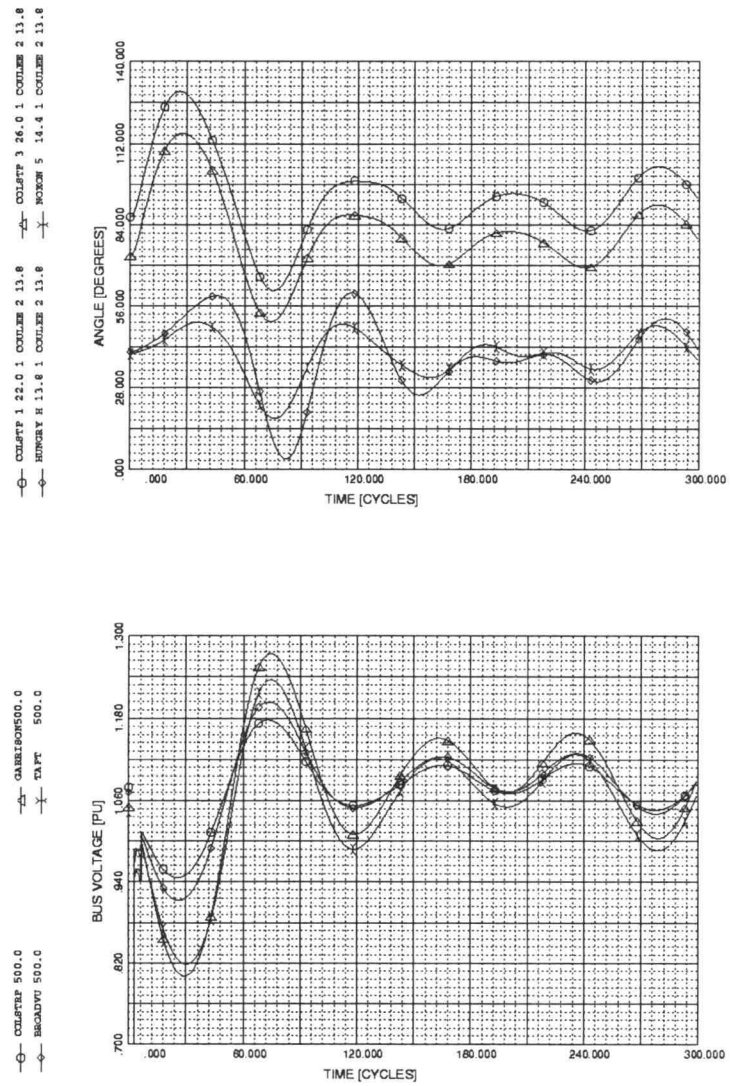


FIGURE 5.12. System transient following Broadview-Garrison three-phase fault

fixed capacitors is plotted versus the system loading in Figure 5.13(b). The installed TCSCs are rated at the full load current given in Table 5.6. When uprating fixed capacitors to values given in Figure 5.13(b), the fixed series compensator reactance is reduced according to (5.1). The compensation percentage of fixed capacitors after they are uprated is plotted in Figure 5.13(c). The balance of the requirement is made

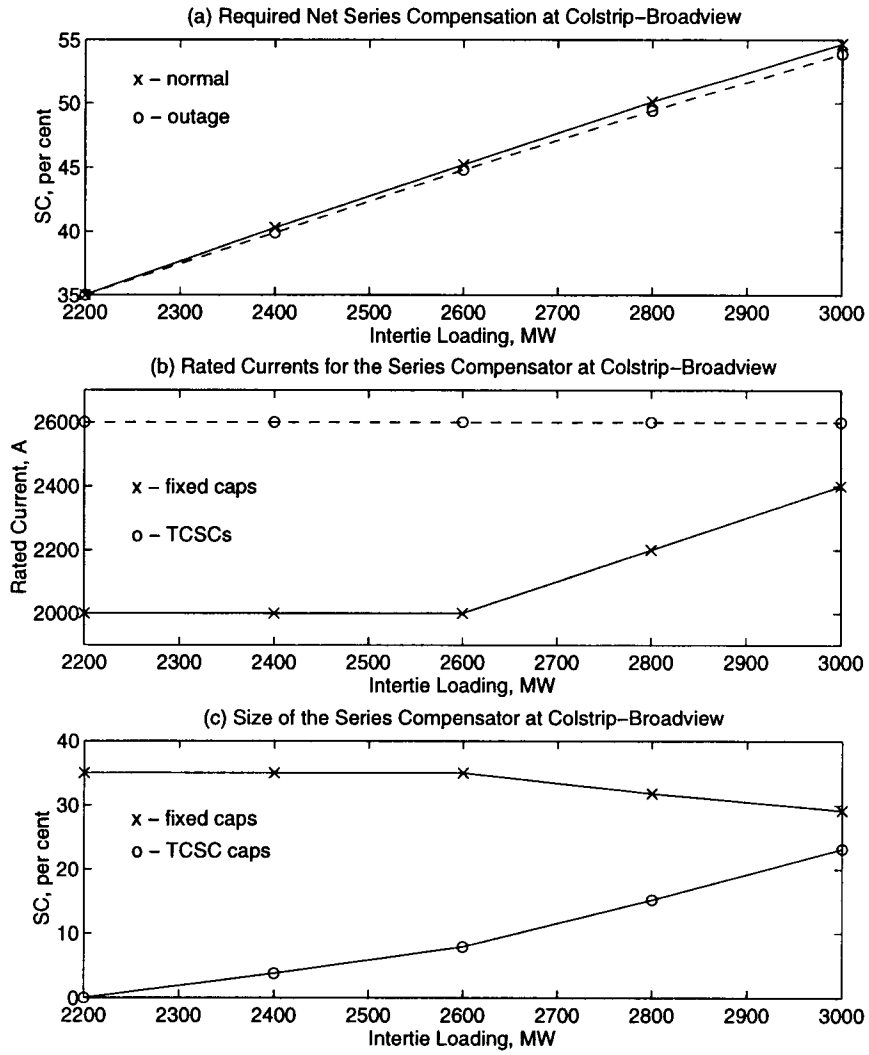


FIGURE 5.13. Installation sequence at Colstrip-Broadview

up by the TCSCs. The required reactance $X_C$ of TCSC capacitors is determined, and its percentage of line ohms is plotted in Figure 5.13(c).

**Broadview-Garrison**

The installation and uprate sequences for this line are similar to those presented for the Colstrip-Broadview line.

**Garrison-Taft**

This case is somewhat different from the one presented above. Figure 5.14(a) shows

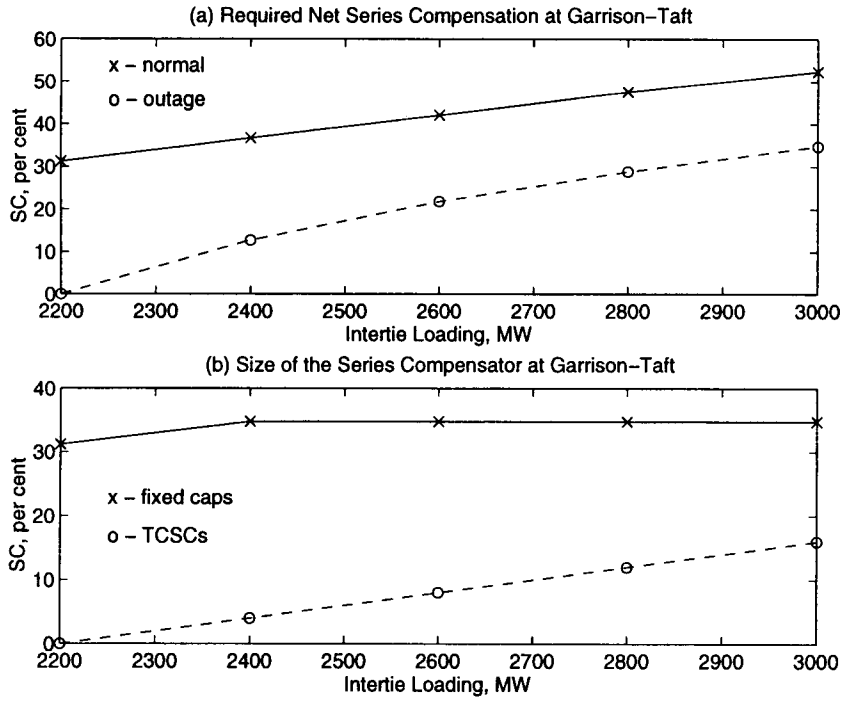


FIGURE 5.14. Installation sequences at Garrison-Taft

compensation requirements for normal and outage conditions. The outage requirement remains below 35%, so that it can be met entirely by fixed compensation, and TCSCs are required only for normal conditions. A suggested approach is to replace the present low rated fixed banks with new fixed banks at full current rating and to add TCSC modules at full normal system rating to meet the increasing normal compensation requirement. Fixed capacitor and TCSC current ratings are given in Table 5.6. The required fixed and TCSC reactances are determined and their percentage of line ohms are given in Figure 5.14(b).

## 5.9. Conclusions

This chapter presents a step-by-step procedure for rating and sizing controlled series compensation. It is assumed that the power transfer from Montana

to Pacific Northwest has to be increased from 2200MW to 3000MW, and that the series compensation is chosen as a means of increasing the transfer capability in the system.

First, powerflow studies are conducted to determine required system reinforcements at the ultimate 3000MW loading. Poweflow studies determined the net series compensation requirements and transmission line currents at the increased loading. Studies determined that the current ratings of the existing fixed capacitors have to be increased to meet higher loading conditions, and the uprate procedure for the capacitor banks is presented.

Next, the SSR studies are performed to determine which series compensator designs are neutral to the sub-synchronous interactions between the compensator and the Colstrip generators. The studies showed that if the series compensation is increased only by conventional fixed capacitors, the SSR will occur in the system. At the same time, controlled compensation such as the TCSC operating in vernier mode and the SSSC are shown to be SSR neutral.

Series compensation share and equipment ratings for the TCSC and SSSC designs are determined based on powerflow and SSR studies. The TCSC design is more economical and has technological advantages over the SSSC in the considered application. Thus, the TCSC design is chosen in this application. Transient stability studies are performed for the TCSC design and confirmed equipment ratings and size. Multi-module TCSC realization is proposed and equipment installation sequence is developed related to the system loading.

This study provides an example of selection, sizing and rating of controlled series compensation, and is a useful reference for similar transmission planning projects.

# 6. CONCLUSIONS

The dissertation addresses planning issues for controllable network devices. Controllable network devices represent the effective means of improving the system stability, and their deployment allows better utilization of the existing transmission facilities and can help to avoid or at least to delay construction of new transmission lines.

The fundamental concepts of transient angle controllability are presented first in this dissertation. A transmission network with controllable network devices (series and shunt compensators, braking resistors) is considered, and the compensation effect on parameters of the transmission system and the multi-machine swing equation is derived. The controls affect transmission system parameters non-linearly and that the parameters of the swing equation are finite for any control value in most practical cases. Next, the controllability results are presented for a two-machine multi-bus system with controllable network devices. The presented results apply to series and shunt compensators as well as braking resistors. The novel approach taken in the dissertation allows to quantify controllability and to relate it to the device type, size, and location in the power transmission network. The main results are obtained under very non-restrictive practical assumptions.

The developed concepts of transient angle controllability can be extended to a multi-machine power system. The first step is made in this direction by showing how parameters in a multi-machine swing equation depend on the device compensation. From a practical standpoint, it will be more useful to consider output instead of state controllability, when generators states are projected on lower dimensional sub-space, representing dynamics of interest, e.g. inter-area swings.

Transient stability controllers are used to maximize the device effect on transient angle stability enhancement, and their functional structure is considered next. The proposed structure of a transient stability controller includes: operating characteristic, control law, and restraint characteristic. The operating characteristic performs on-line stability assessment and disturbance severity classification to activate the controller. The control law determines the compensation policy required to meet the specified control objectives. The restraint characteristic disables the controller based on the system dynamic performance and device transient overload ratings. Design requirements for each of the controller components are specified, and examples of the controller designs are discussed.

Emerging technologies such as Thyristor-Controlled Series Compensators and Synchronous Voltage Sources offer superior control capabilities and performance characteristics as compared to conventional compensators. Unlike conventional compensators, the new controllable network devices are very complex dynamical systems and require more comprehensive modeling for time-domain studies and controller designs. Detailed models of a Thyristor-Controlled Series Compensator and a Synchronous Voltage Source for powerflow, transient stability, and electro-magnetic transient studies are derived in this dissertation. These models allow power system engineers to perform more accurate evaluation of the device effect on the system dynamic performance, and to design better controllers.

Finally, a planning study for increasing power transfer capability of the Montana transmission system is presented. The study assumes that the power transfer from Montana to Pacific Northwest has to be increased from 2200MW to 3000MW, and that the series compensation is chosen as a means of increasing the transfer capability in the system. First, powerflow studies are conducted to determine net series compensation requirements and transmission line currents at the ultimate 3000MW

loading. The studies determined that the current ratings of the existing fixed capacitors have to be increased, and the uprate procedure for the capacitor banks is presented. Next, the SSR studies are performed to determine the series compensator designs neutral to the sub-synchronous interactions between the compensator and the Montana generators. The studies demonstrated danger of the SSR conditions if the series compensation is increased using only conventional fixed capacitors. At the same time, controlled series compensators such as the TCSC operating in vernier mode and the SSSC are shown to be SSR neutral. Series compensation share and equipment ratings for TCSC and SSSC designs are determined based on powerflow and SSR studies. The TCSC design is more economical and has technological advantages over the SSSC in the considered application. Thus, the TCSC design is chosen in this application. Transient stability studies are performed for the TCSC design and confirmed equipment ratings and size. Multi-module TCSC realization is proposed and equipment installation sequence is developed related to the system loading. This study provides an example of selection, sizing and rating of controlled series compensation required to meet a variety of design and performance considerations, and is a useful reference for similar transmission planning projects.

## BIBLIOGRAPHY

[1] Institute of Electrical and Electronics Engineers, *IEEE Standard Dictionary of Electrical and Electronics Terms,* New York, 1988.

[2] E.W.Kimbark, "Improvement of System Stability by Switched Series Capacitors," *IEEE Transactions on Power Systems and Apparatus,* vol.85, pp.180-188, 1966.

[3] R.M.Maliszewski, B.M.Pasternack, H.N.Scherer Jr., M.Chamia, H.Frank, L.Paulsson, "Power Flow Control in a Highly Integrated Transmission Network," CIGRE paper 37-303, 1990.

[4] N.Christl, R.Hedin, K.Sadeck, P.Lutzelberger, P.Krause, S.McKenna, A.Montoya,D.Torgerson, "Advance Series Compensation (ASC) with thyristor-controlled impedance," CIGRE, paper 14/37/38-05, 1992.

[5] J.Urbanek, R.J.Piwko, E.V.Larsen, B.L.Damsky, B. Furumasu, W.A.Mittelstadt, J.D.Eden, "Thyristor Controlled Series Compensator Prototype installation at the Slatt 500 kV Substation," *IEEE Transactions on Power Delivery* vol.8, pp.1460-1469, 1993.

[6] L.Gyugyi, C.D.Schauder, K.K.Sen, "Static Synchronous Series Compensator: A Solid State Approach to the Series Compensation of Transmission Lines," presented at 1996 Winter IEEE Power Engineering Society Meeting, paper 96 WM 120-6 PWRD, 1996.

[7] E.Larsen, N.Miller, S.Nilsson, S.Lindgren, "Benefits of GTO-based Compensation Systems for Electric Utility Applications," *IEEE Transactions on Power Delivery,* vol.7, pp.2, October 1992.

[8] L.Gyugui, "Dynamic Compensation of AC Transmission Lines by Solid-State Synchronous Voltage Sources," *IEEE Transactions on Power Delivery,* vol.9, pp.904-911, April 1994.

[9] C.Schauder, M.Gernhardt, E.Stacey, T.Lemak, L.Gyugyi, T.W.Cease, A.Edris, "Development of a ±100 MVAr Static Condenser for Voltage Control of Transmission System," *IEEE Transactions on Power Delivery,* vol.10, pp.1486-1496, July 1995.

[10] L.H.Walker, "10-MW GTO Converter for Battery Peaking Service," *IEEE Transactions on Industry Applications,* vol.26, pp.63-72, January/February 1990.

[11] M.Shelton, P.Winkelman, W. Mittelstadt, W.Bellerby, "Bonneville Power Administration 1400 MW Braking Resistor", *IEEE Transactions on Power Systems and Apparatus*, vol. 94, pp.602-611, 1975.

[12] L.Gyugyi, C.D.Schauder, S.L.Williams, T.R.Rietman, D.R.Torgrson, A.Edris, "The Unified Power Flow Controller: A New Approach to Power Transmission Control," *IEEE Transactions on Power Delivery,* vol.10, pp.1085-1097, April 1995.

[13] L.Perko, *Differential Equations and Dynamical Systems,* Springer-Verlag, 1991.

[14] D.N.Kosterev, W.J.Kolodziej, "Series Capacitor Bang-Bang Transient Stability Control," *IEEE Transactions on Power Systems,* vol.10, pp.915-924, May 1995.

[15] D.N.Kosterev, W.J.Kolodziej, R.R.Mohler, W.A.Mittelstadt, "Robust Transient Stability Control Using Thyristor-Controlled Series Compensation," *Proceedings of the 4th IEEE Conference on Control Applications*, pp. 215-220, Albany, NY, 1995.

[16] D.N.Kosterev, W.J.Kolodziej, R.R.Mohler, A.Y.Khapalov, "Controllability and Placement of FACTS Devices," *Proceedings of 1995 Stockholm PowerTech,* International Symposium on Electric Power Engineering, paper SPT IS-06-3, Stockholm, 1995

[17] C.W.Taylor, *Power System Voltage Stability,* McGraw-Hill, 1994.

[18] M.Klinger, W.A.Mittelstadt, C.W.Taylor, "Transient Stability Controls Used by Bonneville Power Administration to Mitigate Delays of Planned Facilities," CIGRE paper 32-01, 1982.

[19] E.V.Larsen, J.J.Sanchez-Gasca, J.H.Chow, "Concepts for Design of FACTS Controllers to Damp Power Swings," 1994 Summer IEEE Power Engineering Society Meeting, paper 94SM 532-2-PWRS, 1994.

[20] J.J.Paserba, N.W.Miller, E.V.Larsen, R.J.Piwko, "A Thyristor Controlled Series Compensation Model for Power System Stability Analysis," *IEEE Transactions on Power Delivery* vol.10, pp.1471-1478, July 1995.

[21] S.Jalali, R.Hedin, M.Pereira, K.Sadek, "A Stability Model for the Advanced Series Compensator (ASC)," presented at the 1995 IEEE Power Engineering Society Meeting in Portland OR, paper 95SM 404-4 PWRD, 1995.

[22] E.V.Larsen, K.Clark, S.A.Miske, J.Urbanek, "Characteristics and Rating Considerations of Thyristor Controlled Series Compensation," *IEEE Transactions on Power Delivery* vol.9, pp.992-1000, 1994.

[23] L.Angquist, G.Ingestrom, H.Othman, "Synchronous Voltage Reversal Scheme - A New Control Method for Thyrsitor-Controlled Series Capacitors," Flexible AC Transmission System Symposium (FACTS 3), Baltimore, October 1994.

[24] L.Dube, I.Bonanti, "MODELS: A new simulation tool in EMTP," *European transactions on Electrical Power Engineering,* vol.2, no.1, pp.45-50, January/February 1992.

[25] G.Lee, D.Goldsworthy, "BPA's Pacific AC Intertie Series Capacitors Experience, Equipment and Protection," presented at 1995 Summer IEEE Power Engineering Society Meeting in Portland OR, paper 95SM 367-3 PWRD, 1995.

[26] A.Hammad, "Comparing the Voltage Control Capabilities of Present and Future VAR Compensating Techniques in Transmission Systems," *IEEE Transactions on Power Delivery,* vol.11, pp.475-484, January 1996.

[27] CIGRE Task Force 38.02.12, *Criteria and Countermeasures for Voltage Collapse,* edited by C.W.Taylor, June 1995.

[28] IEEE Special Stability Controls Working Group (Power System Engineering Committee), "Static Var Compensator Models for Power Flow and Dynamic Performance Simulation," *IEEE Trans. on Power Systems,* vol.9, pp.229-240, February 1994.

[29] G.Seguier, F.Labrique, *Power Electronic Converters, DC-AC Conversion,* Springer-Verlag, 1993.

[30] Bonneville Power Administration, *BPA Powerflow Program: User's Guide,* 1995.

[31] J.H.Chow, K.W.Cheung, "A Toolbox for Power System Dynamics and Control Engineering Education and Research," *IEEE Transactions on Power Systems,* vol.7, pp.1559-1564, November 1992.

[32] D.N.Kosterev, W.A.Mittelstadt, R.R.Mohler, W.J.Kolodziej, "An Application Study for Rating and Sizing Controlled and Conventional Series Compensation," accepted for publication in *IEEE Transactions on Power Delivery,* presented at 1995 Summer IEEE Power Engineering Society Meeting, paper 95SM 401-0 PWRD, 1995.

[33] K.B.Stump, R.A.Hedin, W.A.Mittelstadt, D.N.Kosterev, "Preliminary Analysis of Subsynchronous Resonance in Colstrip West 500kV Transmission System," scheduled for *EPRI: Future of Power Delivery Conference,* Washington DC, April 9-11, 1996.

[34] J.M.Barcus, S.A.Miske, A.P.Vitols, H.M.Maynard, W.G.Peterson, "The Varistor Protected Series Capacitors at the 500kV Broadview Substation," *IEEE Transactions on Power Delivery,* vol.3, pp. 1976-1985, 1988.

[35] E.V.Larsen, C.Bowler, B.L.Damsky, S.L.Nilsson, "Benefits of Thyristor-Controlled Series Compensation," CIGRE paper SC 14/37/38-04, Paris, 1992.

[36] R.A.Hedin, S.Weiss, D.Torgerson, L.E.Eilts, "SSR Characteristics of Alternative Types of Series Compensation Schemes," *IEEE Transactions on Power Systems,* vol.10, pp.845-852, May 1995.

[37] IEEE Committee Report, "Single Phase Tripping and Autoreclosing of Transmission Lines," *IEEE Transactions on Power Delivery,* vol.7, pp.182-191, 1992.

[38] C.W.Taylor, A.L.Van Leuven, "CAPS: Improving Power System Stability Using the Time-Overvoltage Capability of Large Shunt Capacitor Banks," presented at 1995 Summer IEEE Power Engineering Society Meeting, paper 95 SM 356-6 PWRD, 1995.